CRANFIELD UNIVERSITY

DANIEL KAMUNGE

A NON-LINEAR WEIGHTED LEAST SQUARES GAS TURBINE DIAGNOSTIC APPROACH AND MULTI-FUEL PERFORMANCE SIMULATION

SCHOOL OF ENGINEERING

PhD. Thesis
CRANFIELD UNIVERSITY

SCHOOL OF ENGINEERING

PhD THESIS

Academic Year: 2010- 2011

DANIEL KAMUNGE

A NON-LINEAR WEIGHTED LEAST SQUARES GAS TURBINE DIAGNOSTIC APPROACH AND MULTI-FUEL PERFORMANCE SIMULATION

Supervisor: Dr. Y.G. Li

January 2011

This thesis is submitted in fulfilment of the requirements for the degree of Doctor of Philosophy

ABSTRACT

The gas turbine which has found numerous applications in Air, Land and Sea applications, as a propulsion system, electricity generator and prime mover, is subject to deterioration of its individual components. In the past, various methodologies have been developed to quantify this deterioration with varying degrees of success. No single method addresses all issues pertaining to gas turbine diagnostics and thus, room for improvement exists. The first part of this research investigates the feasibility of non-linear Weighted Least Squares as a gas turbine component deterioration quantification tool. Two new weighting schemes have been developed to address measurement noise. Four cases have been run to demonstrate the non-linear weighted least squares method, in conjunction with the new weighting schemes. Results demonstrate that the non-linear weighted least squares method effectively addresses measurement noise and quantifies gas path component faults with improved accuracy over its linear counterpart and over methods that do not address measurement noise.

Since Gas turbine diagnostics is based on analysis of engine performance at given ambient and power setting conditions; accurate and reliable engine performance modelling and simulation models are essential for meaningful gas turbine diagnostics. The second part of this research therefore sought to develop a multi-fuel and multi-caloric simulation method with the view of improving simulation accuracy. The method developed is based on non-linear interpolation of fuel tables. Fuel tables for Jet-A, UK Natural gas, Kerosene and Diesel were produced. Six case studies were carried out and the results demonstrate that the method has significantly improved accuracy over linear interpolation based methods and methods that assume thermal perfection.

ACKNOWLEDGEMENTS

The Author would like to sincerely acknowledge and appreciate the following persons who contributed in one way or another to the success of this project.

To the Aviation industries of China for their kind sponsorship; I am truly grateful.

To my supervisor Dr Ivan Li, for his patience and for all the helpful and insightful comments throughout the project; I am truly grateful.

To Professor Pericles Pillidis and Professor Riti Singh for the blessed opportunity to be a doctorate researcher in Cranfield and for all departmental support; I am truly grateful.

To Mr Jonathan Haynes in the computer centre, for his help with Fortran 90 programming; I am truly grateful.

To Robert Sawko, for helping with understanding some of the hard concepts and for always having his door open; I am truly grateful and I pray that he finishes well – and soon.

To my Cranfield friends who have been a second family in England – the Ubadykes, the Governor and Co., the Jemitolas, Ade, Isaac, Gareth and Ro'; for all the love and friendship, I am truly grateful. Special thanks to Ade, Gareth and Ro' for their help, hospitality and late nights of scrabble.

To my Pastor, Pastor Biyi Ajala and the entire 'Holding forth' community who have been a loving family to me. I appreciate all the encouragement, concern, support and the blessed opportunity to serve God and develop my God-given talents in his house.

To anyone and everyone else not mentioned here but all the same contributed in some way to the success of this project; the exclusion was not intentional. In addition, my gratitude to you is by no means less.

And saving the best for last –

To Mum and Dad, John, Michael and Elizabeth; the wind beneath my wings. This PhD was one of the greatest risks I have ever undertaken in my life but God was kind enough to give me a loving family like you who cushioned most of the risk. For all the sacrifices, prayers and support, I am eternally grateful.

To Almighty God; I sincerely thank you.

To Mum and Dad and,

in loving memory of Cucu.

TABLE OF CONTENTS

LIST OF FIGURES

LIST OF TABLES

NOMENCLATURE

A	General matrix
AI	Artificial intelligence
ANN	Artificial Neural Network
Atm	Atmospheres
$\vec{b}$	Vector of sensor biases
BBN	Bayesian Belief Network
C	Carbon, centigrade
CEA	Chemical Equilibrium with Applications
C_p	Isobaric heat capacity
C_v	Isochoric heat capacity
FAR	Fuel to Air Ratio
FCM	Fault Co-efficient Matrix
GA	Genetic Algorithms
GP	Gas property
GPA	Gas path analysis
H, *h*	Influence co-efficient matrix, enthalpy, Hydrogen, integer counter, matrix of interpolation point spacings
H/C	Hydrocarbon ratio
i	Integer counter

ICM	Influence Co-efficient Matrix
J	Joules
K	Kilo
K,k	Kelvin, iteration number
Kg	Kilogram
Kg/hr	Kilograms per hour
Kg/s	Kilograms per second
M,m	Number of measurements, matrix of interpolation point gradients
Ma	Mach Number
MB	Megabytes
MFI	Multiple fault isolation
NASA	National Aeronautics and Space Administration
N,n	Number of engine health parameters, number of days in averaging interval
NLWLS	Non-linear weighted least squares
O	Oxygen
P	Pressure
PCN	Compressor non-dimensional rotational speed
PDF	Probability density function
PR	Pressure ratio
psia	Pounds per square inch absolute

PT	Power turbine
r	residuals
R	Gas constant, set of real numbers
RMS	Root mean square
RPM	Rotations per minute
s	Matrix of second derivatives, second
S	Entropy, sum of residuals
SD	Standard deviation
SFI	Single fault isolation
T	Temperature
TET	Turbine entry temperature
u	Speed of sound
UK	United Kingdom
V	Velocity
w	mass flow
W	Watts
WAR	Water to Air Ratio
WLS	Weighted Least Squares
WS	Weighting Scheme
x	Interpolant value

$\vec{X}$	Vector of engine health parameters
$\vec{Z}$	Vector of measurement parameters

SUPERSCRIPTS

‘	ideal, differential
o	Reference condition
T	Transpose

SUBSCRIPTS

0	Reference condition
c	Compressor
eff	Effective
f	fuel flow
is	Isentropic
p	pressure
s	Static
T	Total
v	volume

GREEK LETTERS

α	Smoothing parameter
Δ	Increment, change
σ	Standard deviation, measurement noise level
κ	Matrix condition number
μ	Mean value
ω	'Percentage- noise-value'
ρ	Density
η	Efficiency
Γ	Flow capacity
γ	Ratio of specific heat capacities
λ, ϕ	Equivalence ratio
φ	Entropy function

1 BACKGROUND, AIMS AND OBJECTIVES

In this chapter, a brief overview of gas turbine diagnostic schemes and performance simulation models developed in the past is presented. Based on work done in the past, requirements for improved diagnostic schemes and performance simulation models are presented; these will form the framework of the aims and objectives of this project as presented in the following section.

1.1 Background - Gas turbine diagnostic methods

The gas turbine has proven to be an indispensable tool and has found use in Air, Land and Sea applications, as a Propulsion system, electricity generator and prime mover. Gas turbine components inevitably deteriorate with use over time; this is normally accompanied by deterioration in performance (shaft power, thrust, etc). The goal of gas turbine performance diagnostics is thus to accurately detect, isolate and assess the changes in engine module performance as a result of deterioration, engine system malfunctions and instrumentation problems from knowledge of measured parameters taken along the engines gas path.

Engine related costs constitute a significant portion of an aircrafts' direct-operating-costs; this is attributed to the required maintenance of the gas turbine. As such, engine diagnostics has been recognised as an important means for making more informed decisions related to engine usage and maintenance; in particular, overhaul schedules and/or component replacement. Such improved monitoring and maintenance methods are employed to ensure cost-effective and safe operation of the gas turbine.

The ever increasing need for condition based monitoring with a view to prioritize and optimize gas turbine maintenance resources has placed a demand for advanced gas turbine diagnostic techniques. In the past, numerous diagnostic schemes have been designed, developed and employed with varying degrees of success, each scheme having its own merits and demerits. Some of these

schemes include linear gas path diagnostic approaches that are based on the assumption that any changes in an engines' health parameters are relatively small and the engine performance variation due to engine gas path component degradation is approximately linear. The errors due to this linearity assumption may however not be negligible; this inadequacy of linear models led to the development of non-linear counterparts which showed significant improvement over their linear counterparts.

No single technique developed so far meets all the requirements for an advanced diagnostic scheme. Such requirements include (and not limited to): based on a non-linear model, freedom from black box behaviour, able to deal with measurement noise, exemption from training and tuning, etc. Discernible shifts in measured gas-path parameters such as temperatures, pressures, shaft speeds, fuel flow, etc, provide the necessary information for determining the shift in engine performance from a nominal (or "clean") state. However, such measurements are always subject to random noise and bias, the magnitude of which may often be comparable to the variations of measurements caused by engine degradation. Thus, failure to address measurement noise and bias may significantly deteriorate the accuracy and precision of diagnostics results. In the past, the methods employed to deal with measurement noise include exponential averaging of measurement samples or to weight individual measurements based on respective measurement variances (reciprocals of respective measurement variances). Therefore, large measurement samples will be required; in the absence of such large measurement samples, the aforementioned methods of dealing with measurement noise fail. In addition, measurement samples with both large variances and very small variances will produce (using the reciprocal-of-variance method) significantly small and significantly large weights, respectively. Such significantly large values of weights may (mathematically) affect the diagnostic algorithm negatively, thus impeding any diagnostic effort.

1.2 Background-Performance simulation models

Gas turbine diagnostics is based on analysis of engine performance at given ambient and power setting conditions; therefore, accurate and reliable engine performance modelling and simulation models are essential for meaningful gas turbine diagnostics. Caloric properties e.g. Specific Heat Capacity, Enthalpy, Entropy etc, can be calculated for simulation purposes, at various levels of fidelity. Selection of fidelity levels is dependent upon simulation objectives, time and computational constraints.

Early technical models based on experimental setups and ambient temperature measurements were able to obtain isobaric heat capacity with high precision; however, the temperature range where such data could be available was restricted to the temperature range which can be covered with accurate experimental setups. Thus, theoretical models that generally consider contributions to the heat capacity from molecular translation, rotation and vibration, were developed; with such methods, the temperature ranges were unrestricted.

The perfect-gas hypothesis that is based on the assumption of constant values of Isobaric heat capacity, C_p and ratio of heat capacities, γ yields inaccuracies of more than a few Kelvin in temperature calculations. To reduce this error, more accurate calculations would involve using constant values of C_p and γ but evaluated at mean component temperature. Fully rigorous approaches involve the use of the fundamental definitions of entropy and specific enthalpy. The inaccuracy of the results produced by these fully rigorous approaches is primarily dependent on the technical model used for calculation of caloric properties and uncertainty of the perfect-gas assumption. This approach is commonly used in gas-turbine simulation codes and yields smaller errors as compared to methods based on the perfect-gas assumption (constant values of C_p and γ).

"No dissociation" models are based on a constant gaseous composition of the fluid in question; composition is allowed to change only after combustion and/or mixing. As a result, mole fractions remain the same at any temperature; this implies that the mean molecular weights of the combustion products remain constant regardless of the pressure or temperature. However, at high temperatures (above 1200K) and/or low pressures dissociation effects start becoming noticeable and can induce increasingly significant deviations in C_p and γ calculations for temperatures beyond 1500K. Caloric properties are sensitive not only to temperature (and pressure) but also to H/C ratio; thus failure to consider the effects of fuel chemistry in the evaluation of these caloric properties for combustion products will lead to significant errors. For fuels with similar H/C ratio, only minor deviations would be expected. For instance, simulation models based on polynomials are suitable for combustion products for both Kerosene and Diesel since these fuels' H/C ratio are not significantly different. However, these polynomial-based models are unsuitable for fuels with significantly different H/C ratios. For fully rigorous thermodynamic calculations, appropriate tables or polynomials should be used.

1.3 Project Aims and Objectives

In light of the previously highlighted issues, accurate multi-fuel simulation models based on fully rigorous approaches in conjunction with advanced diagnostic algorithms are desirable in as far as accurate Gas turbine performance simulation and diagnostics are concerned. Therefore, the aims of this research project are;

- **To investigate the fidelity of a non-linear weighted least squares diagnostics algorithm for fault quantification of gas path components.**
- **To develop a multi fuel and multi-caloric property to improve the potential of gas turbine performance simulation accuracy.**

To achieve this aims, the following are the key objectives:

- Develop measurement weighting schemes that will work in conjunction with the non-linear weighted least squares (NLWLS) algorithm.
- Formulate the mathematical basis of the NLWLS algorithm and further code it using a suitable programming language.
- Compare diagnostics results of NLWLS algorithm with an available gas turbine diagnostics algorithm.
- Identify parameters that affect caloric properties of fluids; four fuels will be considered: Kerosene gas (Jet-A), UK Natural gas, Diesel and Hydrogen fuel.
- Identify a suitable technical model that will be used to obtain caloric properties of the aforementioned fuels. Once identified, this model will be used to develop dedicated tables of caloric properties for the four stated fuels.
- Develop a multi-dimensional non-linear interpolation algorithm for use with the dedicated caloric property tables.

2 LITERATURE REVIEW

2.1 Gas Path Diagnostic Schemes

During operation, gas turbine performance deterioration caused by component degradation is inevitable. A few of the principal faults that affect performance are *fouling* where the accumulation of deposits on blade surfaces results in an increase in surface roughness, changes in the aerofoil shape and a narrowing of the aerofoil-throat aperture, *erosion* where the aerofoil and seal surfaces are worn away by hard particles in the gas path, blade tip clearance damage that influences both efficiency and flow capacity, *corrosion* where the chemical reaction between component material and contaminants entering the gas turbine causes the loss of material from flow path components, *foreign object damage* that is the result of a foreign body striking the flow path components of the gas turbine engine, etc (AGARD-LS-183, 1992).

Any performance degradation due to the above stated causes may be detected by gas path diagnostics; to that end, different linear and non-linear gas path diagnostic approaches have been developed to detect, isolate and quantify faults in any of the engine components. Such actions are performed within the framework of condition based monitoring, with a view to optimise maintenance schedules and thus operate the engine safely and cost-effectively.

In the past, various thermodynamic performance-based diagnostic schemes have been designed and applied with relative success. Such techniques relate measureable engine parameters with the engine health parameters i.e. Flow capacity indexes and efficiency indexes. The review of these methods now follows.

2.1.1 Linear Weighted Least Squares

The weighted-least-squares method has been the predominant algorithm for gas turbine diagnostics for about a decade and has been utilised by a number of authors such as (Urban and Volponi, 1992; Barwell, 1987), amongst others. A linear weighted least squares approach was demonstrated by (Doel, 1994; Doel, 2003). The method was implemented within a diagnostic tool, *TEMPER*. *TEMPER* uses weighted-least-squares to apportion observed measurement deviations between engine health parameter deviations and sensor errors. Such apportionment is based on expected variation of both engine health parameters and measurement errors. Engine "baselines" represent expected values of test-cell or on-wing measurements; these baselines are the ones that permit recognition of abnormal engine behaviour. Development of such baselines is a time consuming effort that requires data assembly from as many engine runs as possible. Further, each engine or test-cell requires a unique expected-value baseline. Any changes to engine configurations or test-cells will subsequently require an update to respective baselines. New engines provide even greater difficulty since there exists no data from which to generate baselines. Users must either await gathering of sufficient data for the generation of the engine baseline or some other technique must be developed for providing the initial baselines.

(Doel, 1994) also made it clear that user interpretation of results is an essential part of the algorithm; further, that the variance of user interpretation may be more significant than any faults being sought or than any problem with the algorithm. As a solution, the author proposed a framework that allows incorporation of useful information such as maintenance history and borescope results in addition to the weighted-least-squares results. Such frameworks may be based on technologies such as expert systems or neural networks.

2.1.2 Linear gas-path analysis with ICM inversion

The relationship between measurements and performance parameters can be expressed analytically by Equation 2.1

$$\vec{z} = h(\vec{x}) + \vec{v} + \vec{b} \quad \textbf{(2.1)}$$

Where

- $\vec{z}$ is the vector of measurement parameters.
- $\vec{x}$ is the vector of engine health parameters
- $\vec{v}$ is the measurement noise vector.
- $\vec{b}$ is the vector of sensor biases.
- $h(\ )$ is a vector valued non-linear function.

This approach is based on the assumption that the changes in the engine health parameters are relatively small and the set of governing equations can be linearized around a given steady state operating point. If measurement noise and sensor bias are neglected, then these linearized equations can be expressed in matrix form by Equation 2.2

$$\vec{z} = h(\vec{x}) \quad \textbf{(2.2)}$$

Equation 2.2 may be written in terms of measurement and health parameter deviations, Equation 2.3.

$$\Delta\vec{z} = H.\Delta\vec{x} \quad \textbf{(2.3)}$$

The matrix *H* is referred to as the Influence co-efficient matrix (ICM). The deviation of component performance parameters can then be calculated by inverting the ICM, Equation 2.4

$$\Delta\vec{x} = H^{-1}.\Delta\vec{z} \quad \textbf{(2.4)}$$

The inverted matrix H^{-1} is referred to as the fault co-efficient matrix (FCM). By inverting the ICM, several assumptions have been made, regarding the relationship between the measurement and engine health parameters:

- A set of accurate measurement deviations are available i.e. there exists a method to faithfully reduce raw observed engine data to a measurement deviation level.
- The fault co-efficients are an accurate engine model descriptor i.e. the faults occurring in the engine are among those being sought.
- The fault co-efficients are invertible, i.e. that changes in the unknowns are adequately manifested in the observations.
- Measurements are noise free.

This method has found use in applications developed by several authors which include diagnostics (Escher, 1995), sensor fault identification (Escher, P.C. 2002), design-point performance adaptation (Li et al, 2006), capabilities. (Staples and Saravanamuttoo, 1975) described a similar method which required minimal computational power, developed to sense the health of a helicopter power plant with a high degree of accuracy and sensitivity. (Lazalier et al., 1978) utilised the same method to design a diagnostic system designed for component diagnostics of the *J75-P-17* engine. (Simani, 2005) presented a model-based procedure for the detection and isolation of faults of a gas turbine system that was based on errors between estimated and measured variables. The proposed fault detection and isolation tool was tested on a single-shaft industrial gas turbine model.

The direct matrix inverse approach shows potential due to the following capabilities:

- It is a relatively simple method as can be seen from the presented mathematical expressions.
- Does not require iterative calculations and is therefore quick.
- The severity of the fault is directly expressed by the changes of performance parameters.
- The technique allows multiple fault diagnostics.

However, any achievements to be obtained by the method would be hindered by the following limitations:

- The method requires many pertinent measurements for the analysis; indeed, the inversion of the ICM requires that the number of engine health parameters be less than or equal to the number of measurements, that is, $N \leq M$.

  (Kyriazis, 2009) presented a method that involved the fusion of GPA with a probabilistic method, to solve this problem of insufficient measurement parameters. This was achieved by means of 'Engine partitioning', where the most probable candidates among a large set of unknown health parameters was selected; this reduces the number of unknown health parameters. Since the number of health parameters for each part of the partition is smaller than the number of available measurements, then the ICM will always be invertible. Calculations are thus performed as many times as the different parts of each partition, estimating each time, the corresponding health parameters.
- The method does not deal with sensor noise or bias.
- Since the method relies on the assumption of linearity, it is only acceptable for very small deviations about the operating condition, of values of health parameters.

(Kamboukos and Mathioudakis, 2005) stated that measurement deviations evaluated by Equation 2.3 differ from the actual ones by the magnitude of the higher order terms neglected in the linear approximation. They stated that, "the assumption of linearity becomes increasingly false when deteriorations cause

the engine to operate further away from the condition for which the matrix was calculated." This consideration led to the development of non-linear GPA.

2.1.3 Non-linear gas-path analysis with ICM inversion

One method of improving the accuracy of Linear GPA is to try to solve the non-linear relationship between the considered engine health-parameters and measurement parameters, using an iterative method, such as the Newton-Raphson method. The method is employed recursively and an improved solution is obtained. Essentially, via this approach, an ICM is generated, taking into account a small deterioration in the engine-components' performance. This ICM is then inverted to calculate the vector of change in the engine-components' performance parameters. From the results calculated, a new ICM is generated and this process is recursively repeated until the solution converges to a set limit. One major benefit of this method is that the difference between the calculated changes in the independent parameters is much smaller for the non-linear approach than the linear approach.

(Escher and Singh, 1995) described such a method that showed significant improvement over its linear counterpart in as far as fault quantification of degraded engine components is concerned. The method is also capable of multiple fault detection, from various combinations of measured parameters.

PYTHIA (Li, 2005) is an integrated gas turbine diagnostic system based on Gas path analysis techniques. It provides the capability of gas turbine performance model generation and adaptation to real engine performance data, instrument selection, measurement data acquisition and simulation, sensor failure detection, measurement data correction against deviated ambient and operating conditions, measurement noise impact reduction and engine component fault diagnosis using the concept of GPA index (Mucino, 2005).

2.1.4 Kalman-filter based GPA

The Kalman filter is a linear model-based estimator and is suitable in those instances where a linear model is available and is known to be a relatively accurate representation of the input-output relationship. In addition the Kalman filter approach utilises all model information available (a priori estimate information, measurement noise information, etc) and can be easily configured to operate with different measurement suites and fault configurations i.e., single fault or multiple fault isolation systems (Volponi et al., 2003b)

Kalman filters reduce any dependency from historical data and estimate current states from previous time steps and current measurements. Deviation of engine component parameters is obtained by minimising a cost function, that is, a function of the difference between the actual measurements and predicted measurements from the model.

Kalman filters were introduced as fault isolation and assessment techniques for engine diagnostics in the late 1970's and found use through the 1980's. One such method is the one described by (Provost, 1988). (Luppold et al., 1989) described an algorithm that estimated both the cause and level of off-nominal engine in-flight performance. Five engine factors that fully characterised off-nominal performance were estimated using a Kalman filter algorithm. The algorithms' inputs comprised of measurements from a standard engine control instrumentation suite.

The success enjoyed in these early programs promoted the use of these techniques in subsequent years, to become the central methodology utilised in many current engine performance analysis programs. (Kobayashi and Simon, 2003) described a method that comprised of a bank of filters applied to aircraft engine sensor and actuator fault detection. From this bank of Kalman filters, each was designed for specific sensor or fault detection. The method was demonstrated to be reliable in sensor and/or actuator fault detection and isolation. More recently, (Simona and Simonb, 2009) presented a method that

takes into account signal information that is normally ignored in Kalman filter applications; such information is normally ignored since it does not fit easily into the structure of the Kalman filter (state variable inequality constraints). The authors noted that inclusion of state variable inequality constraints increases computational effort but at the same time improves diagnostic estimation accuracy. The method was demonstrated via simulation results obtained from a turbofan model and it was confirmed that the method provides improved accuracy in diagnostic estimation of gas turbine components.

The Kalman filter technique displays the following advantages:

- Optimality, in the sense that the cost function is minimised.
- Inclusion of prior knowledge; knowledge about the statistics of engine components deterioration can be introduced through the initial values of the state vector and its covariance matrix.
- Accounts for measurement noise; the actual measurement noise can be assumed to be white and Gaussian, as the Kalman filter requires.
- Sensor errors can be estimated through augmentation of the state vector to include the unknown sensor biases.

Limitations in the use of the Kalman filter include:

- Prior knowledge and tuning are needed: the choice of the covariance matrix (tuning) is often arbitrary.
- The Kalman filter tends to “smear” the fault over many components, i.e. “spreading out” any detected fault over other components apart from the one being analysed. The problem is undetermined and the Kalman filter solution is a maximum likelihood one; as such, concentration on the actual faulty component(s) may be difficult. (Provost, 1994) described and developed a modification to the basic Kalman Filter to solve this smearing effect.

- Non-linearity; the errors due to the assumed approximation to a linear model may not be negligible.
- The Kalman filter produces an optimal solution provided the hypothesis about the system is correct. In the case of gas turbine diagnostics, even though one might assume the measurement equation to be sufficiently precise, almost nothing is known of the system equation which describes the temporal evolution of the fault; therefore the system equation should be somehow estimated and this can impair the final diagnostic accuracy. In fact, the use of techniques to completely estimate the system equation introduces errors and as measurements are collected and used by the algorithm, the system "learns the wrong state too well." The consequence is divergence, i.e. the estimated solution becomes more and more distant from the actual solution.

2.1.5 Non-Linear Model-based optimal estimation by using genetic algorithms

In order to take into account the non-linearity of engine behaviour, a non-linear model based method combined with conventional optimisation was first introduced in 1990 by (STAMATIS et al., 1990)

Unfortunately, conventional optimisation may stop at a local minimum point. In recent years this disadvantage has been overcome by using genetic algorithms. The idea of gas turbine fault diagnosis with genetic algorithms involves initially guessing a component parameter; the engine model provides a predicted performance measurement vector. An optimisation approach is applied to minimise the objective function (which is a measure of the difference between the real measurement vector and the predicted measurement vector). A minimisation of the objective function is carried out iteratively until the best predicted engine component parameter vector is obtained.

(Zedda and Singh, 2002) described a diagnostic system for performance analysis of gas turbine components and sensors; the system estimates performance parameters in the presence of measurement noise and biases. Estimation is performed through optimisation of an objective function by means of genetic algorithms in conjunction with an accurate non-linear steady state performance model of the engine. The technique was tested by the authors on a low by-pass ratio turbofan model and the results showed high level of accuracy.

(Gulati et al., 2000) combined a GA approach with a multiple point diagnostic approach (Stamatis et al., 1991) to produce a GA-based multiple operating-point analysis method for gas turbine diagnostics. The method was used for estimating the shift in the component performance parameters of a relatively poorly instrumented engine in the presence of measurement noise and bias. The technique was based on the use of multiple operating point analysis to overcome the lack of information due to an inadequate sensor set. The technique was demonstrated on a three-spool low bypass ratio turbofan engine, with nine measurements used to determine fourteen performance parameters and showed favourable results.

The following are the advantages of the genetic algorithms method:

- They search for the optimal solution from a population of points, not a single point; this makes it easier to escape from local minimum areas.
- They use objective function information; no use of derivatives is required. This enlarges the area of applicability of genetic algorithms significantly.

Genetic Algorithms do however suffer from the following limitations:

- The method is more computationally burdensome than classic estimation techniques.

- Although multiple-faults can be detected, the technique is limited to four health parameters experiencing simultaneous deteriorations.
- The method requires a trained person for its worthwhile operation. This is because care must be taken when assigning the number of strings. Active awareness of these issues that are necessary for the correct utilization of the technique makes the method difficult to use and thus the requirement for a trained person for its worthwhile operation.

2.1.6 Artificial Neural Networks

Work on artificial neural networks was motivated from the recognition that the human brain computes in an entirely different way from the conventional digital computer. A neural network can be defined as a massively distributed processor made of simple processing units which have a natural propensity for storing experimental knowledge and making it available for use.

Artificial neural networks differ from conventional techniques in many respects. The main difference is that the latter rely on a mathematical model of the process to be analysed (hence they are referred to as 'model-based'), while the former learn from examples.

Generally, Neural Networks operate in two phases; a learning phase and an operating phase. The purpose of the learning phase is to determine the Neural Network parameters, which will enable the network to function properly in the operating phase. (Ogaji and Singh, 2003) presented an artificial neural network system that was trained to detect, isolate and assess faults in some of the components of a single spool gas turbine. The method was tested with data not used for the training process. The authors compared the results with available diagnostic tools and the results showed that significant benefits can be derived from the actual application of the technique.

(Lu et al., 2001) described a back-propagation artificial network based method that was trained and tested using noisy data. The results indicated that under

high noise levels, ANN fault diagnostics could achieve only a 50-60% success rate.

(Yoon, et al, 2008) applied an artificial neural network to predict the deteriorated component characteristics of a micro gas turbine. The neural network was trained with generated deterioration data. Inputs to the system were measurable parameters and characteristic health parameters of each component were predicted. The method was demonstrated to produce sufficiently accurate predictions; however, such accuracy was reduced when a smaller number of input parameters were used.

(Fast, et al, 2009) presented an ANN that was trained to predict the performance parameters of a gas turbine for both on-line and off-line monitoring. The presented method could extrapolate beyond the range of training data and was demonstrated with good diagnostic results.

The multi-layer perceptron (MLP) with back-propagation training is the most common architecture used for gas path analysis purposes, also known as the feed-forward back-propagation neural-network. Various researches have applied this method and they include, (Denney, 1965), (Eustace, 1993), (Kanelopoulos et al., 1997), (Tang et al., 1998)

The following are the main advantages of neural networks as listed by (Bettocchi et al., July 2007)

- They do not require knowledge of the physics of the problem to be modelled, since they allow the reproduction of a system once they are trained by using input-output data of the system itself. This is especially useful when a system model is either unavailable or too complex to be analysed.
- The capability to learn different typologies of information such as quantitative and qualitative rules derived from field experience.
- High robustness in the presence of poor and incorrect input data.

- High computational speed, which allows real time calculation.

On the other hand, the main limitation of Neural networks is high prediction error when they operate outside the field for which they were trained, i.e. they are not able to extrapolate; this implies that a massive amount of data from encountered and foreseeable fault conditions of operation would be required in each development phase of the neural network.

Others limitations include:

- Training times may be long, though this is dependent on network type, size and amount of training data. In the event that machine operating conditions change, e.g. an overhaul, neural networks require retraining.
- It is deficient in as far as providing descriptive results is concerned; besides inspecting predictions by the neural network, there is no way of accessing the neural networks "reasoning".
- It is sometimes difficult to provide the confidence level associated with the output result. This is because neural networks attempt to replicate the behaviour of a system and thus lack the knowledge needed for true understanding of a physical process. (They are thus considered shallow).
- As the number of engine operating points that need to be diagnosed increases, the diagnostics error is bound to increase unless an alternative means of data correction is devised.

2.1.7 Bayesian-belief network based GPA

Bayesian Belief Networks (BBN) are probabilistic expert systems that allow the estimation of the probability of discrete variables even in complicated systems with many variables (and strong relationships among them). A Bayesian Belief Network consists of nodes representing discrete variables, as defined in probability theory. All possible discrete values of a variable compose the set of

states of the corresponding node. The interrelationships among the variables are expressed through the links of the network. Diagnostic BBNs allow the disengagement of the BBN from hard-to-find statistical data and implementation into any type of engine; these two elements make BBN's interesting and promising. The heuristic way of building BBNs however puts some question on its reliability and generality.

(Palmer, 1998) noted that in as much as Gas path analysis codes have been somewhat successful, they have nevertheless not been entirely satisfactory; improvements would therefore consist of the integration of information such as past maintainance records, in order to achieve better results. To that end, the author developed a diagnostic system for the *CF6* family of engines. This system integrated test cell measurements and a gas path analysis program with information regarding engine operational history, build-up work-scope, and direct physical observations, in a Bayesian belief network. A similar approach was presented by (Volponi et al., 2003a) who developed a data fusion system that utilised, in part, a BBN for data fusion. The aim of the method was to integrate data from multiple sources that included maintainance histories and user manuals; such an approach was deemed by the authors to be more worthwhile than using information from a single sensor. The underlying purpose of their method consisted of enhancing diagnostic visibility, reliability and reducing the number of diagnostic false alarms. A general procedure of building a BBN for diagnostic reasons has been presented by (Romessis et al., 2001). (Romessis and Mathioudakis, 2006) presented an alternative BBN method. In comparison with the BBN proposed by (Romessis et al., 2001), it was more efficient even in fault cases with smaller health parameters' deviations. This improvement was due to the way the BBN was constructed; probabilistic relationships among variables were more accurately represented. Further, the following aspects made the BBN by (Romessis and Mathioudakis, 2006) (and all other BBNs in general) more attractive for application:

- Since the diagnostic conclusions are derived through estimated probabilities, confidence levels of diagnostic conclusions are also provided with the diagnostic results.
- The ability to embed BBNs into other diagnostic procedures thus providing a more robust and accurate diagnosis.
- The convenience of inclusion of additional information, whenever available. Additional information such as engine maintainance histories can be included either as independent knowledge by adding network nodes or as a-priori knowledge by modification of the a-priori probability of the network nodes. This inclusion is not a hard task since it does not require a rebuild of the network. In this way, the method offers an alternative to the known problem of gas path diagnostics consisting of the determination of more health parameters, than the available measurements. The BBN solves this problem through the inclusion of this additional information, something that would be possible for GPA only by having additional gas path measurements.

However, the use of BBN in gas path diagnostics experiences the following limitations:

- BBN's in general do not deal with sensor bias. However, recently, (Lee, et al, 2010) developed an off-line fault diagnosis method for industrial gas turbines that made use of multiple Bayesian models. Sensor biases were explicitly included in the multiple models so that the magnitude of biases, if any, could be estimated in addition to component faults.
- Substantial time and effort are required to gather the information needed for setting it up.

2.1.8 Fuzzy Logic based diagnostics

Fuzzy Logic is a method that formalises the human capability of imprecise reasoning. It is a rule-based approach, founded on the formulation of novel algebra, typically used in the analysis of complex systems and to enable decision making processes to be performed.(Ross, 2004) The input and output are discretised and this enables complex mathematical problems to be simplified. Fuzzy logic systems allow the incorporation of the knowledge base in a simpler manner than other artificial intelligence methods, specifically, neural networks. In addition, they are cost effective for a wide range of applications compared to traditional mathematical model-based methods (and neural networks as well), (Bettocchi et al., 2007).

Various gas turbine diagnostic methods based on Fuzzy logic theory have been developed with success. (Siu, 1996) presented a system that consisted of Fuzzy logic in conjunction with an expert system, for diagnosis of vibration in turbo-machinery. The fuzzy part was used to model uncertainty associated with vague knowledge whilst the expert system part was used to rank possible vibration causes. The system also made use of past maintainance records. The system was tested and was demonstrated to be able to identify underlying causes of typical vibration problems. (Tang et al., 1999) presented a jet engine condition monitoring and diagnosis system that was based on Fuzzy logic and neural network technology. The method contained three diagnostic levels, health check, fault diagnosis and prognosis. Fuzzy reasoning acted to classify faults into gas path components, sensor faults and rotor/subsystem faults, whilst the neural network element speculated the fault codes and computed their magnitudes. The system was applied in an airline situation with data acquired from airborne recorders and was demonstrated to be successful in as far as condition monitoring and fault diagnosis are concerned. (Applebaum and Ha'Emek, 2001) presented a fuzzy expert classifier for fault identification that was based on expert reasoning and diagnosis of trend case residuals formed during an airplanes first ten seconds of flight. The implementation of the system

allows an expert to modify the fuzzy rule base ‘on the fly’ so that no further model recompilations are necessary.

(Ganguli, 2003) developed a fuzzy logic system for gas turbine module fault isolation. Inputs to this system were measurement deviations of gas path parameters (deviation from a baseline engine). The system then used rules developed from performance influence coefficients, for fault isolation, whilst accounting for measurement uncertainty. The method was tested with simulated data and showed that the fuzzy system isolated module faults with an accuracy above 95%, even with poor quality data.

(Demirci, et al., 2008) developed an automated fuzzy-logic based method for engine health monitoring for use in commercial aircraft. The inputs to the fuzzy logic system were engine performance parameters gathered from aircraft during cruise. The system produced output values as either ‘faulty’ or ‘not faulty’. The method was found to simplify Engine health monitoring procedures for a certain airline and in addition, minimised drawbacks such as human error, extra labour hours and the requirement for engineering expertise. Limitations to this method include the fact that it does not provide long-term engine maintainance decisions such as scheduling overhaul times or predicting the remaining life of hot-end components.

The use of fuzzy logic systems in gas path diagnostics experiences the following limitations:

- The model free feature that allows data-fusion and computational time reductions comes with the restrictions that a fuzzy system does not admit model-based proofs of stability and robustness.
- Like other artificial intelligence tools, fuzzy systems are unable to extrapolate/approximate credibly, outside their range of exposure; this implies the need to have massive amounts of data in their development, from both encountered and foreseeable fault conditions.

- Fuzzy systems face the problem that the number of rules increases according to the complexity of the process that is being approximated.

2.1.9 Expert Systems

An expert system is a computer program that represents and reasons with knowledge of some specialist subject with a view to solving problems or giving advice. It is usually built by assembling a knowledge base which is then interpreted by an inference engine. A number of expert systems for gas turbine diagnostics have been developed in the past, and include and not limited to, JET-X (Shah et al., 1988) a PC-based expert system, developed at *General Electric* for use on the United States Airforce *A-10* aircraft. It provided the capability to supplement engine fault detection systems by incorporating knowledge from existing troubleshooting manuals, augmented by engineers with a background in engine performance analysis. The system proved quite useful where considerable amounts of information were required to be analysed for multiple interdependent root causes. HELIX, (Hamilton, 1988) developed by *United technologies research centre* and *Sikorsky aircraft,* utilised a *Qualitative Reasoning System (QRS)* that represented a set of constraints that defined the normal behaviour of the engines, flight controls, transmission and rotors of helicopter aircraft. Aircraft health was assessed by determining whether observations (sensor readings and pilot control inputs) were consistent with the constraints of the model. If an inconsistency was detected, a process of systematic constraint suspension was used to test various failure hypotheses. TEXMAS, (Collinge and Schoff, 1987) was developed by *Textron Lycoming* for the *Lycoming T53* engine for both engine condition monitoring and diagnosis. The monitoring of trends in measured parameters lead to prediction of component failures and subsequent deduction of the defective component or system

(Torella and Torella, 1999) presented an expert system for the diagnostics and trouble-shooting of gas turbine apparatuses that constructed probabilistic

relations among symptoms and faults. The authors noted that by using probabilistic expert systems, delicate maintenance actions may be carried out fast and effectively.

(Afgan, et al, 2006) presented a method for diagnosis and monitoring of gas turbine combustion chambers. The method made use of data obtained by means of numerical simulation of gas turbine chambers. The method was meant to solve the problem of scarcity of high-level experts in the energy sector by providing decisions on engine health condition in the absence of the high-level experts.

(Kopytov et al., 2010) presented a hybrid expert system method that consisted of three models. The first was a diagnostic model based on bayes' theorem. This model was built on the basis of prior statistics of respective components. The second model was based on an engine mathematical model that computes engine faults based on measurable parameters from both clean and degraded conditions. The third model was a logical model that was used to determine the engines status condition based on information from the first two models.
This mutual complementation allowed for optimal fault isolation and quantification.

Expert systems have much to offer to integrated diagnostics for gas turbine engines. (Doel and LaPierre, 1989) highlighted the following promising areas:

- Integration of expert systems with Built-in control (BIT) controls; resident in the engine control, and integrated with the flight computer, an expert system will serve to provide interpretation of BIT information that can provide specific maintenance recommendations. Further, the proliferation of information that accompanies BIT systems provides an opportunity for expert systems, as far as management and analysis of large amounts of data are concerned, since these will be beyond the capacity of most maintenance personnel.

- Analysis of acquired engine parameters, particularly from mechanical subsystems; data analysis can often be accompanied independent of expert systems. However, interpretation of many complex symptoms is an appropriate function for expert system technology
- The inclusion of qualitative and expert information (that is generally available to the analyst) in gas path analysis. Kalman filter based tools are certainly effective but they fall short of the performance that can be achieved by a skilled analyst. This short fall results from the inability to make use of qualitative information that includes: prior maintenance history, pilot reports, interpretation of error patterns generated by Kalman filters, impact of unavailable measurements on the analysis. Further, (DePold and Gass, 1999) noted that a minimum of one week of intensive training is required to apply diagnostic knowledge but effective utilisation of current tools requires years of experience. They further stated that the use of expert systems permits the emulation of the required judgment and experience (that takes a long time to acquire).
- The integration of expert systems with the capability to store massive amounts of text and graphic information using CD-ROM or comparable media. By combining these technologies, one can envision a system that assists the mechanic throughout engine diagnostic and maintenance tasks. The expert system could contain the procedure(s) needed to diagnose engine problems

However, there are significant obstacles to be overcome if expert systems (and indeed Artificial Intelligence systems) are to become a robust tool for jet engine diagnostics and they include:

- Defining effective diagnostic procedures for new engines. There are two factors that make this difficult; the first is anticipating the problems that the expert system will need to address. It is not practical to have a system cope with every conceivable situation that could occur. It is also

not unusual to have new engines exhibit one or two problems that were not expected and/or have not been seen before.

- A second difficulty is anticipating the symptoms for some problems; this is difficult because of the limited instrumentation that is provided on jet engines.

2.1.10 Rough-Sets based Diagnostics

The Rough-set method was first introduced by Polish mathematician *Zdislaw Pawlak*, (Pawlak, 1984). The method can be viewed as an extension to classical set theory and is founded on the assumption that with every object of the universe of discourse, one can associate some information (data, knowledge). Therefore, objects characterized by the same information are indiscernible in view of the available information concerning them. Such objects can be considered as belonging to sets with fuzzy boundaries, that is, sets that cannot be precisely characterised using the available set of attributes. This leads to the definition of a set in terms of lower and upper approximations. The lower approximation is a description of the objects which are known with certainty to belong to the subset of interest whereas the upper approximation is a description of the objects which possibly belong to the subset.

Whilst faults in engine gas paths are multi-characteristic in nature, it is not always possible to set as many sensors as would be needed to correctly diagnose these faults. In addition, noise and sensor faults will compromise the quality of sensed data. As such, the situation is one where one needs to precisely diagnose faults with limited information (limited measurement parameters affected by measurement noise). To address this issue, (Chen and Sun, 2005) developed a hybrid method that consisted of Rough-sets in conjunction with Neural Networks. The rough-sets was used as the front end of the Neural networks, where the former served in the area of fault isolation and the latter served in the area of fault quantification. This hybrid method served to improve engine fault diagnosis as opposed to the case where either method

was used on its own; this is because the rough-sets part of the system served to isolate the fault whilst the Neural networks part served to quantify the same fault, taking into account engine non-linearity.

The main advantages of the rough set-theory include:

- Representation of imprecise knowledge; in gas turbine diagnostics, a typical situation is the case of multiple fault diagnosis with limited measurements.
- Ability to incorporate expert knowledge into a system.
- Evaluation of the quality of the available information with respect to its consistency and the presence or absence of repetitive data patterns.

Having mentioned that, it needs to be stated that similar to other artificial intelligence methods such as Fuzzy logic and Artificial Neural networks, rough-sets are not accurate beyond the range of variability for which they were trained.

2.1.11 Diagnostics using Transient measurements

In most cases, gas turbine diagnostics is performed using steady state measurement data. However in certain cases, such steady state data may be either difficult to obtain or altogether unavailable. A good example is combat aircraft that spend 70% of their total mission time with their engines running in non-steady state conditions (Merrington, 1989). In addition, some gas turbine fault phenomena appear only during transient phases; such faults contribute little to performance deviation at steady state operation conditions but are however significant during transient processes. Such phenomena could seriously degrade the operability of the engine during manoeuvres and following missile release, such as mis-scheduled nozzle and compressor blade movement due to control system faults (Merrington, 1988). In such cases gas

turbine diagnostics may best be achieved using transient measurement data. (Meher-Homji and Bhargava, 1994) noted that there is significant diagnostic content in turbine start-up and shutdown data and in data obtained during power or speed changes and that these data can be captured if an automatic on-line system is employed. They further provided an overview of the use of both performance and mechanical transient analysis as a means to detect gas turbine problems. (Li, 2003) presented a method that utilised a non-linear model based diagnostic approach using typical gas turbine transient measurements, combined with genetic algorithms. For this approach, a typical slam acceleration process from idle to maximum was chosen. The method was applied to a model engine implanted with three typical single component faults and was proven to be very successful. (Lunderstaedt and Junk, 1997) presented a method that suited non-stationary operations of jet engines especially in the military field. The method utilised nonlinear parameter estimation algorithms and neural networks for the calculation of the non-stationary reference base lines. The authors further presented results from two jet engines, *LARZAC* and *RB 199*.

(Ogaji, et al., 2003) presented a method that involves the use of Artificial Neural Networks with engine transient data for fault diagnosis of engine components. The approach involved classification and approximation type networks, where engine measurements are first assessed by a trained network and if a fault is diagnosed, it is classified into one of two groups, sensor faults or component faults. Other trained networks proceed with quantification of the diagnosed fault. The method took into account sensor noise and bias. The authors compared fault signatures from a steady state and transient process and concluded that diagnosis with transient data can improve the accuracy of gas turbine fault diagnosis.

(Sampath, et al., 2003) presented a method that compared model-based information with measured data obtained from an engine during a slam-acceleration. The measured transient data was compared with a set of

simulated data from an engine model under similar operating conditions and known faults through a cumulative deviation. The cumulative deviations so obtained were minimised for best fit by means of a genetic algorithm. The method was applied with success to a 2-spool turbofan engine.

2.1.12 Summary of diagnostics methods and recommendations

In as much as engine-fault diagnostics is a mature technology no technique provides a satisfactory and complete answer to all the issues; each method comes with its own limitations. In summary:

1. Some of the approaches such as linear GPA with ICM inversion are based on the assumption that the changes in the health-parameters are relatively small and the set of governing equations can be linearized. The inadequacy of this linearity assumption has led to the development of non-linear counterparts.
2. Techniques, such as WLS and Fuzzy-logic approaches are well suited for dealing with measurement uncertainty.
3. Algorithms based on ICM inversion are suitable only if the number of measurements is more than (or equal to) the number of health parameters; in addition, they are not able to deal with measurement uncertainty.
4. Estimation techniques as well as AI-based methods, can deal with diagnostics with only a few measurements.
5. Some techniques are better suited for estimating gradual deteriorations and others for rapid deteriorations. Such methods may be referred to as MFI (multiple-fault isolation) and SFI (single-fault isolation) respectively. The former implies that all the engine-components deteriorate (slowly) with time, whereas the latter implies a rapid trend shift, probably due to a single (or multiple) entity going awry. AI-based methods are more suitable for SFI problems, because

they approximate all the possible solutions with a limited number of cases used to train the system.

The extension to all the possible combinations (even in a limited search-space) is theoretically possible, but time consuming and extremely burdensome computationally.

6. AI-based techniques do not exhibit the ‘smearing' problem (i.e. the tendency to spread-out the faults over a large number of the engine's components and sensors) that estimation techniques suffer from, but on the contrary have good ‘concentration' capabilities.
7. Estimation techniques require prior information and the solution can be dramatically affected by this choice. Similarly AI-based methods require particular care during the set-up phase. Moreover AI-based algorithms can be excessively time-consuming, both in the actual calculation as in the case of a GA, or in the training phase as for an ANN.

   As far as fuzzy systems are concerned, a large number of rules with many non-linearly-related inputs and outputs are needed.

8. Expert systems, ANNs, BBNs and fuzzy logic systems are referred to as model-free systems. This model-free feature is responsible for data-fusion capability but comes with the limitation that no model-based proofs of stability and robustness are possible. Besides, they are not accurate out of the range of variability for which they have been trained or set-up. Numerous tests are required to validate these techniques. ES, BBN and fuzzy logic approaches have the additional quality that they can be used to encompass expert knowledge in the system.

The techniques are summarised in Table 2.1.

	Methodology										
Strategy	Linear GPA with ICM inversion	Non-linear GPA with ICM inversion	Linear Kalman filter	Linear WLS	Non-linear Kalman filter	Non-linear model based with GA	Artificial neural networks	Bayesian belief networks	Expert systems	Fuzzy Logic	Rough-Sets
Linear/non-linear model	Linear	Non-linear	Linear	Linear	Non-linear	Non-linear	Non-linear	Non-linear			
Small changes of health parameters	X		X	X							
Addresses Random noise			X	X	X	X	X	X	X		
Addresses Bias			X	X	X	X	X		X		
N Parameters, M Measurements	M>=N	M>=N	M<N	M<N	M<N	M<N	M<N	M<N	M<N		M<N
Singe/Multiple fault(s)	MFI	MFI	MFI	MFI	MFI	SFI/Limited MFI	SFI/Limited MFI	SFI/Limited MFI	SFI/Limited MFI		MFI
Smearing Vs concentration			Smearing	Smearing	Smearing	Concentration	Concentration	Concentration			
Difficulty and dependence on training/tuning			Prior knowledge	Prior knowledge	Prior knowledge	Number of string assignment	Long training and data selection	Effort in gathering info for setting-up			Need to generate rules
Artificial intelligence based						X	X	X	X	X	X
Computational burden						X		X			
Model free							X	X			X
Data-fusion capability							X	X			
"Black-box" (not observable)							X				X
Good accuracy in pre-defined ranges only						X	X	X			X
Expert knowledge capability								X	X	X	X
On-wing			X	X	X		X			X	

Table 2.1: Comparison and summary of Gas-path diagnostic methods. [Marinai et al., 2004]

'X' means that the respective scheme possesses the respective capability contained in the "strategy" column.

In conclusion, the critical review of the available literature recommends the following requirements for an advanced diagnostics process:

1. It should be based on a non-linear model.
2. Ability to detect with reasonable accuracy significant changes in performance.
3. Able to deal with measurement random noise and sensor bias.
4. Competent to make a worthwhile diagnosis using only a few measurements.
5. Designed specifically for Single Fault Isolation or Multiple Fault Isolation.
6. Possess a “concentration” capability on the actual fault.
7. Exempt from tuning and training uncertainties and any difficulties and dependences related to the setting-up of parameters.
8. Easily-satisfied computational requirements.
9. Capable of data-fusion.
10. Ability to incorporate expert knowledge.
11. Fast in undertaking diagnosis for on-wing applications.
12. Free from black-box behavior (lack of comprehensibility).

There is no single technique that addresses all these issues; some of the techniques are complementary and each has its own advantages and limitations. Hence it would be worthwhile to try and combine more than one technique to offset the limitations of one with the advantages of another within a combined scheme. This task can be thought of in two ways; one is to use critically the results from different methods to work in concert with one another, exploiting a potential synergistic effect. The second way is to design hybrid systems. On the other hand, industry is showing a major interest in engine-health monitoring and prognostic schemes. The future challenge is to design effective combined engine health monitoring and prognostic procedures, and in so doing, increasing the market value of these technologies.

2.2 Advanced thermo-fluid modelling for gas turbines

Reliable and accurate fluid modelling of caloric properties for gas turbine performance simulation software is essential as it provides a robust foundation for building advanced multi-disciplinary modelling capabilities and improved confidence in simulation results. Such caloric properties e.g. Specific Heat Capacity, Enthalpy, Entropy etc, can be calculated at various levels of fidelity which are dependent upon simulation objectives, time and computational constraints. This section attempts to investigate the common assumptions in thermo-fluid modelling and their subsequent effects on caloric properties. In addition, the common technical models used for calculating caloric properties are reviewed and compared for mutual consistency.

2.2.1 Experimental methods

One method of determining the ideal gas isobaric heat capacity utilises the speed of sound in a perfect gas, (Trusler, 1991), Equation 2.5.

$$u^2 = RT\gamma \tag{2.5}$$

Where,

- $\gamma = \dfrac{C_p}{C_p - R}$ is the zero-pressure (perfect gas) limit of C_p / C_v .
- R is the ideal gas constant, calculated as Equation 2.6.

$$R = \frac{R_{universal}}{MolecularWeight}\left[\frac{J}{Kg.K}\right] \tag{2.6}$$

The temperature is determined by measurement and the speed of sound so obtained is used to obtain the isobaric heat capacity C_p, Equation 2.7

$$\frac{\gamma}{\gamma - 1} = \frac{C_p}{R} \tag{2.7}$$

Typically, the isobaric heat capacity obtained in this manner will be obtained with a precision of 0.01 percent or better. However, the temperature range where such data are available is restricted to the temperature range which can be covered with accurate experimental setups. Thus, an alternative and common method of determining the heat capacity of ideal gases uses theoretical models that depend on molecular constants measured by spectroscopy. These models generally consider contributions to the heat capacity from molecular translation, rotation and vibration and where necessary, from excited electronic states. Each mode has its own distinguished energy scale, denoted by a characteristic temperature. For higher accuracy, especially at high temperatures, contributions from mutual interactions between different modes have to be considered. With this method, the temperature ranges are unrestricted.

Once the isobaric heat capacity and molecular weight of a species are known, then the rest of the caloric properties can be calculated for an ideal gas using Equations 2.8 to 2.10

$$Enthalpy, h(T) = h_o + \int_{T_0}^{T} C_p(T) dT \ \left[J\right] \tag{2.8}$$

$$Entropy, s(T,P) - s(T_o,P_o) = \int_{T_o}^{T} \frac{C_p}{T} dT - R \times \ln\left(\frac{P}{P_o}\right) \left[\frac{J}{Kg}\right] \tag{2.9}$$

$$\gamma = \frac{C_p(T)}{C_V(T)} = \frac{C_p}{C_p - R} \tag{2.10}$$

Where,

- C_p is the isobaric heat capacity
- P is the pressure
- T is temperature
- *H* is the enthalpy
- R is the gas constant

In addition to the equations above, the following equations are fundamental as far as flow continuity models are concerned.

$$P_s = \rho \times R \times T_s \tag{2.11}$$

$$W = \rho \times A_{eff} \times V \tag{2.12}$$

$$h_T - h_s = \frac{V^2}{2} \tag{2.13}$$

$$\varphi = \int_{T_0}^{T} \frac{C_p}{T} dT = s(T,P) - s(T_0,P_0) + R.\ln\left(\frac{P}{P_0}\right) \tag{2.14}$$

$$Ma = \frac{V}{\sqrt{\gamma.R.T_S}} \tag{2.15}$$

The equations presented so far are made without due attention to real-gas effects; however, neglecting real-gas effects poses limits which are discussed in the following section.

2.2.2 Perfect gas hypothesis and its limitations

Gas turbine performance simulation tools employ simplifications depending on the intent of the simulation for which these simplifications are appropriate. A perfect gas consists of the assumption of constant cold end gas properties, that is, $C_p = 1004.7\left[\mathrm{J/(Kg.K)}\right]$ and $\gamma = 1.4$ (Walsh et al., 1998). This assumption can yield inaccuracies of more than a few degrees Kelvin in temperature calculations (Konstantinos Kyprianidis et al., 2009). Particularly at low temperatures and high pressures, intermolecular forces affect the thermodynamic properties of the system leading to considerable deviations from the assumed perfect gas behaviour, (Bücker et al., 2003). For quick evaluation of thermodynamic cycles, especially hand calculations, this method is however useful. (Kurzke, 2007) stated that simplified models are quite acceptable for ideal cycle analysis; however for real cycles and more so combustion models, these simplified models are unacceptable. (Wilcock et al., 2002) noted that cycle performance simulations of future gas turbines may be limited if real gas properties at high temperatures and Fuel-to-air ratios are not taken into account.

For dry air, reliable thermodynamic properties can be calculated using an accurate equation of state, (Jacobsen et al., 1990). (Bücker et al., 2003) made comparisons of isobaric heat capacity and enthalpy for dry air and combustion of a natural gas at an equivalence ratio of $\lambda \approx 3$.

Where

$$\lambda = {FAR}\Big/{FAR_{stoichiometric}} \qquad \textbf{(2.16)}$$

The aforementioned comparison was between thermodynamic properties obtained using an equation of state that considers real gas behaviour, (Jacobsen et al., 1990) and corresponding values obtained assuming a perfect gas mixture, Figure 2.1 to Figure 2.3.

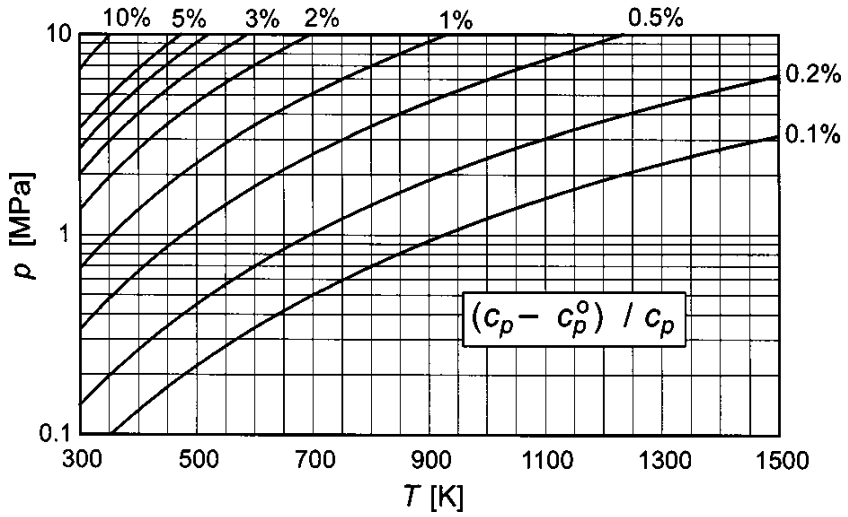

Figure 2.1: Percentage deviations of isobaric heat capacities of dry air considering real gas behaviour versus a perfect gas mixture [Bücker et al., 2003]

With reference to Figure 2.1, it is observed that neglecting real-gas effects results in significant inaccuracies of isobaric heat capacity values especially at high pressures and low temperatures.

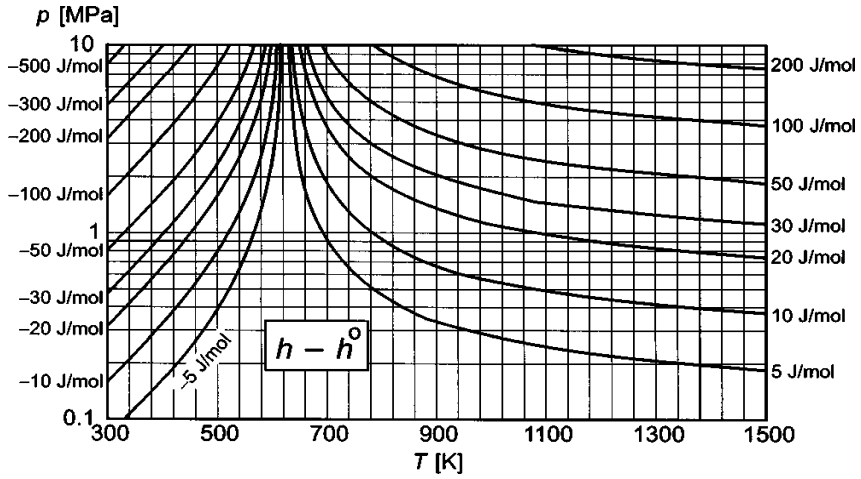

Figure 2.2: Absolute deviations of enthalpies of dry air considering real gas behaviour versus a perfect gas mixture [Bücker et al., 2003]

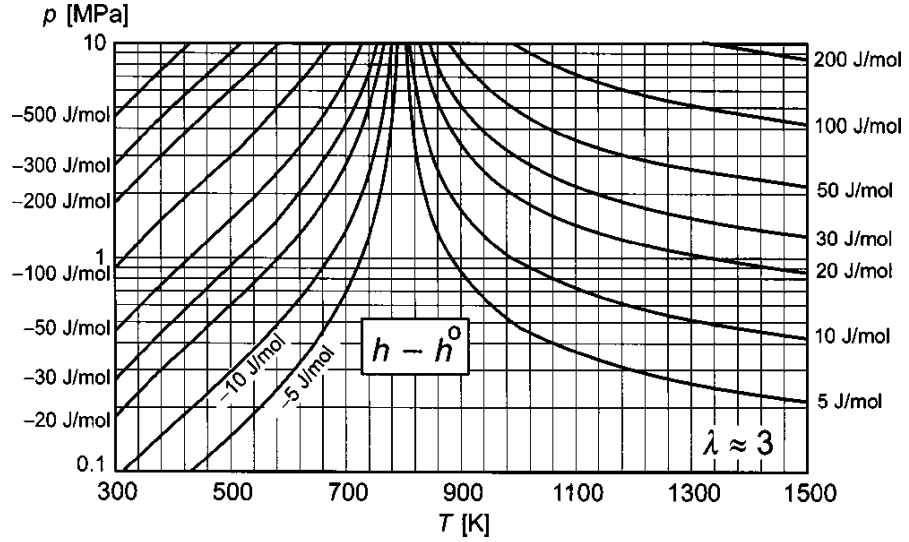

Figure 2.3: Absolute deviations of enthalpies of combustion of a natural gas in air, considering real gas behaviour versus a perfect gas mixture [Bücker et al., 2003)]

With reference to Figure 2.2, it is observed that the deviations in enthalpy are small when absolute differences are considered; however, these small differences may have a major impact if enthalpy differences are calculated between two states at comparable temperatures and different pressures

Real gas effects will rise considerably for moist air and combustion gases due to the presence of water and/or carbon dioxide, depending on the concentration of either (or both). With reference to Figure 2.3, deviations in enthalpy are observed. Though these absolute differences may be small, they may have a major impact when enthalpy differences are considered, between two states at comparable temperatures and different pressures.

More accurate calculations can be obtained if the assumption of constant values of C_p and γ are maintained but evaluated at mean component temperatures. For illustration, Equation 2.17 represents compressor isentropic efficiency:

$$\eta_{c,is} = \frac{W.C_{p,mean}.\left(T_{out}^{'} - T_{in}\right)}{W.C_{p,mean}\left(T_{out} - T_{in}\right)} = \frac{T_{out}^{'} - T_{in}}{T_{out} - T_{in}} \quad \textbf{(2.17)}$$

For a compression calculation, the aim would be to compute compressor exit temperature, T_{out}. Using isentropic compression relations (Walsh et al., 1998), Equation 2.17 can be re-written as:

$$\eta_{c,is} = \frac{PR^{\left(\frac{\gamma_{mean}-1}{\gamma_{mean}}\right)} - 1}{\frac{T_{out}}{T_{in}} - 1} \quad \textbf{(2.18)}$$

Therefore, T_{out} is obtained by substituting values of PR, T_{in}, $\eta_{c,is}$ and γ_{mean}. This method yields less inaccuracy (just a few degrees Kelvin in temperature calculations) as compared to constant cold end gas properties.

Fully rigorous calculations involve the use of the fundamental definitions of specific enthalpy and entropy; any inaccuracies obtained using this method are dependent on the technical model used for calculating caloric properties. (Walsh et al., 1998) state that typical uncertainty levels in calculations using the fully rigorous approach are on average approximately 0.25 %.

The fundamental definition of isentropic efficiency is as given in Equation 2.19 which is a modified version of Equation 2.17:

$$n_{is} = \frac{Ideal\ Power}{Actual\ Power} = \frac{W.\left(h_{out}^{'} - h_{in}\right)}{W\left(h_{out} - h_{in}\right)} \quad \textbf{(2.19)}$$

For an adiabatic isentropic process, there is no change in entropy, thus for an ideal isentropic compression,

$$\varphi_{out}^{'} - \varphi_{in} = R.\ln(PR) \quad \textbf{(2.20)}$$

Equations 2.19 and 2.20 form the foundation for fully rigorous calculations. The following calculation procedure then follows:

1. φ_{in} is obtained from the fluid model and is a function of T_{in} and fluid composition.
2. The gas constant, R, is obtained from the fluid model and is a function of fluid composition.
3. φ'_{out} is obtained from $\varphi'_{out} - \varphi_{in} = R.\ln(PR)$ by substituting in values of R, PR and φ_{in}
4. T'_{out} is then obtained from the fluid model using an inverse fluid function and is a function of φ'_{out} and fluid composition.
5. h_{in} is obtained from the fluid model
6. h'_{out} is obtained from the fluid model and is a function of T'_{out} and fluid composition.
7. h_{out} is then obtained from Equation 2.19 by substituting h_{in}, h'_{out} and n_{is}.
8. Finally, T_{out} is obtained from the fluid model using an inverse fluid function and is a function of h_{out} and fluid composition.

The procedure above is mandatory for rigorous calculations and involves iterations and interpolations.

(Konstantinos Kyprianidis et al., 2009) carried out a compression case to illustrate the differences between the calculation methods; their results are presented in Table 2.2.

Calculation Method	Error in Temperature [K]	Error in compression Power [%]
Constant Cold End C_p and γ	-15.8	-0.61
C_p and γ at mean component temperature	3.7	0.59
Fully Rigorous approach	Acted as reference	Acted as reference

Conditions:

T_{in} = 351.2 K, P_{in}=110.135 [kPa], PR = 10.65, $\eta_{c,is}$ = 0.863

Assumptions:

- $FAR_{in} = FAR_{out}$ *and* $WAR_{in} = WAR_{out}$
- No compressor bleeds.

Table 2.2: Comparison of various calculation methods for a compression case [Konstantinos Kyprianidis et al., 2009]

2.2.1 Chemical Equilibrium and No dissociation models

Dissociation can be defined as, 'A general process in which ionic compounds separate or split into smaller particles usually in a reversible manner.' In other words, the products of combustion of a fuel (hydrocarbon) are Carbon dioxide and water, assuming complete combustion. At relatively high temperatures the otherwise stable products of combustion acquire sufficient energy to break down into intermediate atomic species such as , CO, H, OH and O. In

addition, the Nitrogen content in air breaks down (after acquiring sufficient energy) into N atoms and combines with the O atoms to produce NO.
The corresponding equations are presented in Equations 2.21 to 2.25.

$$CO_2 \Leftrightarrow CO + \frac{1}{2}O_2 \quad \textbf{(2.21)}$$

$$H_2O \Leftrightarrow H_2 + \frac{1}{2}O_2 \quad \textbf{(2.22)}$$

$$H_2O \Leftrightarrow OH + \frac{1}{2}H_2 \quad \textbf{(2.23)}$$

$$\frac{1}{2}O_2 \Leftrightarrow O \quad \textbf{(2.24)}$$

$$\frac{1}{2}N_2 + \frac{1}{2}O_2 \Leftrightarrow NO \quad \textbf{(2.25)}$$

The level of dissociation is highly influenced by both pressure and temperature. LeChateliers' principle states:

If the external constraints under which an equilibrium is established are changed, the equilibrium will shift in such a way as to moderate the effect on the change.

In each of the equations highlighted above and based on LeChateliers' principle, the following can be deduced:

- The forward reactions are endothermic; that is, they absorb energy for bond breaking. Therefore an increase in temperature of the products of combustion would favour the forward reaction and thereby yielding higher levels of dissociated species; therefore higher temperatures imply higher levels of dissociation.

- The sum of moles in each species on the left is less than the sum of moles on the species on the right side of each respective

equation. Pressure is proportional to the number of moles and as such, the pressure on the left side of each respective equation is also less than the pressure on the right side. Therefore, an increase in pressure would favour the reverse reaction thereby yielding higher levels of non-dissociated species. Therefore the lower the pressure, the higher the level of dissociation.

Dissociation fluid models thus take into account products of combustion that are a result of dissociation.

On the other hand, no-dissociation-fluid models assume constant gaseous composition of the products of combustion of a fuel or air. In the case of combustion of a fuel (mixed with air), the products of combustion would thus be Carbon dioxide and water (assuming complete combustion); in the case of a fuel-lean mixture, Argon, Nitrogen and Oxygen are formed as well. Since dissociation is not accounted for then there is no change in the composition of the products even with changes in temperature and/or pressure; thus the mean molecular weight of the products of combustion remains constant regardless of the temperature or pressure.

(Bücker et al., 2003) developed a model for the prediction of caloric properties of moist air and combustion gases. The model predicts ideal gas caloric properties of un-dissociated gas mixtures at temperatures from 200 K to 3300 K. In addition, the authors developed a simple model to account for dissociation at temperatures up to 2000 K. The authors noted that although dissociation reactions considerably affect combustion gas properties at temperatures relevant to gas turbine processes, only two of the common models address this issue, (Gordon and McBride, 1994) and (Brandt, 1999). (Konstantinos Kyprianidis et al., 2009) noted that if dissociation effects are ignored, then errors can be induced in the values of C_p and γ as much as 30% and 5 % respectively.

2.2.2 Polynomial functions and property tables

Conventionally, there are two approaches for fluid model implementation in gas turbine simulations; empirical relations based on polynomial functions and dedicated caloric property tables.

In the polynomial function method, the composition of combustion products is determined depending on the fuel and fuel-to-air ratio. This provides the mass fraction of each constituent gas in the combustion product. The properties of each constituent are then calculated at the prevalent temperature and combined to give the respective values for the mixture. (Walsh et al., 1998) stated, 'for performance calculations this method is now almost mandatory for computer library routines in large companies.' To that end, the authors express the specific heats of air and common gases in combustion products as eighth-order polynomials in temperature, Equation 2.26.

$$C_p = \sum_{i=0}^{n} A_i \left(\frac{T}{1000} \right)^i \qquad \textbf{(2.26)}$$

The authors have provided values of the coefficients, A_i, for various gases. These polynomials can be used in the range 200-2000 K.

(Van Wylen et al., 1994) provide accurate relations for a number of gases, including O_2, CO_2, N_2, and H_2O. Their relations employ fewer terms than those in Equation 2.26.

(Guha, 2001) presented generic equations that are applicable for any fuel, fuel-air ratio and temperature. The devised equations are useful for both hand calculations as well as repetitive computer iterations for thermodynamic cycle analysis.

In the property-tables method, respective caloric values are calculated *a priori* and presented as tabulated data sets. Chemical equilibrium software such as NASAs CEA, (Gordon and McBride, 1994) may be used to generate these data

tables. Required caloric properties are then obtained from these tables my means of interpolation routines. The accuracy of this method depends on the size of the data table; in addition, respective fuels will require unique data tables. Although generating such tables is far more laborious and time consuming than directly implementing polynomial functions, fluid tabulations offer several key advantages which include:(Sethi et al., 2008)

1. Substitution of fluid models is numerically safer if only tabulations are changed.
2. The introduction of alternative function calls for different fluid models may lead to convergence problems due to the internal iterations of the functions.
3. The calculation speed is noticeably faster without these iterations.
4. The constraints of polynomials, with respect to range limits and precision, can be overcome by using high resolution tabulations over a wide range.
5. The required storage space for such dense tables is not a problem for modern computing systems.
6. The use of proprietary fluid models is safer with tabulations because even if keyed tabulations are decoded they reveal nothing more than numbers and not the model itself. This is especially important if developed models are used collaboratively by competitors.
7. In cases where the effects of water to air ratio, unburned fuel to air ratio, dissociation and any other factors need to be considered, it may not be easy to find polynomial relationships which account for these effects in the open literature. Thus, tabulated fluid model tables provide the ability to express any fluid property as a function of as many parameters as required. For modern computing systems, storage and handling of densely populated multi-dimensional tables is not a problem.

2.2.3 Effects of fuel chemistry on Caloric properties

For gas turbine performance calculations, it is important to consider the effects of fuel chemistry in the evaluation of caloric properties for combustion products. The isobaric heat capacity will normally increase with H/C ratio. As expected, the effect of H/C ratio is more important as the mixture gets richer. Moreover, when moving from a weak mixture to a stoichiometric one C_p will become more sensitive not only to H/C ratio but also to temperature. (Konstantinos Kyprianidis et al., 2009)

Since the isobaric heat capacity for combustion products is dependent on the H/C ratio of the fuel used, it is thus expected that for fuels with similar H/C ratio, minor deviations would be expected. The Walsh and Fletcher polynomials (Walsh et al., 1998) are presented as being suitable for combustion products for both Kerosene and Diesel. Some fuels, e.g. Hydrogen fuel, are not catered for.

.

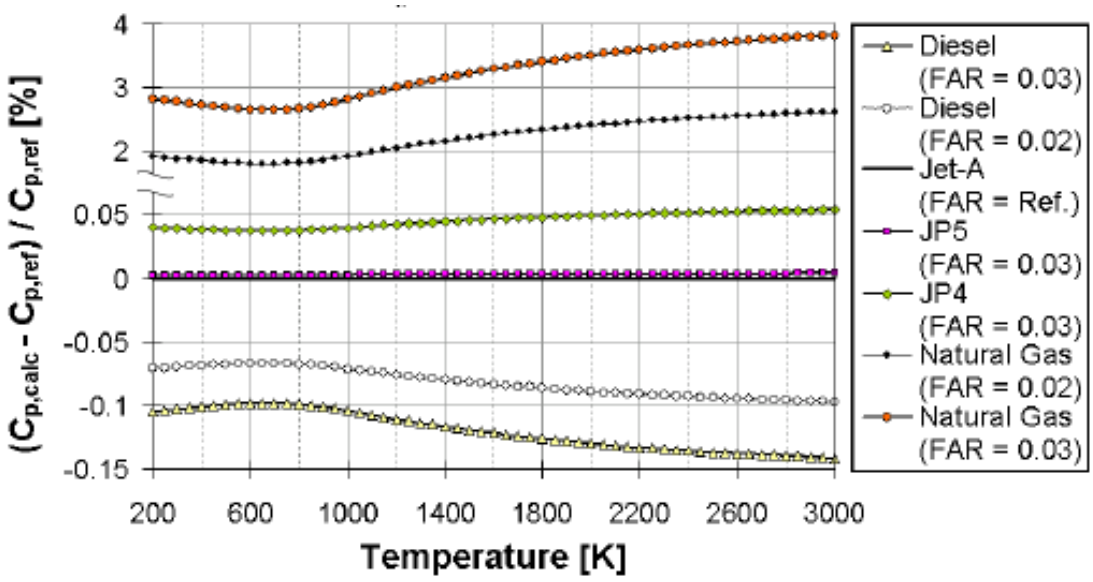

Figure 2.4: deviations of isobaric heat capacities

for various fuels [Konstantinos Kyprianidis et al., 2009]

With reference to Figure 2.4; Jet A was used as the reference for comparison purposes. It is observed that the deviations of isobaric heat capacity for Diesel, JP5 and JP4 fuel, for different FAR's are relatively small and perhaps acceptable. However, as far as Natural gas is concerned, the deviations are unacceptably high compared to Jet A. Therefore, for fuels with significantly different H/C ratios, appropriate tables or polynomials should be used in an attempt to reduce errors related to differences in fuel chemistry.

2.2.4 Uncertainty analysis of common technical models

Various technical models have been developed and accepted as technical standards in industry. The models reviewed in this section comprise of the common ones currently used in industry.

The ANSI/ASME performance test codes (ANSI/ASME, 1981) are widely used in gas turbine design. Equations consisting of up to five terms are presented for the enthalpy of typical combustion gas components. The range of validity of these equations is 300 K to 1350 K. (Bücker et al., 2003) stated that these equations have poor consistency with other technical models, including one developed by the authors. Maximum deviations of more than $\pm 0.5\%$ for isobaric heat capacity have been observed, Figure 2.5.

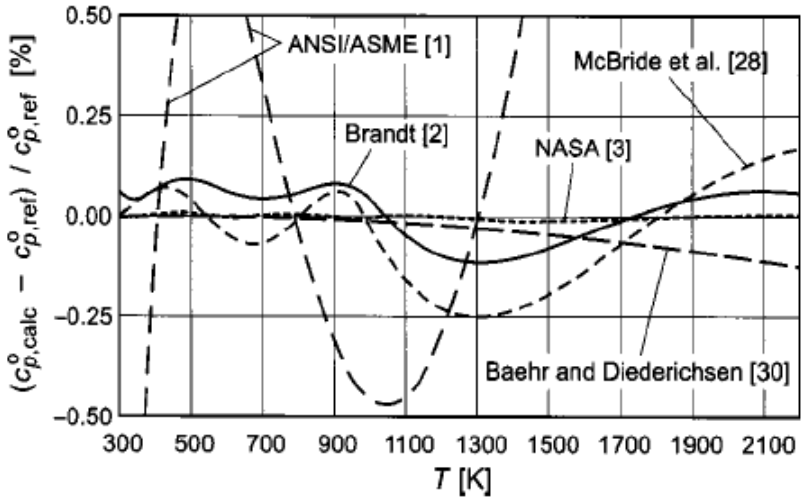

Figure 2.5: Percentage deviations of values for the ideal gas isobaric heat capacity of a typical combustion gas calculated by commonly used technical models versus values calculated using (Bücker et al., 2003) **method. [Bücker et al., 2003**]

The SAE Aerospace Standard AS681 (Society of Automotive Engineers, 1999) contains thermodynamic properties of moist air and combustion gases applicable in gas turbine calculations.

The Association of Steam Boiler, Pressure Vessel and Piping manufacturers (Brandt, 1999) model is used for calculation of combustion processes. This model is based on a 1963 version of NASA polynomials for the calculation of caloric properties. Another set of equations which is widely used in industry were published by (Baehr and Diederichsen, 1988). These equations consist of twelve terms. In the high temperature range above 1500K, these equations deviate systematically from data published by other authors.

The NASA Glenn equilibrium computer program, Chemical Equilibrium with Applications (CEA), is the latest in a series of thermodynamics tools generated at NASA Glenn Research Center to apply equilibrium thermodynamics to practical problems (Gordon, 1994). CEA uses a 9-constant representation of

thermodynamic data; this 9-constant form has been used since 1994. NASA Glenn Research Center maintains a database with 9-constant empirical coefficients for over 2000 species and for a temperature range of 200 [K] to 20,000 [K]. These coefficients were generated by least-squares fits to measured or calculated thermodynamic functions for condensed and gas-phase species (McBride, B.J. 1993). The database is continually updated to reflect new species, improved measurements for current species, and newer physical constants.

(Bücker et al., 2003) performed some comparative analysis for un-dissociated combustion gases and compared caloric properties with their method and CEA; they concluded that deviations of isobaric heat capacity were at most $\pm 0.05\%$. They further stated, 'Among the technical models, CEA is the only one that describes the caloric properties of combustion gases with satisfactory accuracy over the entire temperature range.'

2.2.5 Summary of advanced thermo-fluid modelling and conclusions

Based on the critical review of the available literature, the following are the conclusions and recommendations:

1. Although most models in industry are acceptable standards, their mutual consistency is rather poor. This leads to contradictory results and to conflicts especially in acceptance tests on the relevant machinery.
2. Perfect gas assumptions are not recommended for industry standard calculations; they are however acceptable for classroom instruction.
3. Dissociation reactions and subsequent caloric properties, particularly for temperatures beyond 1200 K should not be ignored. Despite this fact, only two of the common models, (Brandt, 1999) and (Gordon and McBride, 1994; MCBRIDE et al., 1993) address this issue.

4. Among the existing technical models, CEA is the only one that describes the caloric properties of combustion gases with satisfactory accuracy over the temperature range of 200K to 3000 K.
5. Changes in a fuels' H/C ratio will significantly affect the caloric properties; in particular, natural gases which may vary significantly depending on country of origin, require dedicated tables, for accurate caloric properties calculations.

3 NON-LINEAR WEIGHTED LEAST SQUARES DIAGNOSTICS METHODOLOGY

This section provides detailed description of the non-weighted least squares gas turbine diagnostics methodology that was developed and used for this research project. The description of the methods now follows.

3.1 Non-Linear Weighted Least Squares

Gas turbine component health parameters are not directly measurable; they are however thermodynamically correlated with measurable parameters. Consequently, gas-path faults have observable effects on measurable parameters. Therefore, with the availability of an essential measurement set and a model function that relates the measurement set to the health parameters, it is possible to identify faulty components.

Hence, consider the performance of a gas turbine engine represented by a model function, Equation 3.1.

$$\vec{z} = h(\vec{x}) \tag{3.1}$$

Where

- $\vec{z} \in \mathrm{R}^{\mathrm{M}}$ is the vector of measurements and *M* is the number of measurements
- $\vec{x} \in \mathrm{R}^{\mathrm{N}}$ is the vector of component health parameters and *N* is the number of engine health parameters.
- *h* is a vector-valued non-linear function that represents the performance behaviour of gas turbine engines.

The requirement then is to find the vector $\vec{x}$ of component performance parameters such that the model function fits best the given measurement data in the least squares sense. That is, the sum of squares represented by Equation 3.2 is minimised.

$$S = \sum_{i=1}^{m} r_i^2 \qquad \textbf{(3.2)}$$

The residual errors, r_i are given by Equation 3.3.

$$r_{i=1,\,m} = z_i - h(\vec{x}) \qquad \textbf{(3.3)}$$

The minimum value of *S* occurs when the gradient is Zero, that is, Equation 3.4.

$$\frac{\partial S}{\partial x_{j=1,\,n}} = 2\sum_{i=1}^{m} r_i \frac{\partial r_i}{\partial x_j} = 0 \qquad \textbf{(3.4)}$$

In a non-linear system, the derivatives $\frac{\partial r_i}{\partial x_j}$ are functions of both the independent variable (component health parameters) and the measurement parameters. Therefore these gradient equations do not have a closed solution. Instead, initial values must be chosen and thereafter refined iteratively; that is, the values are obtained by successive approximation, Equation 3.5.

$$x_{j=1,n} \approx x_j^{k+1} = x_j^k + \Delta x_j \qquad \textbf{(3.5)}$$

Where,

- *k* is an iteration number

- Δx_j, known as the *shift vector* is the vector of increments between iterations

At each iteration, the model is linearized by approximation to a first-order Taylor series expansion about a specified condition denoted by subscript '0' (baseline condition) and is represented by Equation 3.6.

$$\vec{z} = h(\vec{x}_0) + \left.\frac{\partial h(\vec{x})}{\partial \vec{x}}\right|_0 (\vec{x} - \vec{x}_0) + HOT \tag{3.6}$$

The higher order terms (*HOT*) can be neglected based on the assumption that the engine performance variation is approximately linear due to relatively small deviations of engine health parameters $(\vec{x} - \vec{x}_0)$. Thus, the engine performance model can be represented in Equation 3.7.

$$\Delta\vec{z} = H \cdot \Delta\vec{x} \tag{3.7}$$

The matrix H is known as the 'Influence co-efficient matrix' (ICM) and is defined in Equation 3.8.

$$H = \sum_{\substack{j=1 \\ i=1}}^{\substack{M \\ N}} \left[\frac{\partial \vec{z}_i / \vec{z}_i}{\partial \vec{x}_j / \vec{x}_j} \right]^0 \tag{3.8}$$

The inverse of this matrix is known as the 'Fault co-efficient matrix' (FCM). The ICM changes from one iteration to the next and can be represented by Equation 3.9.

$$\frac{\partial r_i}{\partial x_j} = -H_{ij} \tag{3.9}$$

The residuals represented in Equation 3.3 can then be updated as Equation 3.10

$$r_i = \Delta z_i - \sum_{j=1}^{n} H_{ij} \Delta x_j \tag{3.10}$$

Substituting Equations 3.9 and 3.10 into Equation 3.4 produces Equation 3.11

$$-2\sum_{i=1}^{m} H_{ij} \left(\Delta z_i - \sum_{s=1}^{n} H_{is} \Delta x_s \right) = 0 \tag{3.11}$$

Upon re-arrangement these become the *normal equations,* Equation 3.12

$$\sum_{i=1}^{m} \sum_{s=1}^{n} H_{ij} H_{is} \Delta x_s = \sum_{i=1}^{m} H_{ij} \Delta z_i \tag{3.12}$$

In matrix notation, the normal equations can be re-written as Equation 3.13.

$$\left(H^T H \right) \Delta x = H^T \Delta z \tag{3.13}$$

Measurements are affected by noise; that is, in repeated measurements, there will be no exact agreement, that is, measurement uncertainty. This measurement uncertainty can be measured by variance, Equation 3.14.

$$\sigma^2 = \frac{\sum \left(x_i - \bar{x} \right)^2}{N - 1} \tag{3.14}$$

Where,

- σ^2 is the variance
- x_i is an observation (measurement parameter)
- $\bar{X}$ is the mean of a set of observations
- N is the number of observations

In gas turbine diagnostics, measurement uncertainty is taken into account by weighting individual measurements using their respective sample variances, Equation 3.15.

$$W_{ii} = \frac{1}{\sigma_i^2} \tag{3.15}$$

Therefore, Equation 3.2 with weighting consideration now becomes Equation 3.16

$$S = \sum_{i=1}^{m} W_{ii} r_i^2 \tag{3.16}$$

The gradient equations for this sum of squares then become,

$$\frac{\partial S}{\partial x_j} = -2\sum_i W_{ii} \frac{\partial r_i}{\partial x_j} = 0 \tag{3.17}$$

And, the modified *normal equations* become,

$$\sum_{i=1}^{m}\sum_{s=1}^{n} H_{ij} W_{ii} H_{is} \Delta x_s = \sum_{i=1}^{m} H_{ij} \Delta z_i \tag{3.18}$$

In matrix form, Equation 3.18 may be written as,

$$\left(H^T W H\right)\Delta x = H^T W \Delta z \qquad \textbf{(3.19)}$$

Therefore,

$$\Delta x = \left(H^T W H\right)^{-1} H^T W \Delta z \qquad \textbf{(3.20)}$$

Equation 3.20 forms the basis for the Newton-Raphson iterative algorithm (Stroud, 2001) for a non-linear least squares problem.

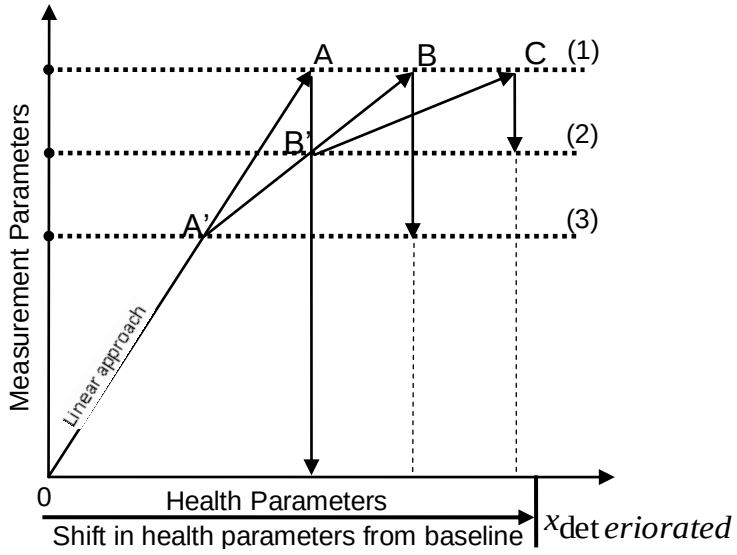

Figure 3.1: Illustration of the non-linear weighted least squares diagnostics method

With reference to Figure 3.1,

1. The point $x_{\det eriorated}$ represents a shift in one or more of the health parameters, efficiency and/or flow capacity from the baseline performance (point '0' in Figure 3.1). This shift in health parameters is accompanied by a shift in some or all of the measurement parameters, line 1 in Figure 3.1.

2. The change in measurement parameters from the baseline state to the deteriorated state forms the column matrix of measurement deviations, Δz. In addition, an FCM is obtained from the baseline state data. Linear weighted least-squares method, Equation 3.20, is employed to obtain an initial solution, point A.
3. To protect from divergence, the method of *shift-cutting* is employed. This involves reducing the vector Δx by a fraction; in this case, a value of 0.5 was used. This reduces the initial solution, *A*, to *A'*. At this new baseline (line 3 in Figure 3.1) a new value of measurement deviations Δz is calculated as the difference between the deteriorated state and the new baseline. In addition, a new ICM, hence FCM is calculated. This new FCM and Δz are then used to obtain a new solution (new set of component performance parameters), point B in Figure 3.1.
4. Once again, shift cutting is performed to protect from divergence and the process is repeated continuously until convergence, point C. With every iteration, the change in the health parameters becomes smaller and smaller and the process is stopped when the convergence criteria is met. A useful convergence criterion is Equation 3.21.

$$\forall_x \left| \frac{x^{k+1} - x^k}{x^k} \right| < 0.001 \qquad \textbf{(3.21)}$$

That is, when the change in health parameters between iterations is less than 0.1%, then the solution is sufficiently precise and the iterations are thus deemed converged.

In computing the above non-linear diagnostics, the following assumptions have been made:

1. That the number of measurements, M, is greater than or equal to the number of performance parameters, N. This assumption is necessary,

as otherwise the matrix $\left(H^T WH\right)$ is not invertible and the normal equations cannot be solved.

2. The $\left(H^T WH\right)$ matrix is non-singular, that is, invertible. (In this second assumption, the non-singularity would be caused by factors other than those stated in assumption 1).

The above two assumptions are made based on the premise of proper measurement selection. In the event of improper measurement selection, the assumptions fail. What follows is a detailed description of the measurement selection process used to ensure the non-singularity of the $\left(H^T WH\right)$ matrix.

3.1.1 Measurement Selection for diagnostics

Improper measurement selection may lead to matrix singularity and hence failure of the diagnostic algorithm. In addition, redundant measurements may be costly. Therefore, proper measurement selection is critical to obtaining correct diagnostic results in a cost-effective manner. In selecting an optimal set of measurements, the following factors were considered:

1. The number of gas path measurements chosen was either equal to or greater than the number of component performance parameters. In the case of the latter, this renders Equation 3.7 *over-determined* and thus, there are redundant equations. A pseudo-inverse defined as Equation 3.20 gives a solution that is best in a least-squares sense. In the case of the former (M=N), a unique solution is obtained.

2. The measurements chosen had a functional relationship to the component performance parameters being sought. This was achieved by means of a sensitivity analysis that involved implanting 1 % drops in efficiency and flow capacity for the respective component, and thereafter analysing corresponding measurement deviations.

3. The chosen measurements had to be independent of each other. The mathematical significance of this is illustrated below.

Consider a general linear system, Equation 3.22,

$$A\vec{x} = \vec{b} \tag{3.22}$$

Where,

- $A = \begin{bmatrix} a & b \\ c & d \end{bmatrix}$ **(3.23)**
- *x* and *b* are column matrices

The inverse of Matrix A in Equation 3.23 can be obtained using the direct inverse technique when M=N. This method involves decomposing matrix A into two elements, the Determinant, Det(A) and the Adjugate, Adj(A), Equation 3.24.

$$A^{-1} = \frac{1}{Det(A)}.Adj(A) \tag{3.24}$$

The determinant Det(A) is calculated as shown in Equation 3.25.

$$|A| = Det(A) = ad - bc \tag{3.25}$$

From Equation 3.24, it may be deduced that the determinant of matrix A, Det(A) should not be zero otherwise the matrix will be singular/non-invertible. In addition, as the determinant approaches Zero the integrity of the matrix deteriorates; the matrix approaches singularity and there may be numerical difficulties in calculating the inverse.

From Equation 3.25, if the determinant of matrix A is Zero, then it implies,

$$ad = bc \text{ or } \frac{a}{b} = \frac{c}{d} \quad \textbf{(3.26)}$$

If we re-write Equation 3.22 as,

$$\begin{bmatrix} a & b \\ c & d \end{bmatrix} \begin{bmatrix} x \\ y \end{bmatrix} = \begin{bmatrix} e \\ f \end{bmatrix} \quad \textbf{(3.27)}$$

Then,

$$\begin{aligned} ax + by &= e \\ cx + dy &= f \end{aligned} \quad \textbf{(3.28)}$$

Therefore,

$$y = \frac{e}{b} - \frac{ax}{b} \quad \textbf{(3.29)}$$

$$y = \frac{f}{d} - \frac{c}{d}x \quad \textbf{(3.30)}$$

From Equations 3.29 and 3.30 the following can be deduced:

- If $\frac{a}{b} = \frac{c}{d}$ and $\frac{e}{b} \neq \frac{f}{d}$ then both equations have similar gradients and different y-intercepts, thus, parallel lines. In diagnostics, this implies that there is no solution (since a solution would be the intersection of the two lines).
- If $\frac{a}{b} = \frac{c}{d}$ and $\frac{e}{b} = \frac{f}{d}$ then both equations have similar gradients and y-intercepts. In diagnostics, this implies that there are infinitely many solutions which all lie on these lines, thus, no unique solution.

The solution then is to choose measurements that give an ICM matrix that is full-column rank; that is, as many independent columns as there are component performance parameters being sought. This will ensure that no column is a linear combination of any other; as such, whatever solution will be produced will be a unique solution.

It needs to be mentioned that the above analysis may be applied for non-square matrices. In this case, the pseudo-inverse $H^{\#}$ is decomposed as,

$$H^{\#} = \left[\frac{1}{Det\left(H^T W H\right)} . Adj\left(H^T W H\right) \right] . H^T \qquad \textbf{(3.31)}$$

As mentioned earlier, matrix integrity is compromised as values of determinants approach Zero. This integrity can be assessed using the *matrix condition number* (Kamboukos et al., 2001). This *condition number* measures stability or sensitivity of a matrix to numerical operations, and more so after changes to the data (right hand-side of Equation 3.22) or changes to the co-efficient matrix A of Equation 3.22 (In the case of diagnostics, changes to the ICM). The *condition number* gives a bound on how inaccurate the solution will be after approximate solution. Therefore, a system of equations is considered to be *well-conditioned* if a small change in the coefficient matrix or a small change in the data results in a small change in the solution vector, and *ill-conditioned* if a small change in the coefficient matrix or a small change in the data results in a large change in the solution vector.

Matrix condition number for any $m \times n$ A matrix is calculated using the matrix *row sum norm* defined in Equation 3.32.

$$\|A\|_{\infty} = \max_{1 \le i \le m} \sum_{j=1}^{n} |a_{ij}| \qquad \textbf{(3.32)}$$

That is, once the sum of the absolute values of the elements of each row of the matrix is calculated, then the maximum of these values is the *row sum norm*. Then, the *condition number* κ may be defined as,

$$\kappa = \|(A)\|_\infty \left\|(A)^{-1}\right\|_\infty \quad \textbf{(3.33)}$$

If matrix A is well-*conditioned* then $\kappa(A)$ is small (close to 1).

If matrix A is *ill-conditioned* then $\kappa(A)$ is large:

(Kamboukos, et al., 2001) Utilised this method of *matrix condition number* as a criteria for optimal measurement selection.

3.1.2 Measurement Uncertainty

Measurements are affected by noise; the order of magnitude of the noise may often be comparable to the variations in the measurements caused by an actual component fault. Neglecting this effect may completely impair diagnostics, hence the need to account for measurement noise.

Bias is a constant or systematic error; in repeated measurements, each measurement has the same bias. To determine the magnitude of bias in a given measurement, one must define the true value of the quantity being measured; this true value is usually unknown and unknowable. Therefore bias is not easily determined; there is no statistic to estimate bias from data. *Random/Precision* error on the other hand is seen in repeated measurements. The measurements do not agree exactly; they exhibit a degree of scatter about a certain value, normally the mean. Variance (Equation 3.14) is used as a measure of precision error; a smaller value of variance indicates relatively less measurement scatter and vice versa. This scatter may however be more adequately expressed in terms of a probability density function (PDF) and is described below.

Gas turbine measurement and component health parameters are continuous variables. Since continuous probability functions are defined for an infinite number of points over a continuous interval, the probability at a single point is always zero. Instead, probabilities (for continuous variables) are defined over intervals.

We may then define the *probability density function* as,

$$\mathrm{Prob}\left[x \le x' \le x + dx\right] = f(x)dx \qquad \textbf{(3.34)}$$

That is, 'The probability that the actual value yielded, x' will be contained in the small interval extending from x to $x + dx$ is equal to $f(x)dx$

Where,

- x' is the actual outcome.
- x is one of the infinitely many values that could be the outcome.
- dx is a small interval of values.
- $f(x)$ is the probability density function.

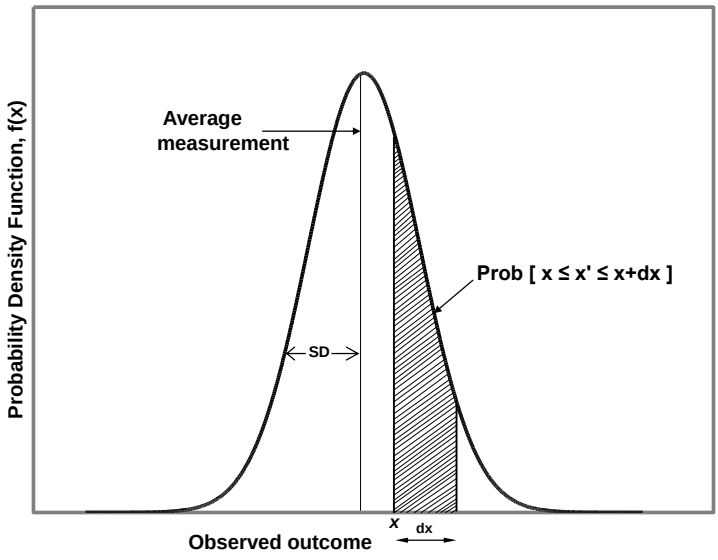

Figure 3.2: Probability distribution of a continuous variable

From Figure 3.2 it can be deduced that quantities with greater uncertainty and hence more scatter, will produce PDF plots with longer tails and broader peaks. This increased degree of uncertainty is measured by the variance (which is the square of the standard deviation, SD). From Equation 3.34 and Figure 3.2 it follows that the probability corresponding to a particular interval starting at x and of length dx is measured by the area of the rectangle of height $f(x)$ and base dx; this is the shaded region in Figure 3.2.

Various methods were employed in this work to account for measurement uncertainty. What follows is a description of these methods

3.1.2.1 Exponential Moving Average method

To reduce the impact of measurement noise for diagnostic analysis, an exponential moving average method may be used; its mathematical expression is presented in Equation 3.35.

$$\bar{z}_i = \alpha.\bar{z}_{i-1} + (1-\alpha)z_i \qquad \textbf{(3.35)}$$

Where

- $\bar{z}_i$ is the exponential moving average of respective measurement values at time i
- α is the smoothing factor = $\dfrac{2}{1+N}$
- N is the number of days in the averaging interval
- z_i is a measurement sample at time i.

With this method, all previous data remains in the computation for every successive value, just to an exponentially decreasing amount (hence the name). This gives the method an advantage over other moving average

methods that forsake old values for new ones. In addition, this method responds more quickly to changing measurement trends compared to other moving average methods.

3.1.2.2 Reciprocal of variance

Given samples of respective measurements, weighting can be performed based on the variances of respective samples; the variance is as presented in Equation 3.14 and the formula of weighting in Equation 3.15. Equation 3.15 ensures that measurement samples with greater uncertainty and thus greater values of variance will have smaller weights, and therefore have less influence on the diagnostic calculation. On the other hand, measurement samples with less uncertainty and thus smaller values of variance will have larger weights and thus more influence the diagnostic calculation.

This method however suffers two setbacks:

1. The method requires availability of samples of measurements (for the calculation of variance). In the absence of such samples, the method fails.

2. In the event that measurement samples have either significantly large values or significantly small values of variance, the resulting weights will be significantly small or significantly large, respectively. Consequently, multiplying the ICM with the weight matrix may affect the integrity of the resulting matrix and therefore impede the diagnostic process. This effect on the integrity of the ICM is quantified by Equation 3.33.

To overcome these setbacks, two weighting schemes were developed and are described in the following sections.

3.1.2.3 Weighting Scheme 1 (WS1)

Measurement noise is often assumed to be normally distributed. The maximum measurement noise of a measurement sample is expected to be around two standard deviations from the mean, where standard deviation is the square root of variance, presented in Equation 3.14. It is thus expected that the mean value of a measurement sample will fall within the bounds of two standard deviations, Equation 3.36.

$$\mu \pm 2\sigma \tag{3.36}$$

Where,

- μ is the mean value of measurement sample**s**
- σ is the standard deviation of measurement samples

In formulation WS1, maximum noise values (2σ) are utilised to calculate respective measurement weights. Such values would be provided by sensor manufacturers. For this work, the maximum measurement noise for different gas path measurement parameters was based on the information provided by (Dyson and Doel, 1987) and is presented in Table 3.1

Measurement	Range	Typical Error
PT Speed, N2	10-50% RPM	$\pm$0.2%
	50-125% RPM	$\pm$0.1%
Pressure	3 – 45 psia	$\pm$0.5%
	8 – 460 psia	$\pm$0.5% or 0.125 psia whichever is greater
Temperature	-65 – 145 ^oC	$\pm$2.6% ^oC
	-65 – 290 ^oC	$\pm$3.3% ^oC
	290 – 1000 ^oC	$\pm \sqrt{2.5^2 + (0.0075 \times T)^2}$
	1000 – 1300 ^oC	$\pm \sqrt{3.5^2 + (0.0075 \times T)^2}$
Fuel flow	Up to 250 Kg/hr	41.5 Kg/hr
	Up to 450 Kg/hr	34.3 Kg/hr
	Up to 900 Kg/hr	29.4 Kg/hr
	Up to 1360 Kg/hr	23.7 Kg/hr
	Up to 1815 Kg/hr	20.8 Kg/hr
	Up to 2270 Kg/hr	23.0 Kg/hr
	Up to 2725 Kg/hr	25.9 Kg/hr
	Up to 3630 Kg/hr	36.2 Kg/hr
	Up to 5450 Kg/hr	63.4 Kg/hr
	Up to 12260 Kg/hr	142.7 Kg/hr

Table 3.1: Instrumentation non-repeatability (Dyson, 1987)

With reference to Table 3.1 the following procedure was followed:

1. The maximum-noise values for respective measurements were calculated based on the specifications given in the “typical error” column.

For example, for a (arbitrary) value of temperature of 800 K, the maximum-noise value is thus:

$$\sqrt{6.25+(0.0075\times 800)^2} = 6.5K\left(=2\sigma\right)$$

In the case of measurement samples, the value to be used is the sample average.

2. The maximum-noise values so obtained were then normalized by dividing them with their respective 'clean' measurement values. This 'clean' value is a simulated noise-free measurement. The obtained value, termed 'percentage-noise-value', ω represents the maximum-noise (2σ) expressed as a percentage of relative to the noise-free measurement. Small values indicate precise measurements and vice versa. This value is calculated as given in Equation 3.37.

$$\forall_Z, \omega = \frac{2\sigma}{z_{clean}} \times 100 \qquad \textbf{(3.37)}$$

The percentage- noise- values once obtained were then used to calculate the weights, Equation 3.38.

$$\forall_z, W_{ii} = \frac{\omega_{\min}}{\omega_i} \qquad i = 1 \text{ to } m \qquad \textbf{(3.38)}$$

In Equation 3.38, weighting was hinged on the least noisy measurement; this guaranteed that the least noisy measurement obtained the largest weight of 1, since its percentage-noise-value would divide itself. On the other hand, the noisiest measurement got the smallest weight.

3.1.2.4 Weighting Scheme 2 (WS2)

Given a measurement sample, *Range* is defined as the difference between the sample maximum and the sample minimum.

WS2 utilises the *Range* of respective measurement samples. The formulation is thus:

1. The percentage- noise- value ω was calculated as,

$$\forall_z \ \omega = \frac{z_{\max} - z_{\min}}{z_{clean}} \times 100 \quad \textbf{(3.39)}$$

   Where,

   - $z_{\max}$ is the sample maximum.
   - $z_{\min}$ is the sample minimum.
   - z_{clean} is the noise-free value for respective measurements.

2. Thereafter, the weights were calculated using Equation 3.38.

WS1 and WS2 were then used as the weighting schemes in the non-linear WLS diagnostic algorithm.

4 MULTI-FUEL PERFORMANCE SIMULATION METHODOLOGY

This section provides detailed description of the multi-fuel performance simulation methodology that was developed and used for this research project. The description of the methods now follows.

4.1 Fuel caloric properties and file organisation

Tabulated fuel caloric properties were provided for four fuels: United Kingdom natural gas, Jet-A (Kerosene), Diesel and Hydrogen fuel.

Table 4.1 presents the formulae of three of the considered fuels and Table 4.2 presents the formulae and components of the fourth fuel, UK natural gas.

Fuel	Formula
JetA	$C_{12}H_{23}$
Diesel	$C_{12.9}H_{23.22}$
Hydrogen	H_2

Table 4.1: formulae for 3 of the considered fuels

Component	Formula	Mole Fraction
Methane	CH_4	0.926
Ethane	C_2H_6	0.036
Propane	C_3H_8	0.009
n-butane	C_4H_{10}	0.004
n-pentane	C_5H_{12}	0.003
Nitrogen	N_2	0.022

Table 4.2: Composition of UK Natural Gas (Gesser, 2001)

Each tabulated fuel comprised of properties which are presented in Table 4.3.

Caloric Property	Symbol	Units
Density	ρ	Kg/m^3
Enthalpy	h	J/Kg
Entropy	s	J/Kg K
Isobaric Heat	C_p	J/Kg K
Gas Constant	R	J/Kg K
Gamma	γ	
Viscosity	μ	Kg/ms

Table 4.3: Tabulated Fuel Caloric properties

These fuel caloric properties were tabulated as functions of four variables, FAR, WAR, pressure and temperature. These four variables and their respective caloric properties were organised in such a way as to optimise file-size and accuracy without compromising either one. The criterion for selection of points for FAR, WAR, Pressure and Temperature along with the interpolation points for FAR, WAR, Pressure and temperature are presented in the following chapter under analysis. The description of these four variables now follows.

- Fuel-to-air ratio (FAR) is the mass ratio of Fuel to air present during combustion. If exactly enough air is provided to completely burn all of the fuel, the ratio is known as a *stoichiometric* mixture. For this work, FARs ranged from a minimal value of Zero (air) to a maximum value of $FAR_{stoichiometric} \times \phi$.

  Where ϕ is the *equivalence ratio* = $\dfrac{FAR}{FAR_{stoichiometric}}$

  This was done to accommodate *rich-burn, quick-mix, lean-burn* combustors (TACINA, 1990). An equivalence ratio of 1.8 was selected based on literature (Peterson et al., 2002). Table 4.4 presents the

stoichiometric FARs and the maximum FARs based on the equivalence ratio, for the four fuels considered.

	UK Natural Gas	Jet-A	Hydrogen	Diesel
$FAR_{stoichiometric}$	0.063	0.068	0.029	0.069
Max FAR	0.113	0.123	0.052	0.124

Table 4.4: Stoichiometric and maximum FARs for the 4 considered fuels

- Water to air ratio (WAR), also known as *mixing ratio* is the ratio of the mass of water vapour in grams to a Kilogram of dry air. For this work, WARs ranged from a minimum value of Zero (dry air) to a maximum value of 0.1. Only values of WAR $\leq$ 0.10 are considered; this is because for values of WAR > 0.10 the mixture cannot be treated as a perfect gas.
- Pressures were tabulated from a minimum value of 0.04 atmospheres to a maximum value of 200 atmospheres. The minimum value of 0.04 atmospheres was conceived with typical steam turbine exit pressures in mind, which are approximately 0.04 atmospheres. The maximum value of 200 atmospheres was based on future/conceptual designs of high pressure ratio gas turbines in mind.
- The initial temperature distribution was based on work by (Sethi V., 2008) who developed gas property tables using NASAs' Chemical equilibrium program (Gordon, 1994). This model employed linear interpolation between values for FAR, WAR, temperature and a fixed pressure of 50 bars. In this model, the temperature distribution was 200 [K] to 3000 [K] in steps of 50 [K]. This temperature distribution was sufficient since only one pressure was considered; that is, dissociation at low pressures was not an issue. However, in light of dissociation at high temperatures and low pressures and subsequent interpolation accuracy,

the temperature distribution was reviewed and the values are presented in the following chapter.

Table 4.5 is a schematic presentation of the structure of the fuel tables. As can be seen, temperature lines form one pressure table; pressure tables form one WAR and all WARs form one FAR. Finally, all FARs form one fuel table.

Temperatures	**Pressures**	**WARs**	**FARs**
w number of temperatures form 1 pressure	*x* number of pressures form 1 WAR	*y* number of WARS form 1 FAR	All FARS combined form 1 Fuel-table
Increasing file-size →			

Table 4.5: Layout of fuel tables

- Where w, x, y and z in Table 4.5 are integers

A section of a fuel-file is presented in Appendix 1. This presented table represents the caloric properties at a given FAR, WAR and pressure, for respective temperatures.

These tabulated caloric properties were then interpolated using the method described in the following section.

4.2 Natural Cubic Spline Multi dimensional Interpolation

The essential limitation of polynomial approximation is that if the function to be approximated is badly behaved anywhere in the interval of approximation, then

the approximation is poor everywhere (De Boor, 2001). This global dependence on local properties can be avoided by using piece-wise cubic polynomial approximants also known as *Cubic splines*. What follows is a description of cubic splines.

Given an interpolant value, *x*, the aim is to approximate a function represented by four points, $(x_n, y_n), (x_{n+1}, y_{n+1}), (x_{n+2}, y_{n+2}), (x_{n+3}, y_{n+3})$

(x_n, y_n), (x_{n+1}, y_{n+1}) represent the two points before the interpolant and (x_{n+2}, y_{n+2}), (x_{n+3}, y_{n+3}) represent the two points after the interpolant.

The task then is to determine the spacing between the points h_n the slopes m_n and then through the solution of a system of equations, the second derivatives of the splines, s_n

$$h_n = x_{n+1} - x_n \tag{4.1}$$

$$m_n = \frac{y_{n+1} - y_n}{x_{n+1} - x_n} \tag{4.2}$$

We may adopt a general cubic function for each spline as

$$y = a_n(x - x_n)^3 + b_n(x - x_n)^2 + c_n(x - x_n) + d_n \tag{4.3}$$

In Equation 4.3, the value of n is 2, that is, the point just before the interpolant value.

Then, the first and second differentials can be expressed as:

$$y' = 3a_n(x - x_n)^2 + 2b_n(x - x_n) + c_n \tag{4.4}$$

$$y'' = 6a_n(x - x_n) + 2b_n \tag{4.5}$$

The next step involves imposing requirements that are key characteristics of spline interpolation.

The first requirement is to enforce C^o continuity; that is, each curve segment passes through its control points. This can be represented as,

$$y_n = f(x_n), y_{n+1} = f(x_{n+1}) \quad \textbf{(4.6)}$$

With reference to Equation 4.3: at $x = x_n$ we obtain,

$$d_n = y_n \quad \textbf{(4.7)}$$

And, at $x = x_{n+1}$, we obtain,

$$y_{n+1} = (x_{n+1} - x_n)^3 a_n + b_n (x_{n+1} - x_n)^2 + c_n (x_{n+1} - x_n) + y_n \quad \textbf{(4.8)}$$

The next requirement is to enforce C^1 continuity; that is, the curve segments have the same slope where they join. Therefore, for two joined splines, we can equate their first derivatives (Equation 4.4) to obtain,

$$3a_n (x_{n+1} - x_n)^2 + 2b_n (x_{n+1} - x_n) + c_n = 3a_{n+1} (x_n - x_n)^2 + 2b_{n+1} (x_n - x_n) + c_{n+1} \quad \textbf{(4.9)}$$

Thus,

$$3a_n (x_{n+1} - x_n)^2 + 2b_n (x_{n+1} - x_n) + c_n = c_{n+1} \quad \textbf{(4.10)}$$

The next requirement is to enforce C^2 continuity; that is, the curve segments have the same curvature where they join together.

This implies that $y'' = y_n''$ at $x = x_n$ and $y'' = y_{n+1}''$ at $x = x_{n+1}$. With respect to Equation 4.5, at $x = x_n$

$$y_n'' = 6a_n(x_n - x_n) + 2b_n \tag{4.11}$$

Therefore,

$$b_n = \frac{y_n''}{2} \tag{4.12}$$

And at $x = x_{n+1}$

$$y_{n+1}'' = 6a_n(x_{n+1} - x_n) + 2b_n = 6a_n h_n + y_n'' \tag{4.13}$$

Therefore,

$$a_n = \frac{\left(y_{n+1}'' - y_n''\right)}{6h_n} \tag{4.14}$$

The co-efficients a_n (Equation 4.14), b_n (Equation 4.12), d_n (Equation 4.7) can be substituted into Equation 4.8 to get the co-efficient c_n (Equation 4.15)

$$c_n = \frac{(y_{n+1} - y_n)}{h_n} - \frac{y_{n+1}'' h_n}{6} - \frac{y_n'' h_n}{3} \tag{4.15}$$

And

$$c_{n+1} = \frac{(y_{n+2} - y_{n+1})}{h_{n+1}} - \frac{y_{n+2}'' h_{n+1}}{6} - \frac{y_{n+1}'' h_{n+1}}{3} \tag{4.16}$$

Having fulfilled the above requirements, then the co-efficients a_n, b_n, c_n can be substituted into Equation 4.10 to produce the following two general equations; these are the governing equations of spline interpolation (for convenience y_n'' is now replaced by s_n)

$$2(h_n + h_{n+1})s_{n+1} + h_{n+1}s_{n+2} + h_n s_n = 6(m_{n+1} - m_n) \quad \textbf{(4.17)}$$

$$2(h_{n+1} + h_{n+2})s_{n+2} + h_{n+1}s_{n+1} + h_{n+2}s_{n+3} = 6(m_{n+2} - m_{n+1}) \quad \textbf{(4.18)}$$

There will be [n-1] of these equations when the spline interpolates [n+1] points. Since there are [n+1] second derivatives (s_n's) there is the need to apply end conditions of the splines to determine s_1 and s_4 at the end points. The option used for this research project was the 'Natural Spline' option, where second derivatives at the ends are set to zero. Hence, for a 4 point cubic spline interpolation,

$$\begin{aligned} s_1 &= 0 \\ h_1 s_1 + 2(h_1 + h_2)s_2 + h_2 s_3 &= 6(m_2 - m_1) \\ h_2 s_2 + 2(h_2 + h_3)s_3 + h_3 s_4 &= 6(m_3 - m_2) \\ s_4 &= 0 \end{aligned}$$

In matrix format,

$$\begin{bmatrix} 1 & 0 & 0 & 0 \\ h_1 & 2(h_1 + h_2) & h_2 & 0 \\ 0 & h_2 & 2(h_2 + h_3) & h_3 \\ 0 & 0 & 0 & 1 \end{bmatrix} \begin{bmatrix} s_1 \\ s_2 \\ s_3 \\ s_4 \end{bmatrix} = \begin{bmatrix} 0 \\ 6(m_2 - m_1) \\ 6(m_3 - m_2) \\ 0 \end{bmatrix} \quad \textbf{(4.19)}$$

For simplicity, we may write Equation 4.19 as,

$$Hs = m \tag{4.20}$$

Where,

- H is the matrix of spacings, h
- s is the matrix of second derivatives
- m is the matrix of gradients (Right hand side of Equation 4.19)

Therefore

$$s = H^{-1}m \tag{4.21}$$

Having obtained the actual values of the second derivatives, the co-efficients, a_n, b_n, c_n can then be computed and substituted into Equation 4.3 along with the interpolant (x) to obtain an interpolation result.

The multi-dimensional interpolation may be illustrated as,

$$GP = f(FAR, WAR, P, T) \tag{4.22}$$

Where,

- GP (Gas property) is the respective caloric property presented in Table 4.3
- FAR is the Fuel-to-air ratio
- WAR is the Water-to-air ratio
- P is the Pressure in atmospheres
- T is the temperature in degrees Kelvin

We may therefore define an interpolation function $INT_x(u_1, u_2, u_3, u_4)$ as the value of the unique cubic polynomial with $f(1) = u_1 ..... f(4) = u_4$ evaluated at an interpolant value *x*.

Where,

- $INT_x(u_1, u_2, u_3, u_4)$ is essentially Equation 4.3
- x is the interpolant value; in this context, it could be FAR, WAR, pressure or temperature.
- u_1 to u_4 are the corresponding functional values (caloric properties) of the points x_1 to x_4 ; x_1 and x_2 are the two points before the interpolant value and x_3 and x_4 are the two points after the interpolant value.

By considering a 4 dimensional grid composed of four points per dimension, then we end up with 256 co-efficients (4^4). The function to be evaluated is fitted to the 256 points on the corners of this 4 dimensional grid (since the interpolant is considered to be in the middle of the grid).

The procedure then is to set,

$$A(T, P, WAR) = INT_{FAR}((T, P, WAR, 1), (T, P, WAR, 2), (T, P, WAR, 3), (T, P, WAR, 4)) \quad \textbf{(4.23)}$$

$$B(T, P) = INT_{WAR}(A(T, P, 1), A(T, P, 2), A(T, P, 3), A(T, P, 4)) \quad \textbf{(4.24)}$$

$$C(T) = INT_P(B(T, 1), B(T, 2), B(T, 3), B(T, 4)) \quad \textbf{(4.25)}$$

$$GP = INT_T(C(1), C(2), C(3), C(4)) \quad \textbf{(4.26)}$$

The function $A(T, P, WAR)$ is determined at the grid points. Thereafter, subsequent evaluations use (as functional values) interpolation results from previous dimensions as demonstrated in Equations 4.24 to 4.26.

This procedure requires 85 calls in total, to INT_x as opposed to the multiplication of a 256 by 256 matrix by a column vector with 256 functional values, which a direct solution would entail.

The next section presents the pseudo-code of the interpolation process.

4.3 Gas property interpolation Pseudo-code

If FAR $\neq 0$ and WAR $= 0$

FAR Dimension

Make 16 calls to A= INT_{far} (T, P, n), n=1 to 4, to obtain 64 functional values of respective caloric property from fuel table

Calculate co-efficients a_n, b_n, c_n, d_n

Substitute co-efficients and given interpolant value (FAR) into Equation 4.3 to obtain 16 values of respective caloric property

Pressure Dimension

Use 16 values obtained from previous dimension,
A= INT_{far} (T, P, n) as functional values in this dimension.

Make 4 calls to C=INT_P (A (T, n)) n = 1 to 4

Calculate co-efficients a_n, b_n, c_n, d_n

Substitute co-efficients and given interpolant value (P) into Equation 4.3 to obtain 4 values of respective caloric property

Temperature Dimension

Use 4 values obtained from previous dimension,
C=INT_P (A (T, n)) as functional values in this dimension.

Make 1 final call to GP=INT_TC(n), n = 1 to 4

Calculate co-efficients a_n, b_n, c_n, d_n

Substitute co-efficients and given interpolant value (T) into Equation 4.3 to obtain final single value of respective caloric property

Else If FAR $= 0$ and WAR $\neq 0$

WAR Dimension

Make 16 calls to B= INT_{war} (T, P, n), n=1 to 4, to obtain 64 functional values of respective caloric property from fuel table

Calculate co-efficients a_n, b_n, c_n, d_n

Substitute co-efficients and given interpolant value (WAR) into Equation 4.3 to obtain 16 values of respective caloric property

Pressure Dimension

Use 16 values obtained from previous dimension,
B= INT_{war} (T, P, n) as functional values in this dimension.

Make 4 calls to C=INT_P (A (T, n)) n = 1 to 4

Calculate co-efficients a_n, b_n, c_n, d_n

Substitute co-efficients and given interpolant value (P) into Equation 4.3 to obtain 4 values of respective caloric property

Temperature Dimension

Use 4 values obtained from previous dimension,
C=INT_P (A (T, n)) as functional values in this dimension.

Make 1 final call to GP=INT_TB(n), n = 1 to 4

Calculate co-efficients a_n, b_n, c_n, d_n

Substitute co-efficients and given interpolant value (T) into Equation 4.3 to obtain final single value of respective caloric property

Else if FAR and WAR $=$ 0

Pressure Dimension

Make 4 calls to C= INT_P (T, n), n=1 to 4, to obtain 16 functional values of respective caloric property from fuel table.

Calculate co-efficients a_n, b_n, c_n, d_n

Substitute co-efficients and given interpolant value (P) into Equation 4.3 to obtain 4 values of respective caloric property

Temperature Dimension

Use 4 values obtained from previous dimension,
$C=INT_P$ (T, n)) as functional values in this dimension.

Make 1 final call to $GP=INT_TC$ (n), n = 1 to 4

Calculate co-efficients a_n, b_n, c_n, d_n

Substitute co-efficients and given interpolant value (T) into Equation 4.3 to obtain final single value of respective caloric property

Else if FAR and WAR $\neq 0$

FAR Dimension

Make 64 calls to $A=INT_{far}$ (T, P, WAR, n), n=1 to 4, to obtain 256 functional values of respective caloric property from fuel table

Calculate co-efficients a_n, b_n, c_n, d_n

Substitute co-efficients and given interpolant value (FAR) into Equation 4.3 to obtain 64 values of respective caloric property

WAR Dimension

Use 64 values obtained from previous dimension,
$A= INT_{far}$ (T, P, WAR, n) as functional values in this dimension.

Make 16 calls to $B=INT_{war}$ (A (T, P, n)) n = 1 to 4

Calculate co-efficients a_n, b_n, c_n, d_n

Substitute co-efficients and given interpolant value (WAR) into Equation 4.3 to obtain 16 values of respective caloric property

Pressure Dimension

Use 16 values obtained from previous dimension,
$B= INT_{war}$ (A (T, P, n)) as functional values in this dimension.

Make 4 calls to $C=INT_P (A (T, n))$ n = 1 to 4

Calculate co-efficients a_n, b_n, c_n, d_n

Substitute co-efficients and given interpolant value (P) into Equation 4.3 to obtain 4 values of respective caloric property

Temperature Dimension

Use 4 values obtained from previous dimension, $C=INT_P (A (T, n))$ as functional values in this dimension.

Make 1 final call to $GP=INT_T C(n)$, n = 1 to 4

Calculate co-efficients a_n, b_n, c_n, d_n

Substitute co-efficients and given interpolant value (T) into Equation 4.3 to obtain final single value of respective caloric property

End

5 NON-LINEAR WEIGHTED LEAST SQUARES RESULTS AND ANALYSIS

The methods that pertain to non-linear WLS diagnostics that were described in previous sections were applied and demonstrated by means of case studies. These case studies were run to demonstrate the effectiveness of the non-linear WLS method in conjunction with WS1 and WS2. Some of the test cases compare the non-linear WLS results with those of non-linear GPA (Escher, 1995). What follows is a presentation of the results obtained.

5.1 Non-linear Weighted Least Squares diagnostics

The non-linear Weighted-Least-Squares diagnostics method was applied to the diagnostic analysis of various component degradations of a model turbo-shaft gas turbine engine that consists of one compressor, one burner, one compressor turbine and one power turbine, Figure 5.1 (Hereafter referred to as 'the engine model')

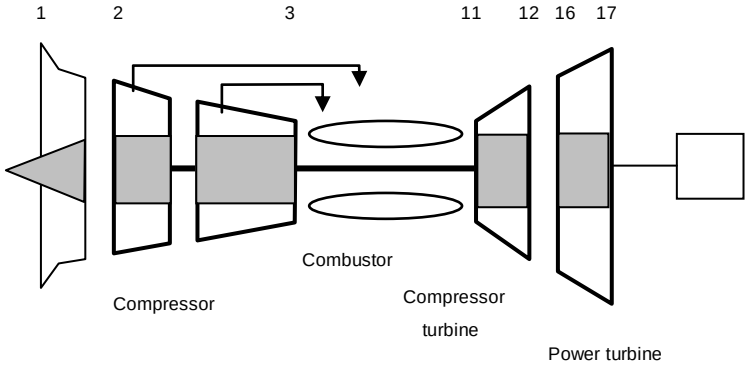

Figure 5.1: Model turbo-shaft gas turbine

Four test cases are described in Table 5.1 where different component degradations were implanted into the model engine.

CASE	DESCRIPTION
1	Comparison of Linear and non-linear WLS using WS1 and WS2 weighting methods
2	Effect of significantly large or significantly small weights on matrix integrity
3	Compressor turbine diagnostics using multiple measurement samples, WS1, WS2 and reciprocal of variance weighting methods
4	Use of a single measurement sample and WS1 weighting method

Table 5.1: Description of test cases

5.1.1 Case Study 1: Comparing Linear WLS with Non-linear WLS

Non-linear diagnostic methods are developed on the premise that engine non-linearity needs to be accounted for. To compare Linear with non-linear WLS, compressor and compressor turbine degradations were implanted into the model engine. Compressor degradation was implanted as follows:

Deviation of Flow capacity index, $\Delta\Gamma$: -3 %;

Deviation of Efficiency index, $\Delta\eta$: -1%

1000 samples of the measurements presented in Table 5.2 were simulated at a noise level of $2\times 2\sigma$

MEASUREMENT PARAMETERS	SYMBOL	UNITS
Compressor outlet temperature	T3	Kelvin
Compressor outlet pressure	P3	Atmospheres
Fuel flow	w_f	Kg/s
Compressor non-dimensional rotational speed	PCN	Non-dimensional
Power turbine exit temperature	T17	Kelvin
Power turbine outlet pressure	P17	Atmospheres

Table 5.2: Compressor diagnostic measurement parameter set

The respective weights for the chosen measurement set are presented in Table 5.3

	WEIGHTING SCHEME AND WEIGHTS	
MEASUREMENT PARAMETER	**WS1**	**WS2**
T3	0.118	0.152
P3	0.2	0.2002
w_f	0.869	0.925
PCN	1.0	1.0
T17	0.122	0.196
P17	0.2	0.212

Table 5.3: Compressor diagnostics measurement set weights

Linear and non-linear weighted least squares were run for these 1000 measurement samples using the presented measurement weights. The averages of the results produced from these samples are presented in Figure 5.2 and Figure 5.3 for both flow capacity and efficiency indices.

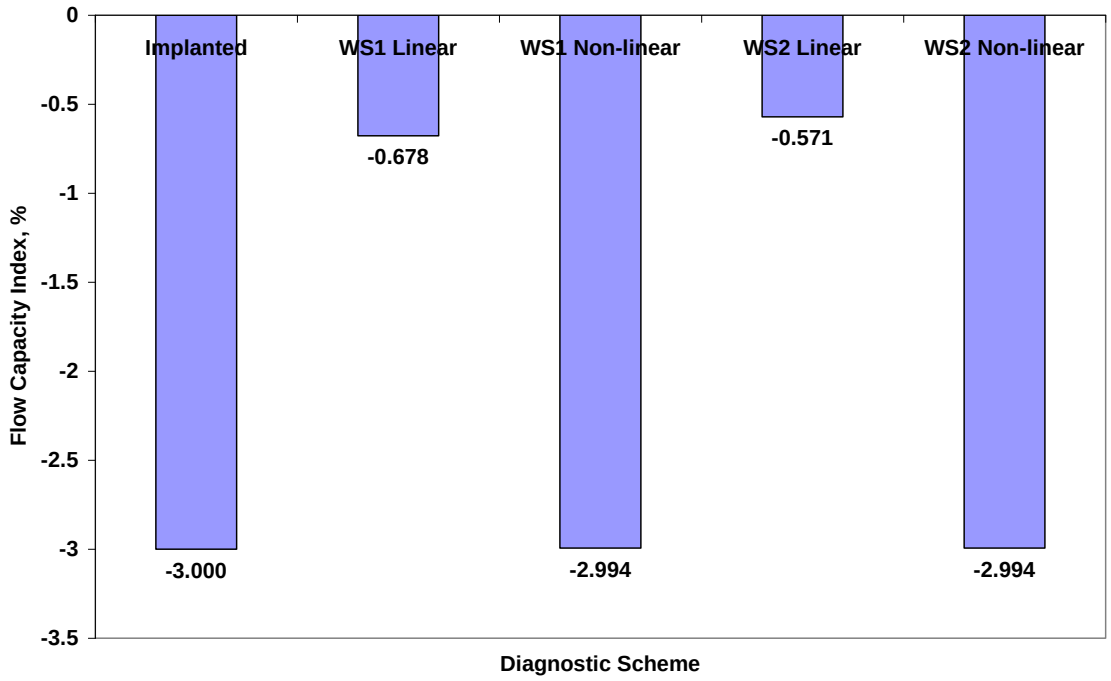

Figure 5.2: Average values of Flow capacity index, Compressor diagnostics

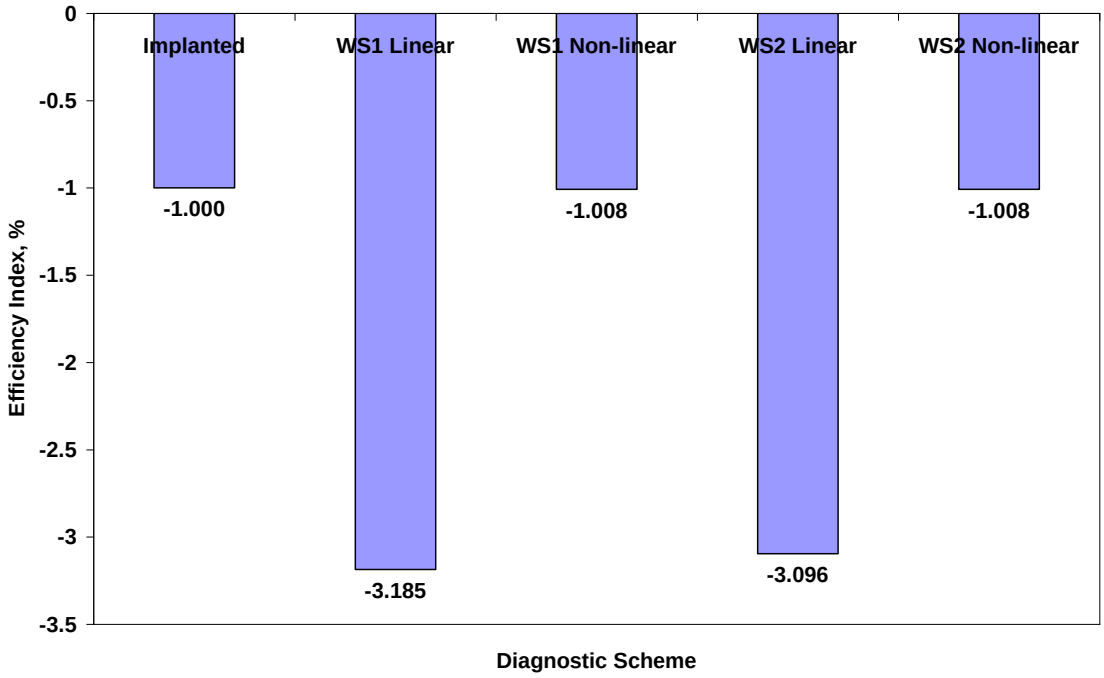

Figure 5.3: Average values of Efficiency index, Compressor diagnostics

With reference to Figure 5.2 and Figure 5.3 it is observed that the non-linear WLS algorithm produces more accurate results when compared to linear WLS. That is, the mean values produced by the non-linear WLS algorithm are closer to the actual (implanted) value than those produced by linear WLS, for both flow capacity and efficiency indices.

For further demonstration compressor turbine diagnostics was carried out by implanting compressor turbine degradation in the engine model as follows:

Deviation of Flow capacity index, $\Delta\Gamma$: 2 %;

Deviation of Efficiency index, $\Delta\eta$: -1%

1000 samples of the measurements presented in Table 5.4 were simulated at a noise level of $2\times 2\sigma$

MEASUREMENT PARAMETERS	SYMBOL	UNITS
Compressor non-dimensional rotational	PCN	Non-dimensional
Fuel flow	w_f	Kg/s
Compressor exit pressure	P3	Atmospheres
Compressor turbine exit pressure	P12	Atmospheres

Table 5.4: Measurement parameter set, compressor-turbine diagnostics

The respective weights for the chosen measurement set are presented in Table 5.5.

	WEIGHTING SCHEME AND WEIGHTS	
MEASUREMENT PARAMETER	**WS1**	**WS2**
PCN	1.0	1.0
w_f	0.868	0.923
P3	0.2	0.225
P12	0.2	0.206

Table 5.5: Compressor-turbine diagnostics, measurement set weights

Linear and non-linear weighted least squares were run for the 1000 measurement samples using the presented measurement weights. The averages of these samples are presented in Figure 5.4 and Figure 5.5 for both flow capacity and efficiency indices.

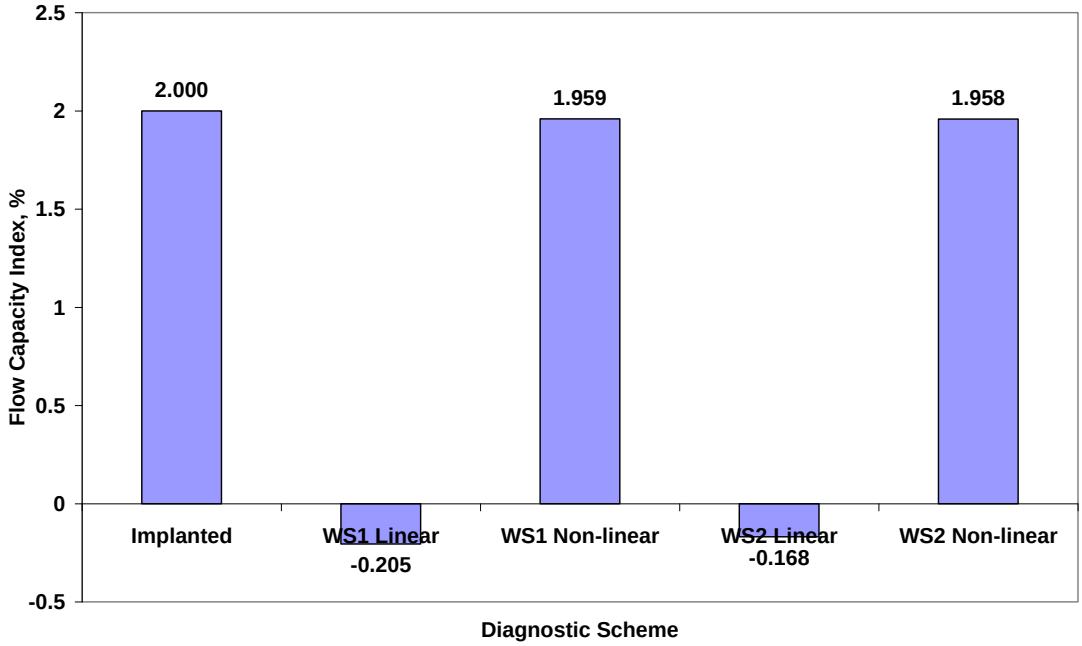

Figure 5.4: Average values of Flow capacity index, Compressor-turbine diagnostics

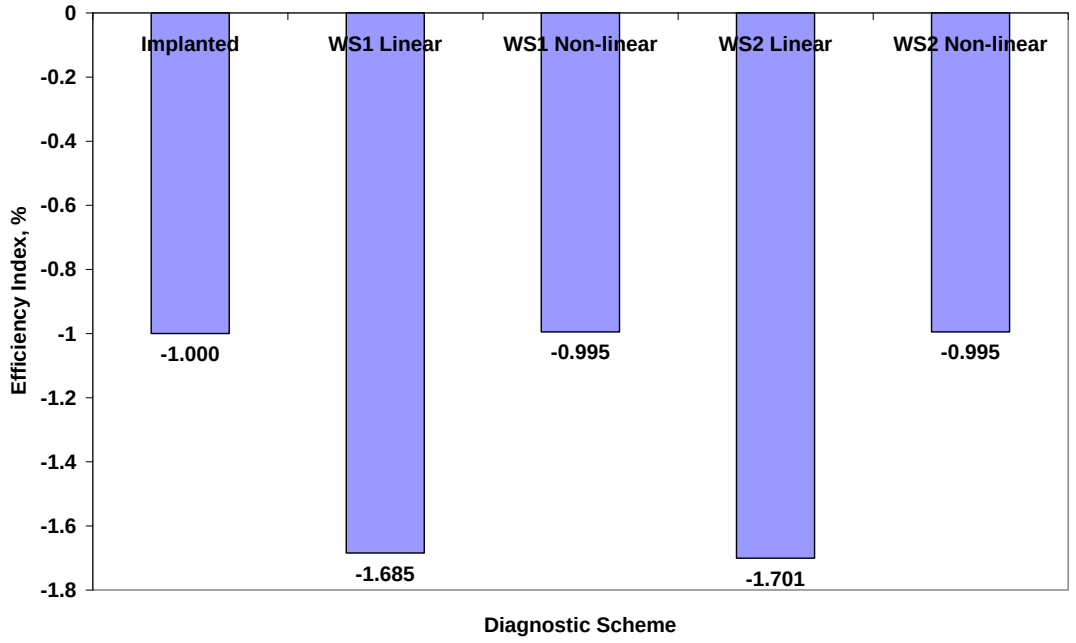

Figure 5.5: Average values of Efficiency index, Compressor-turbine diagnostics

With reference to Figure 5.4 and Figure 5.5 it is observed that, once again, the non-linear WLS algorithm produces more accurate results when compared to its linear counter-part, linear WLS. The mean values produced by the non-linear WLS algorithm are closer to the actual (implanted) value than those produced by linear WLS, for both flow capacity and efficiency indices.

In both cases (Compressor and compressor turbine diagnostics) results produced by linear WLS are not useful for diagnostic purposes; this is because the results are very inaccurate. On the other hand, non-linear WLS produces much more accurate results. We may define the root mean square (RMS) as Equation 5.1:

$$RMS = \sqrt{\left[\left(\Gamma_{implanted} - \Gamma_{predicted}\right)^2 + \left(\eta_{implanted} - \eta_{predicted}\right)^2\right] / 2} \qquad \textbf{(5.1)}$$

Therefore, a RMS value close to Zero implies improved accuracy and vice versa. Then, we may compare respective RMS values, Figure 5.6 and Figure 5.7.

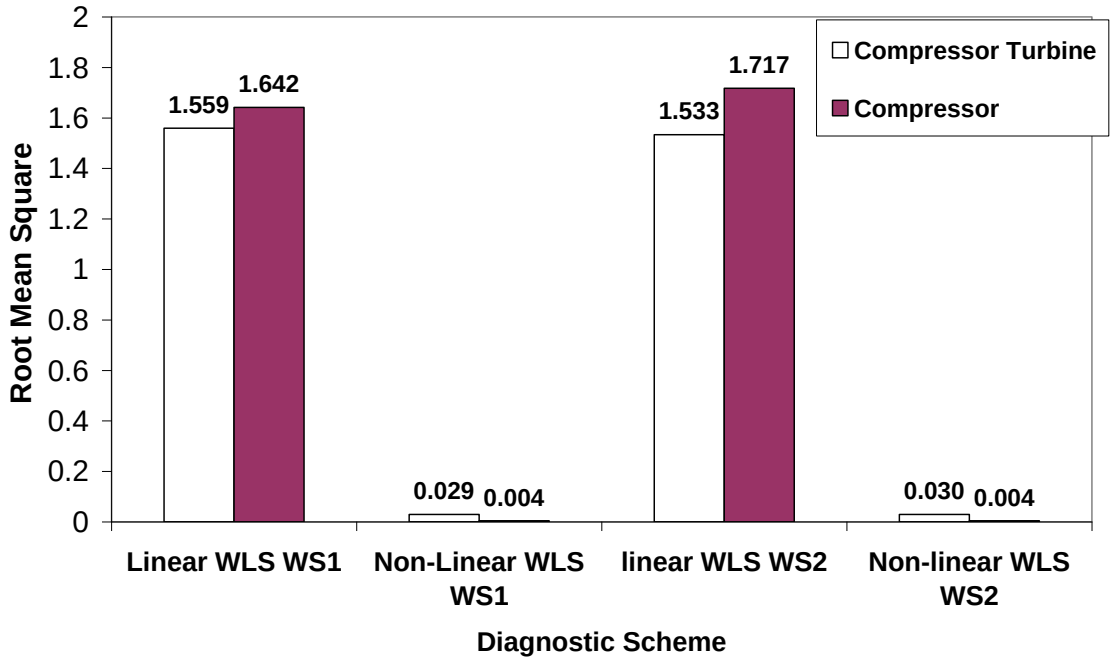

Figure 5.6: Root mean square values, Flow capacity index

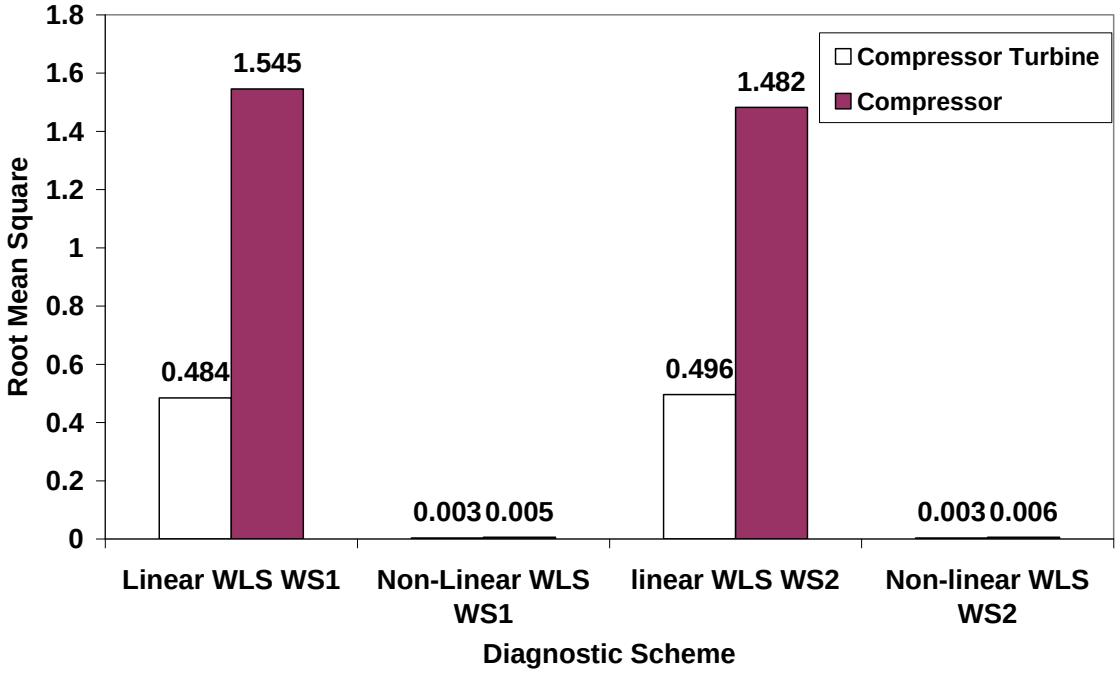

Figure 5.7: Root mean square values, Efficiency index

Figure 5.6 and Figure 5.7 further confirm the improved accuracy of non-linear WLS over linear WLS.

Therefore, it can be concluded that non-linear WLS should be the preferred choice over linear WLS for gas turbine diagnostics.

5.1.2 Case Study 2: Effect of significantly large and/or small weights on matrix integrity

The effect that significantly large and/or significantly small weights on matrix condition number (and hence matrix integrity) was investigated in this case study. This was achieved by means of compressor turbine degradation which was implanted into the engine model as follows:

Deviation of Flow capacity index: $\Delta\Gamma$ 2 %;

Deviation of Efficiency index: $\Delta\eta$ -1%

1000 samples of the measurements presented in Table 5.4 were simulated at 3 noise levels: $1\times 2\sigma$, $2\times 2\sigma$ and $3\times 2\sigma$.

Where,

- 2σ is the maximum measurement noise
- 1, 2 and 3 are multipliers (of measurement noise)

Table 5.6 to Table 5.8 are the presented measurements and their respective measurement weights for all three weighting methods (reciprocal of variance, WS1 and WS2) and for all three measurement noise levels.

	WEIGHTING SCHEME AND WEIGHTS		
MEASUREMENT PARAMETER	**RECIPROCAL OF VARIANCE**	**WS1**	**WS2**
PCN	4006909.008	1.0	1.0
w_f	453720121.688	0.868	0.9403
P3	1403.163	0.2	0.193
P12	22985.374	0.2	0.201

Table 5.6: measurement weights, 1x2σ

	WEIGHTING SCHEME AND WEIGHTS		
MEASUREMENT PARAMETER	**RECIPROCAL OF VARIANCE**	**WS1**	**WS2**
PCN	1000963.562	1.0	1.0
w_f	106079634.597	0.868	0.923
P3	354.885	0.2	0.225
P12	5537.23	0.2	0.206

Table 5.7: Measurement weights, 2x2σ

	WEIGHTING SCHEME AND WEIGHTS		
MEASUREMENT PARAMETER	**RECIPROCAL OF VARIANCE**	**WS1**	**WS2**
PCN	445492.09	1.0	1.0
w_f	50413915.62	0.868	0.889
P3	154.046	0.2	0.1903
P12	2489.65	0.2	0.224

Table 5.8: Measurement weights, 3x2σ

The condition numbers of the matrix $\left(H^T WH\right)^{-1}$ were calculated for each weighting method presented in Table 5.6, Table 5.7 and Table 5.8 and the results are presented in Figure 5.8.

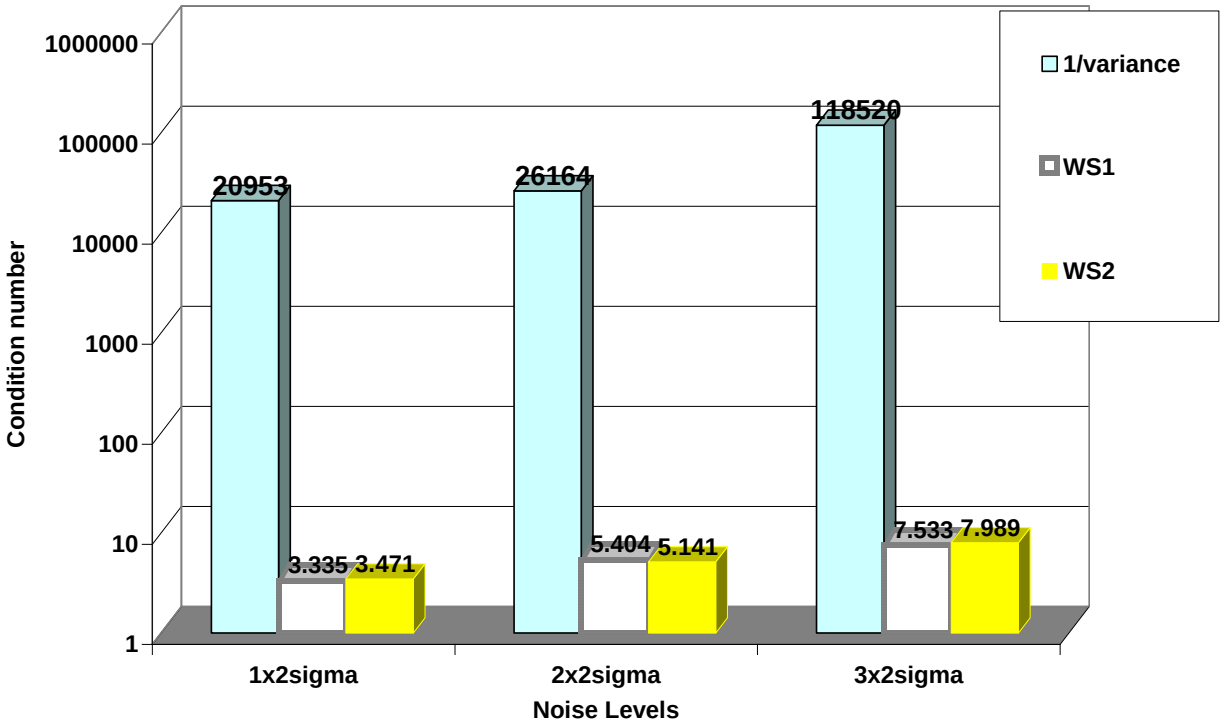

Figure 5.8: condition numbers of the matrix $(H^T WH)^{-1}$

With reference to Figure 5.8, it is observed that the reciprocal-of-variance method produces large condition numbers (in this case) whilst the other two weighting methods produce relatively small condition numbers. Further, these condition numbers increase with an increase in noise; this is because the large weighting values serve to amplify the measurement noise present in measurement parameters. It is expected that these large condition numbers will have an impeding effect on the diagnostic effort. It needs to be mentioned at this point that with the reciprocal-of-variance weighting method, large

condition numbers are not always to be expected; it has been observed that the method may or may not produce large condition numbers.

1000 measurement samples of the measurements presented in Table 5.7 (at a noise level of 2x2σ) were simulated and used for compressor turbine diagnostics. The non-linear WLS results were compared with those of non-linear GPA, (Escher, 1995) a diagnostic algorithm that does not account for measurement noise.

Figure 5.9 and Figure 5.10 are plots of the mean values of the diagnostic results obtained from the 1000 samples, for both flow capacity and efficiency.

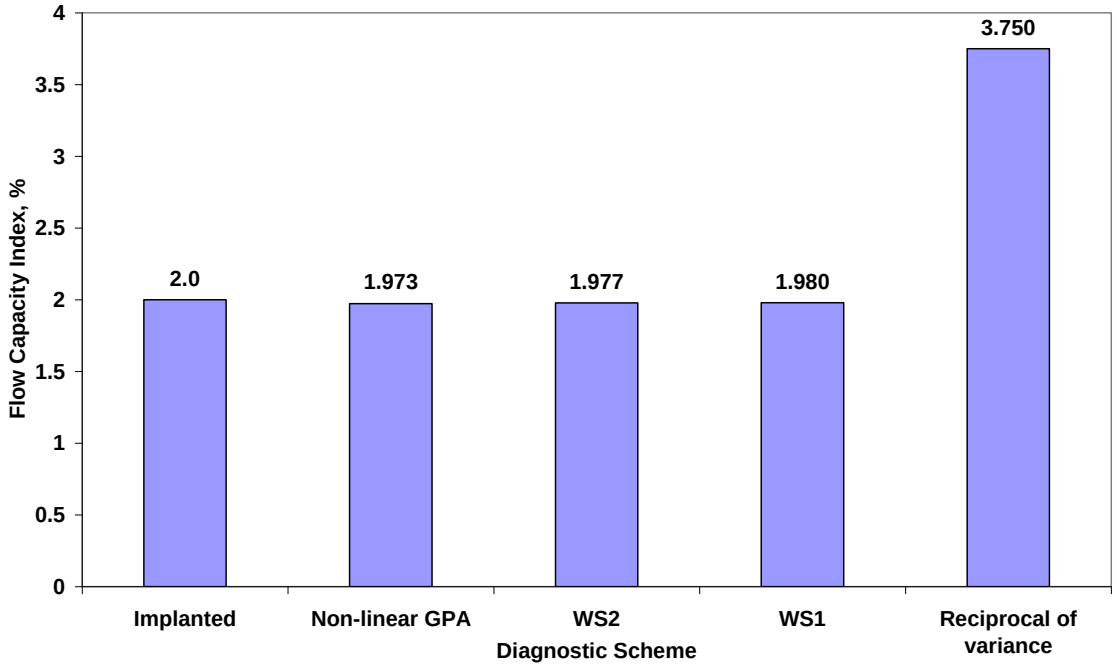

Figure 5.9: Flow capacity mean values, compressor turbine diagnostics

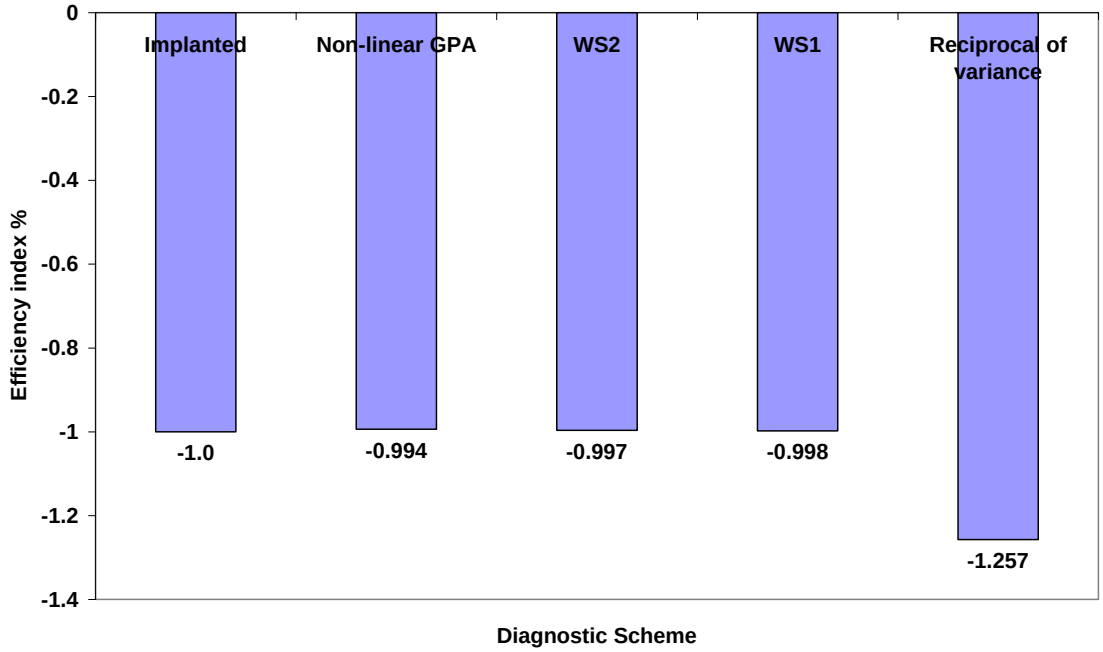

Figure 5.10: Efficiency mean values, compressor turbine diagnostics

From Figure 5.9 and Figure 5.10 it is observed that the results are reasonably accurate for all methods except for the reciprocal of variance method. The large condition numbers of the $\left(H^T WH\right)^{-1}$ matrix served to impede the diagnostic effort. We may further observe the trend of the 1000 results by looking at their standard deviations. Smaller values of standard deviation imply that the results are closer to the mean value while larger values of standard deviation imply that the results are more scattered from the mean value. Figure 5.11 and Figure 5.12 are plots of standard deviation; it is observed that the reciprocal of variance method has the largest standard deviations for both flow capacity and efficiency. The non-linear WLS method in conjunction with WS1 and WS2 produced the most accurate results, demonstrated by the smaller values of standard deviations, for both flow capacity and efficiency. The non-linear GPA method which does not account for measurement noise produces results with less accuracy than non-linear WLS.

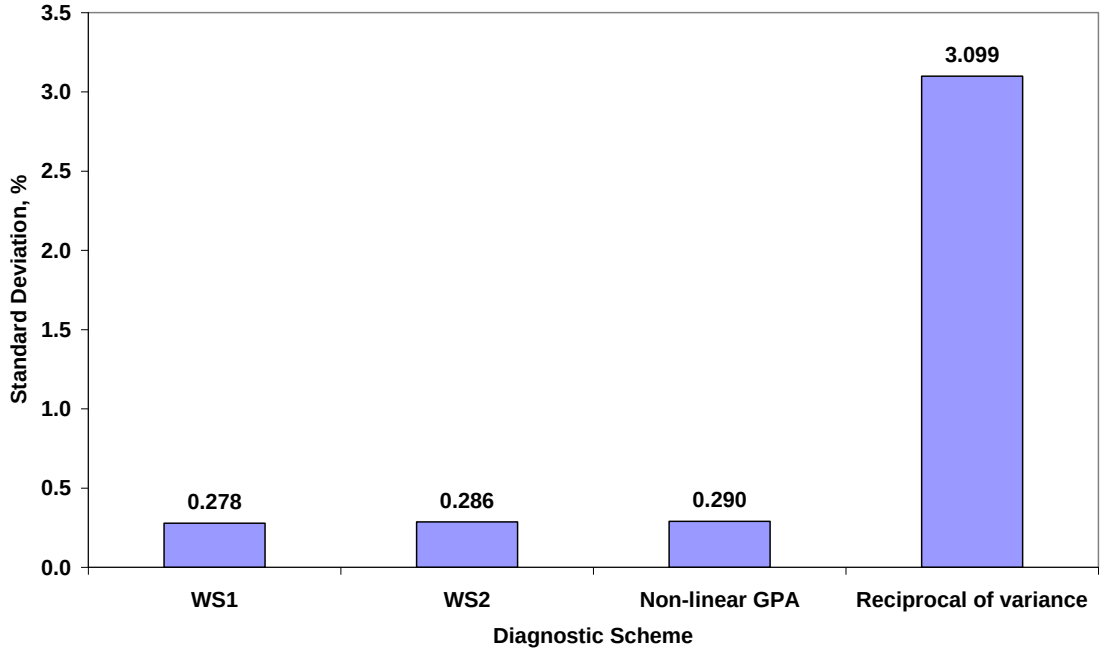

Figure 5.11: Flow capacity index standard deviation, compressor turbine diagnostics

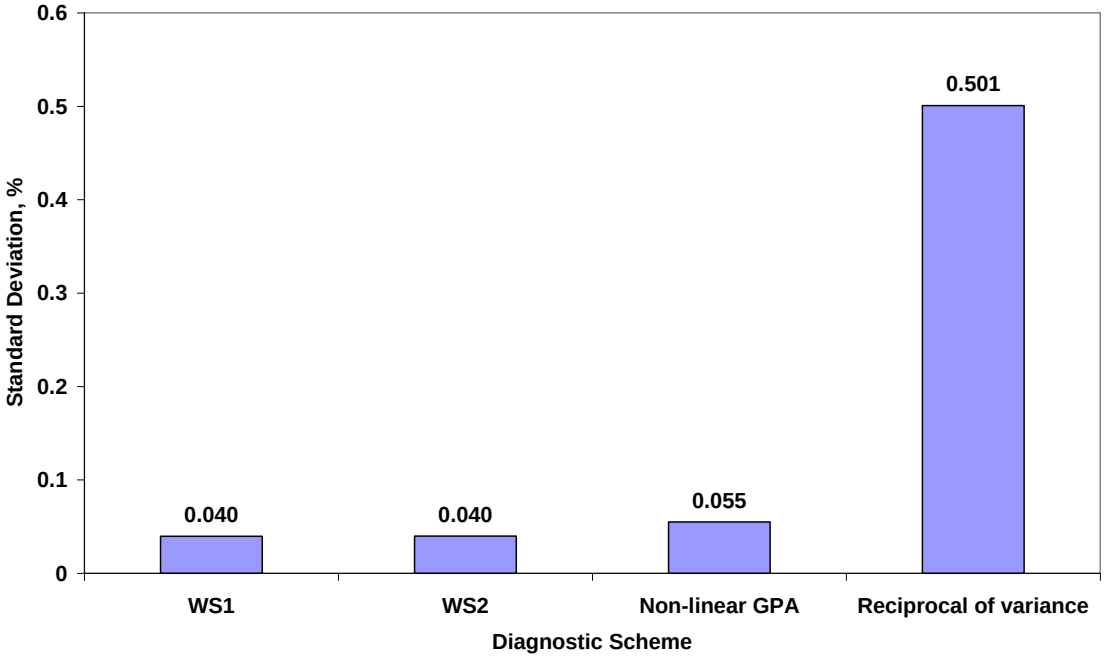

Figure 5.12: Efficiency index standard deviation, compressor turbine diagnostics

Figure 5.13 and Figure 5.14 are the normal distribution/probability density function plots for both flow capacity and efficiency. The reciprocal of variance plots are observed to have long tails, lower and wide peaks as opposed to the other diagnostic schemes that have shorter tails, higher and narrow peaks. This implies that the values (reciprocal of variance method) are far spread about the mean (long tails). Therefore, the probability that the diagnostic result would be close to the mean value is low. It can therefore be concluded at this point that due to the high condition number of the $\left(H^T WH\right)^{-1}$ matrix occasioned by the large absolute values of the weight matrix, the reciprocal of variance method does not produce any useful diagnostic results. Non-linear GPA results are both less accurate and less precise when compared to non-linear WLS in conjunction with WS1 or WS2; this can be attributed to the fact that non-linear GPA does not account for measurement noise. Figure 5.15 and Figure 5.16 are presented without the reciprocal of variance method so that the improved accuracy of non-linear WLS over non-linear GPA is clearer.

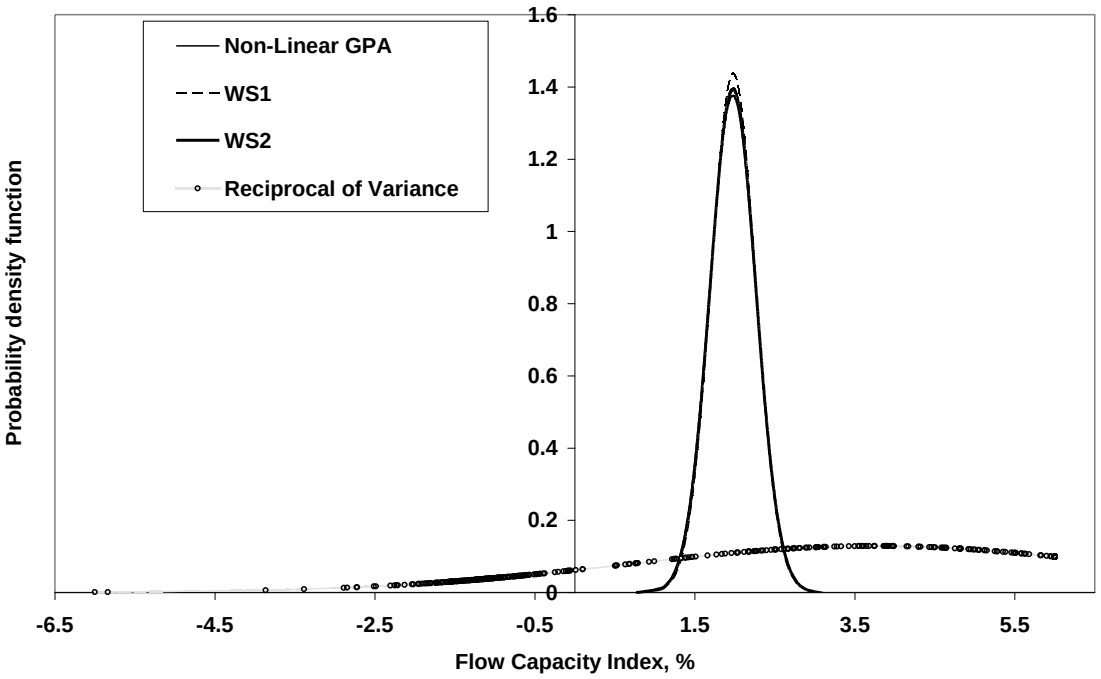

Figure 5.13: Probability density function, flow capacity index, compressor turbine diagnostics

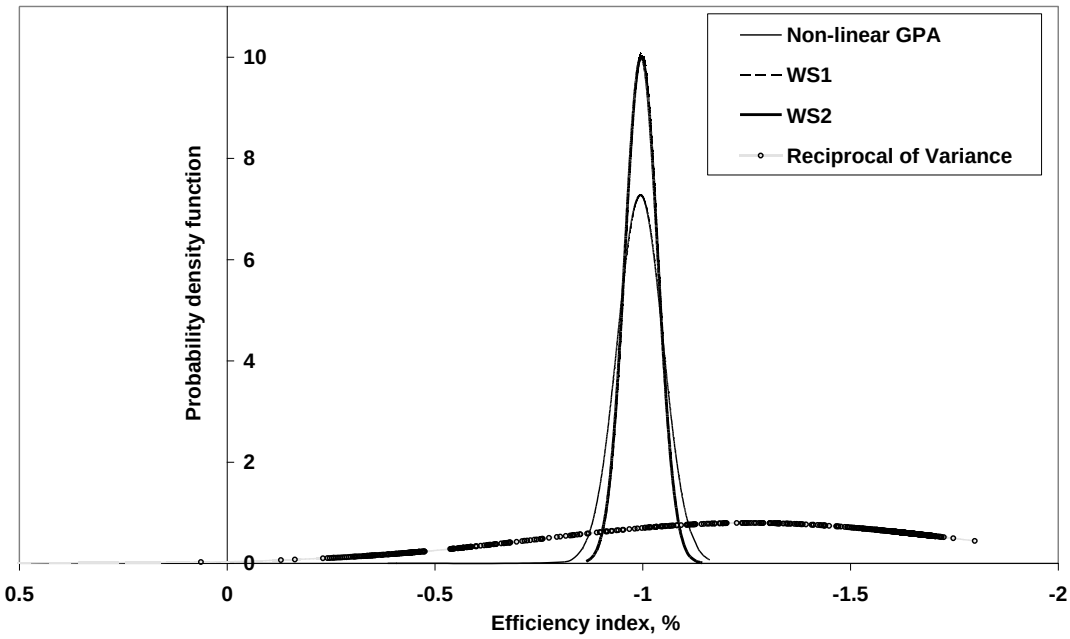

Figure 5.14: probability density function, efficiency index, compressor turbine diagnostics.

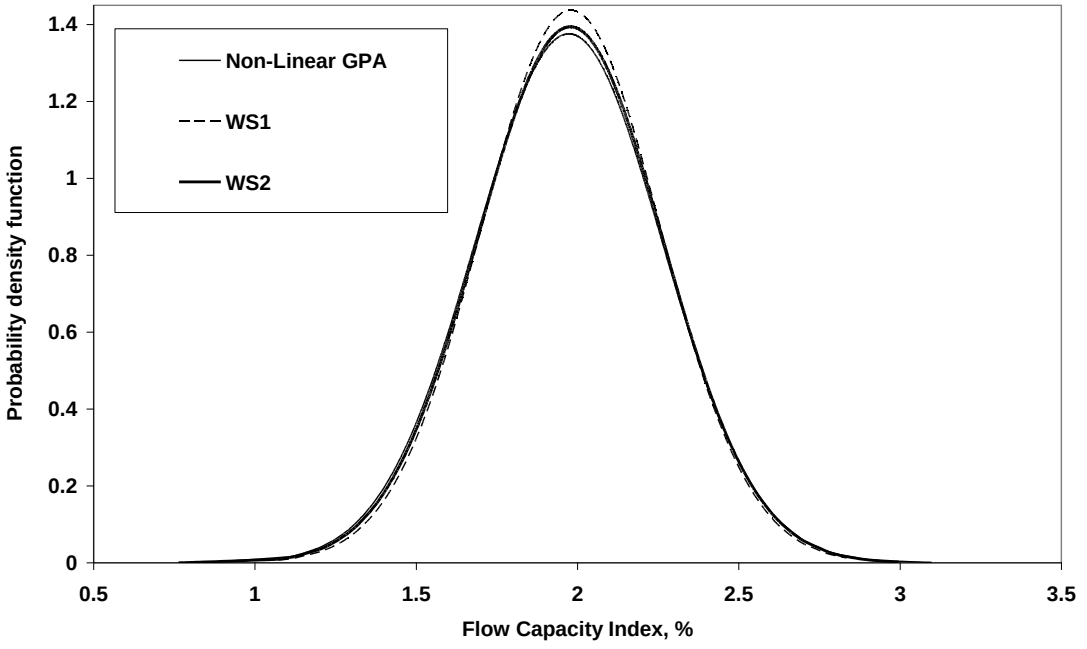

Figure 5.15: Probability density function, flow capacity index, compressor turbine diagnostics

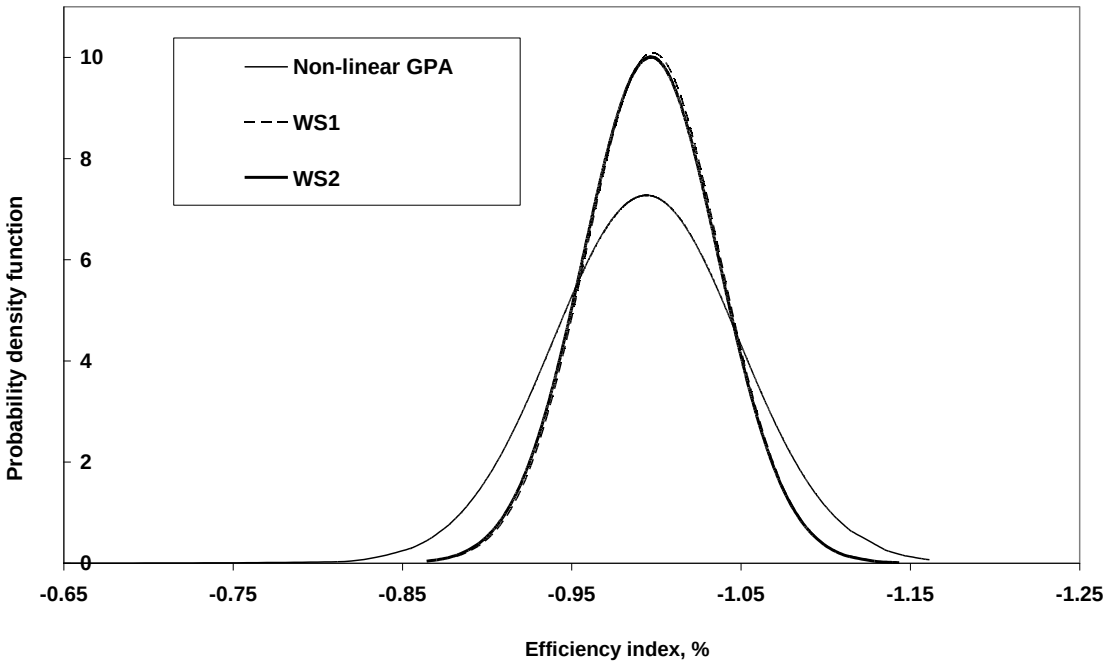

Figure 5.16: probability density function, efficiency index, compressor turbine diagnostics.

Therefore, it may be concluded at this point that where the reciprocal-of-variance method fails, WS1 and WS2 are still dependable and will produce improved diagnostic results in terms of accuracy and precision.

5.1.3 Case Study 3: Compressor diagnostics

The developed non-linear WLS method was further tested by implanting compressor degradation into the model engine as follows:

Deviation of Flow capacity index, $\Delta\Gamma$: -3 %;

Deviation of Efficiency index, $\Delta\eta$: -1%

Table 5.9 is a presentation of the selected measurement set for compressor diagnostics and respective weights. 1000 samples of these measurements were simulated at a noise level of $2 \times 2\sigma$

	WEIGHTING SCHEME AND WEIGHTS		
MEASUREMENT PARAMETER	**RECIPROCAL OF VARIANCE**	**WS1**	**WS2**
T3	0.07	0.118	0.152
P3	382.837	0.2	0.2002
w_f	114,617,977	0.869	0.925
PCN	1031554.561	1.0	1.0
T17	0.0372	0.122	0.196
P17	39195.8895	0.2	0.212

Table 5.9: Compressor diagnostics measurement parameter set weights

Figure 5.17 and Figure 5.18 are plots of accuracy; that is, the means of the 1000 diagnostic results obtained from the 1000 measurement samples. It is observed that each diagnostic scheme produces reasonably accurate results, that is, a mean value close to the implanted value. The non-linear WLS method in conjunction with WS1 and WS2 produces the most accurate results compared to non-linear GPA and the reciprocal of variance weighting method.

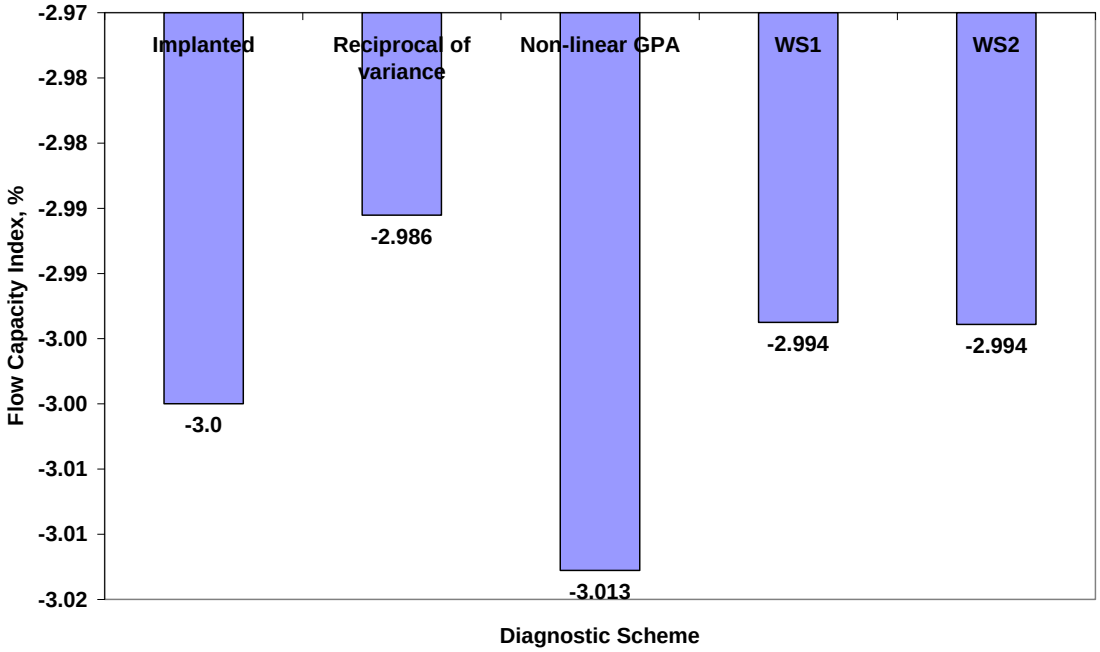

Figure 5.17: Flow capacity index mean values, compressor diagnostics

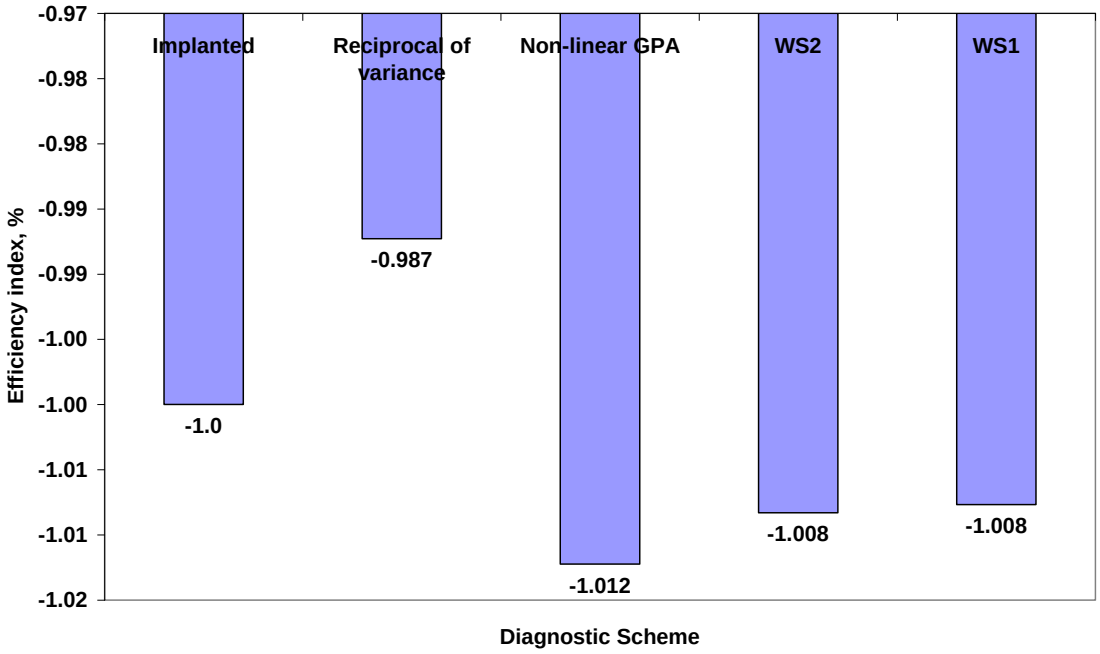

Figure 5.18: Efficiency index mean values, compressor diagnostics

Figure 5.19 and Figure 5.20 are plots of precision; that is, standard deviations of the 1000 diagnostic results for flow capacity and efficiency indices respectively. It is observed that non-linear GPA produces the least precise results, demonstrated by the largest values of standard deviation for both flow capacity and efficiency indices. For flow capacity index, non-linear WLS in conjunction with WS1 produces the most precise results whist for efficiency index, the reciprocal of variance method produces the most precise results.

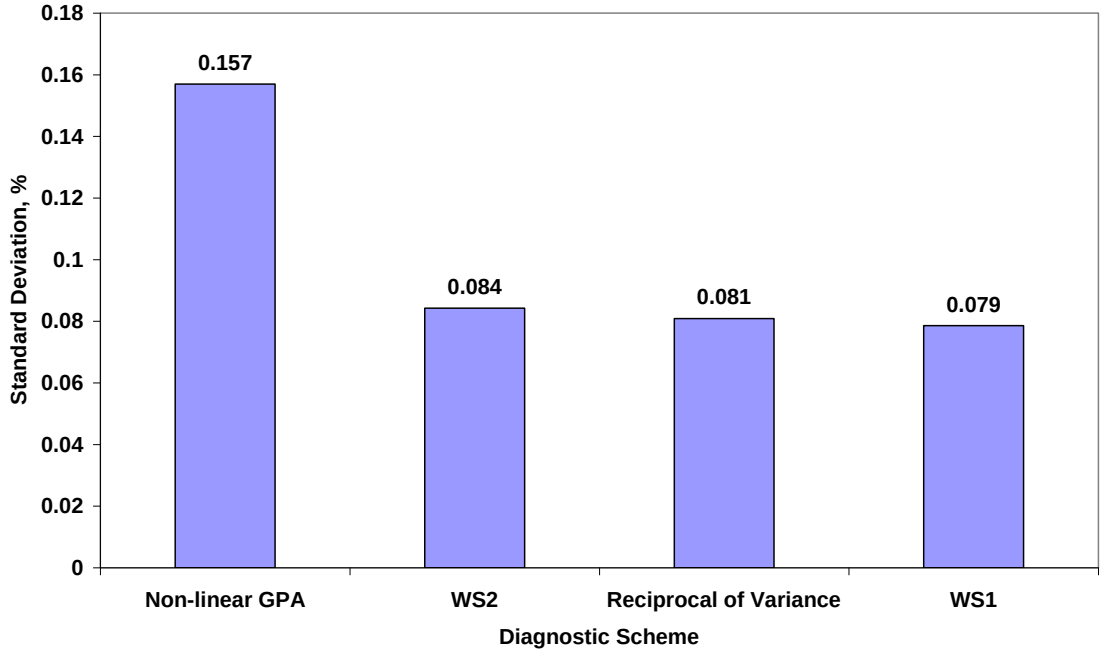

Figure 5.19: Flow capacity index standard deviation, compressor diagnostics

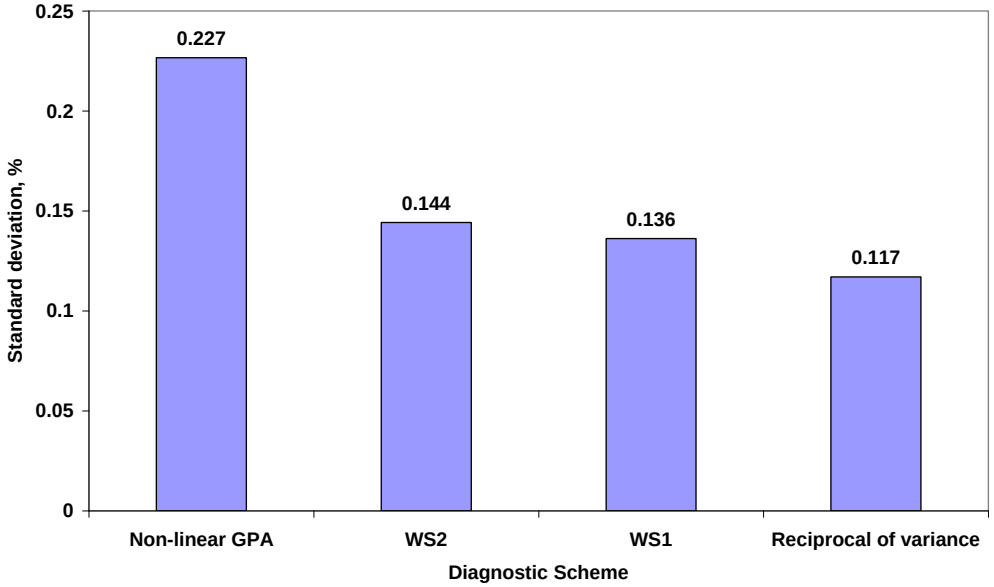

Figure 5.20: Efficiency index standard deviation, compressor diagnostics

Figure 5.21 and Figure 5.22 are the normal/probability density function (PDF) plots for flow capacity and efficiency indices respectively. It is observed that non-linear GPA produces the least precise diagnostics results for both flow capacity and efficiency indices. This is demonstrated by the longer tails and wider peaks of the PDF plots; this implies that the diagnostic results are further spread out from the mean. In addition, the probability of obtaining a diagnostic result that is close to the mean value is low. On the other hand, non-linear WLS in conjunction with WS1 and WS2 and the reciprocal of variance method produce diagnostics results with improved precision (compared to non-linear GPA). It needs to be stated that the reciprocal of variance method did not fail in this case. When the condition number of the $\left(H^T WH\right)^{-1}$ matrix in this context was investigated, it was found to have a value of 217, which is significantly smaller than the values obtained in the previous case, case study 2.

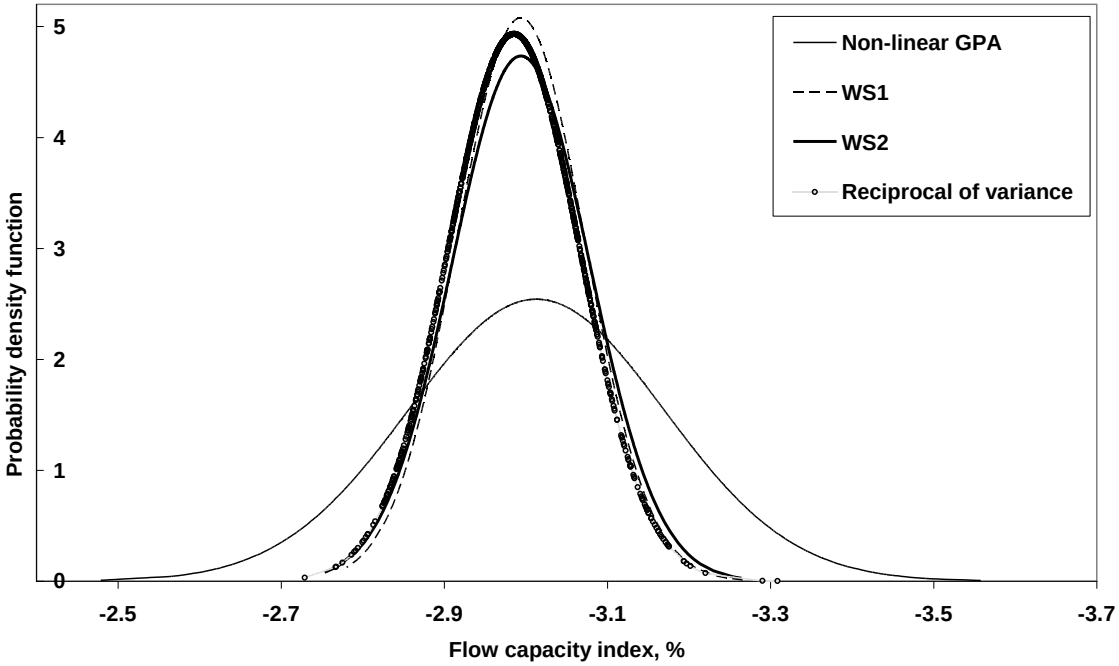

Figure 5.21: Flow capacity index probability density function, compressor diagnostics

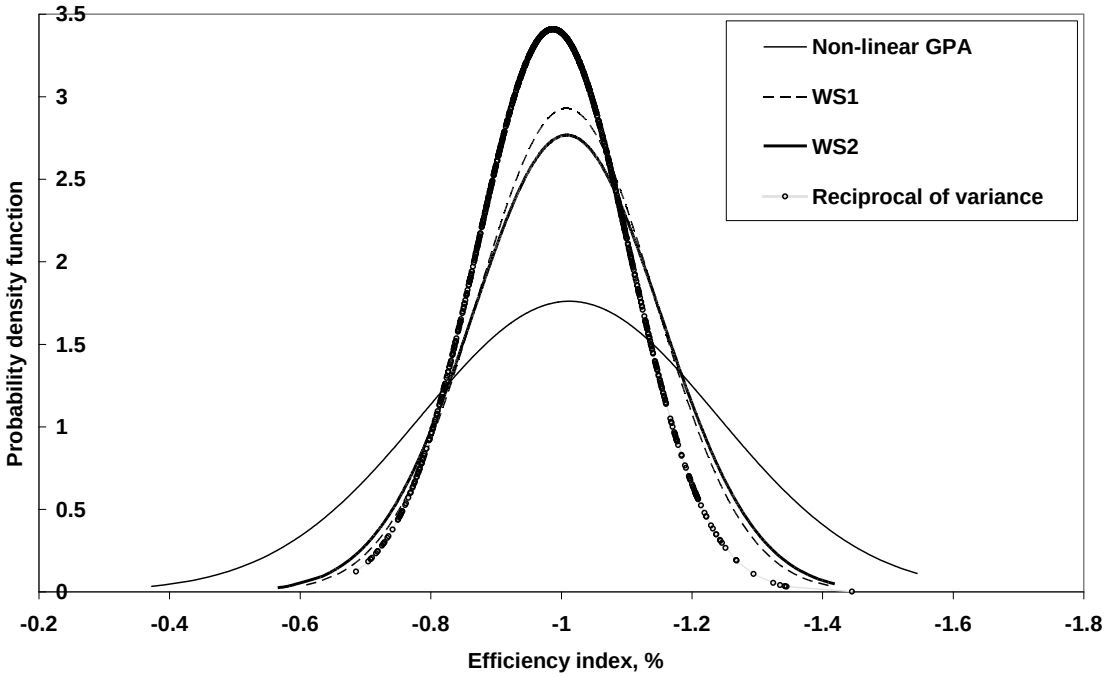

Figure 5.22: Efficiency index probability density function, compressor diagnostics

5.1.4 Case Study 4: Use of a Single sample and WS1

In all cases presented so far, measurement samples were available (1000 simulated samples). In the event that only a single sample of measurement data is available for diagnostic analysis of component faults, then calculation of variance is impossible. In such a case, measurement weighting is possible only with method WS1, since this scheme can weight individual measurements without the need for multiple measurement samples. To demonstrate this, compressor degradation was implanted into the model engine as follows:

Deviation of Flow capacity index, $\Delta\Gamma$: -3 %;

Deviation of Efficiency index, $\Delta\eta$: -1%

A single sample of the measurements in Table 5.9 was simulated at a noise level of $2\times 2\sigma$. Using WS1, respective measurement weights were calculated and are presented in Table 5.10. The simulated measurement sample was then used by the non-linear Weighted-Least-Squares diagnostic approach to predict the engine degradation in order to test the effectiveness of the approach.

MEASUREMENT PARAMETER	WS1 WEIGHTS
T3	0.118
P3	0.2
w_f	0.869
PCN	1.0
T17	0.122
P17	0.2

Table 5.10: WS1 weights, compressor diagnostics using a single sample

The non-linear WLS diagnostics approach was run and the predicted degradation was compared with those of non-linear GPA, Figure 5.23 and Figure 5.24.

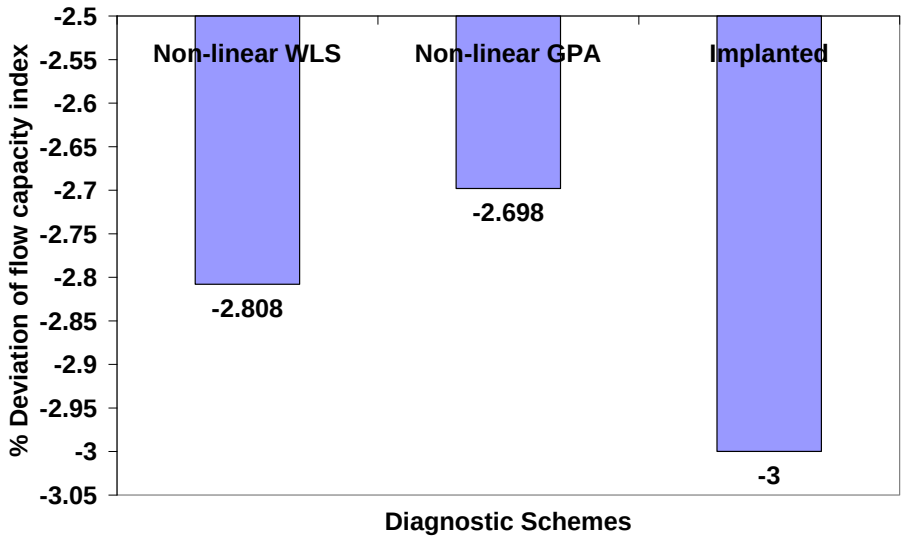

Figure 5.23: Comparison of diagnostic schemes, compressor flow capacity index

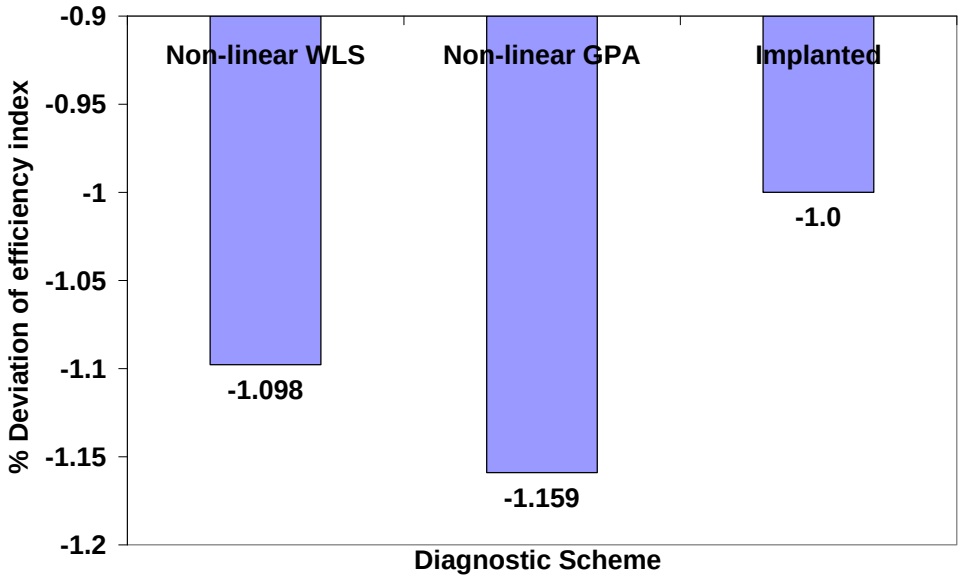

Figure 5.24: Comparison of diagnostic schemes, Compressor efficiency index

With reference to Figure 5.23 and Figure 5.24, it is observed that the non-linear WLS algorithm in conjunction with WS1 predicts the implanted degradation with greater accuracy than non-linear GPA for both flow capacity and efficiency indices. This reduced accuracy of non-linear GPA can be attributed to measurement noise, whilst the non-linear WLS algorithm took account of the measurement noise (by weighting using WS1) thus producing improved results.

5.2 Non-linear WLS discussion of results

This section aims to discuss the findings of the nonlinear WLS method and further reconcile them with the insights gained from the literature review.

From the literature review, a number of requirements were highlighted as necessary components for an advanced diagnostic scheme. The developed non-linear WLS method met a few of those requirements which are discussed below.

1. The method is non-linear based. This was in line with findings from literature that made it clear than non-linear methods are more accurate than linear methods. One such finding is (Kamboukos, P. 2005) who carried out comparisons of linear and non-linear diagnostic methods and concluded that the use of linear methods may lead to substantial inaccuracies in the estimation of degradation. This has been demonstrated by results from case study 1 where the non-linear WLS algorithm detected compressor and compressor turbine components with greater accuracy than linear WLS. In addition, it has been demonstrated that the linear WLS results may not be useful in as far as detection of component faults are concerned. However, the linear results can serve as a starting point for the non-linear algorithm for further iterations and thereby obtaining improved results.

2. The method is able to deal with random measurement noise. This was achieved by means of two weighting schemes, WS1 and WS2 which replaced the traditional method of the reciprocal of variance. Results from case studies 2, 3 and 4 have demonstrated that these methods are able to deal with measurement noise and produce useful diagnostic results. Case study 2 in particular presented a scenario where the reciprocal of variance method failed as a result of large matrix condition numbers which were in turn a result of significantly large or significantly small measurement weights. However, both WS1 and WS2 methods sufficed. This can be attributed to the fact that WS1 and WS2 are designed to produce weights with values no greater than 1. As such, the probability of producing significantly large values of weights which have the capacity to degrade the ICM, H, is eliminated. WS1 proved further useful in that in the absence of large samples of measurement data, weighting was still possible by means of sensor maximum noise specifications as has been demonstrated in case study 4. This is quite helpful in real cases where only a single measurement sample of data is available for diagnostics. In all case studies, the method has shown significant improvements over non-linear GPA that does not account for measurement noise.

3. The method is model-based as opposed to non-model based (Artificial intelligence). (Marinai et al., 2004) highlighted the advantage of model-based methods over non-model based methods, that is, model-based proofs of stability and robustness. The mathematical foundation behind the non-linear WLS model has been clearly presented; therefore, the method is comprehensible. In addition, the method is robust in the sense that, it was not generated from experimental data that may be subjective to a particular case; any other user may thus use the same mathematical foundation to re-produce the method, for diagnostic purposes. In addition, the non-linear WLS method is free from tuning and training

uncertainties and therefore free from any difficulties related to setting-up parameters.

4. Based on experience with testing the method, the author can conclusively state that the non-linear WLS algorithm is not computationally expensive. That is, the method does not require more processing power than can be provided for by modern days' computer systems. This ensures that diagnostic results can be obtained without unnecessary delays.

6 MULTI-FUEL PERFORMANCE SIMULATION RESULTS AND ANALYSIS

The methods that pertain to multi-fuel performance simulation that were described in previous sections were validated, applied and demonstrated. This demonstration was by means of case studies in order to demonstrate the effectiveness of these methods. What follows is a presentation of the results obtained.

6.1 Validation of tabulated data

The tabulated data for the four fuels was validated using values obtained from literature. The purpose of this validation was to ascertain that the tabulated values agree, within reasonable limits, to published data and can therefore be used with confidence.

6.1.1 Dry Air

(Keenan, 1980) presents thermodynamic properties of air, based on examination of data from spectroscopic sources. The properties are provided at selected temperatures and for a pressure of 1 atmosphere. These values were compared to those presented in the fuel tables (herein referred to as *tabulated data*) produced for this work.

A % difference was defined as Equation 6.1,

$$\frac{GP_{ref} - GP_{tables}}{GP_{ref}} \times 100 \qquad \textbf{(6.1)}$$

Where,

- GP_{ref} is the reference caloric property, obtained from literature

- GP_{tables} is the caloric property that is being validated, obtained from the produced fuel tables

Figure 6.1 and Figure 6.2 are figures of change in enthalpy ΔH and change in entropy, ΔS respectively, for dry air at 1 atmosphere.

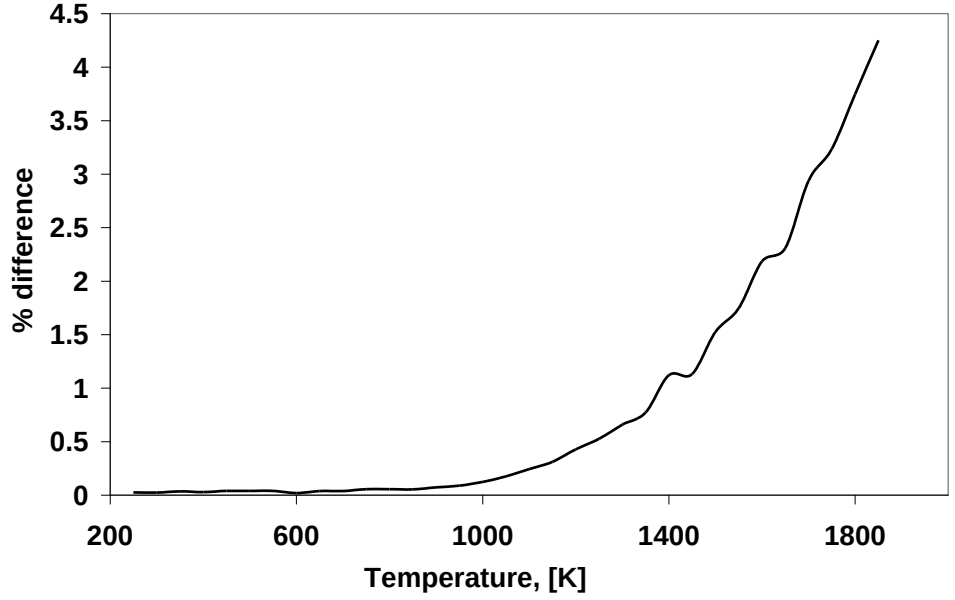

Figure 6.1: Comparison of ΔH, dry air at 1 atmosphere

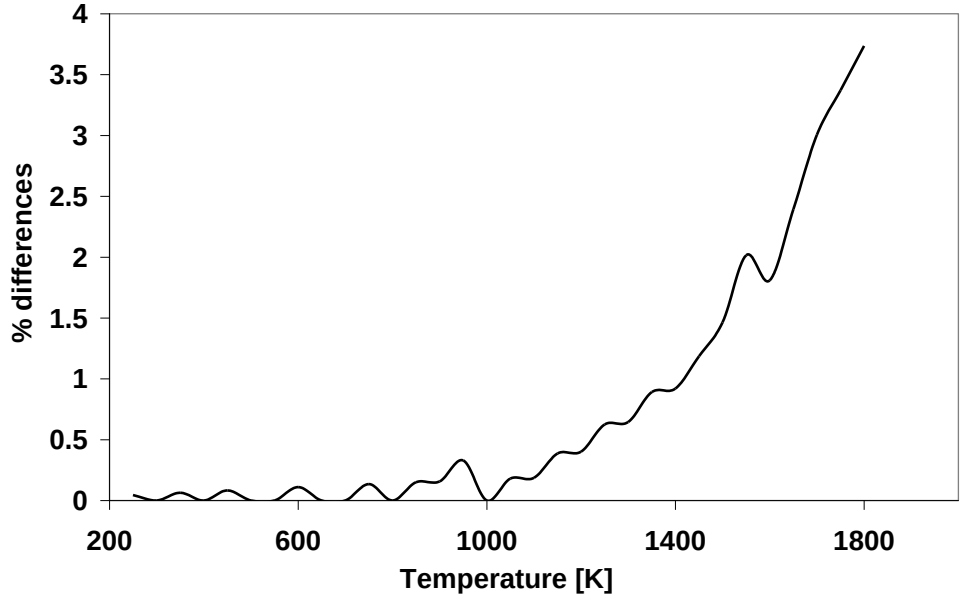

Figure 6.2: Comparison of ΔS, dry air at 1 atmosphere

From Figure 6.1 and Figure 6.2 it is observed that the tabulated data for dry air agrees closely with values from literature until temperatures of 1000 [K] where effects of dissociation begin to become prominent. The model used as the reference for this comparison did not take dissociation effects into account, hence the increase in % difference. Prior to 1000 [K], values of % difference are below 0.5 %.

Figure 6.3 is a comparison of viscosity; this comparison was made between tabulated values and two published sources, (Keenan, 1980) and Sutherlands formula, (Crane, 1988). The latter source is a formula that is valid in the temperature range between 0 [K] and 810 [K] whilst the former has values presented for temperatures between 200 [K] and 1400 [K].

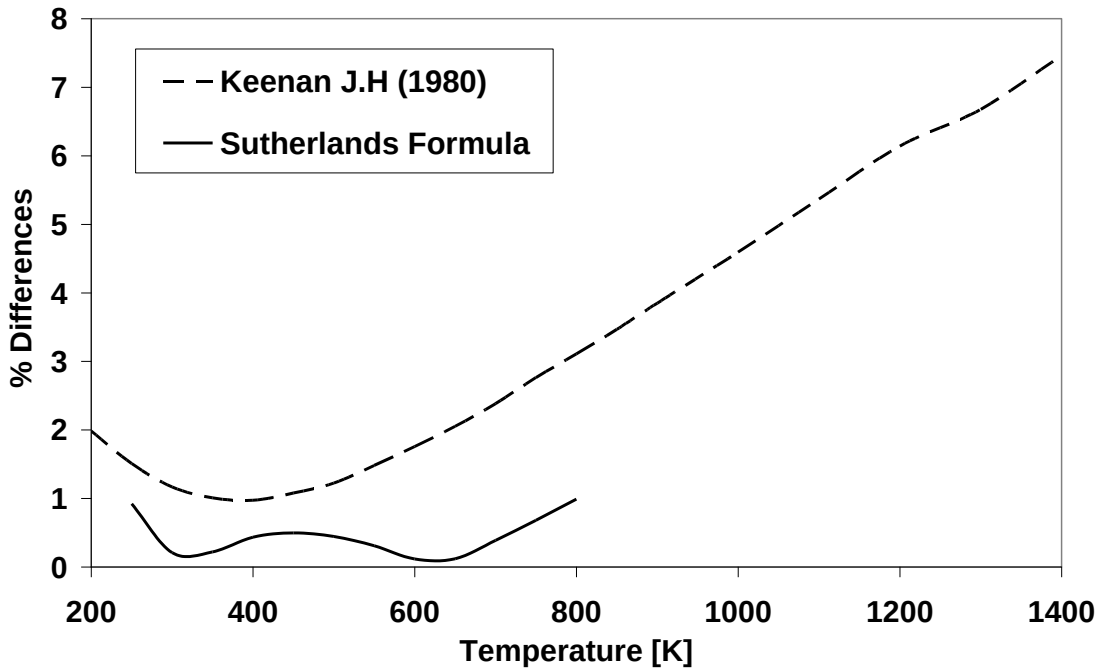

Figure 6.3: Comparison of Viscosity, dry air at 1 atmosphere

With reference to Figure 6.3, it is observed that when tabulated air values of viscosity are compared to values produced by Sutherland's formula, a maximum error of 1 % is observed whilst a maximum error of 7 % is observed

for values produced by (Keenan, 1980). Above 1000 [K], dissociation is responsible for the significant rise in % difference since (Keenan, 1980) does not account for dissociation.

Figure 6.4, Figure 6.5 and Figure 6.6, are comparisons of the ratio of heat capacities, Gamma, γ Gas constant R and Isobaric heat capacity C_p respectively. This comparison was made between tabulated air values and values obtained from (Poferl et al., 1969) who utilised a chemical equilibrium program (Svehla, 1964). The values were obtained at a pressure of 10 atmospheres and for a temperature range of 300 [K] to 2500 [K].

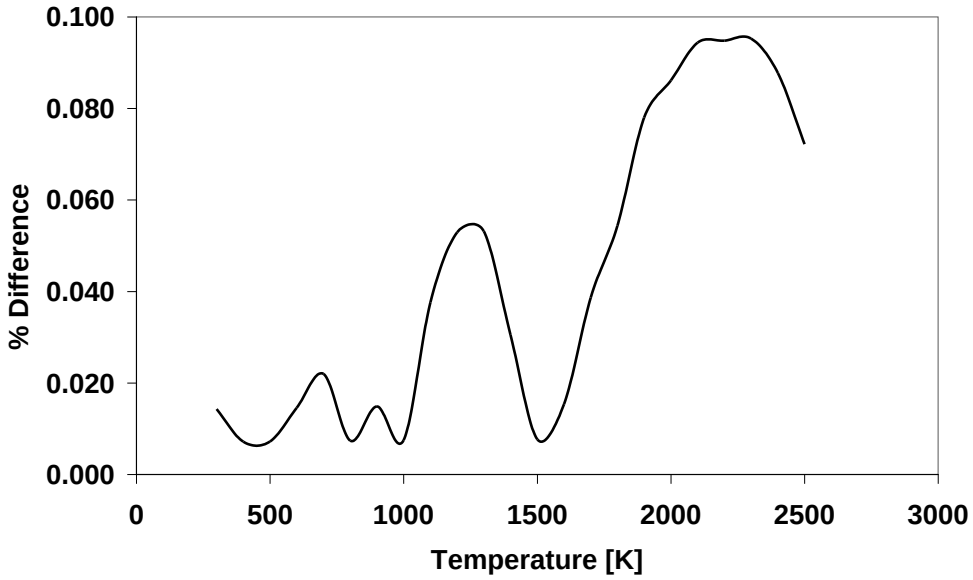

Figure 6.4: Comparison of Gamma, dry air at 10 atmospheres

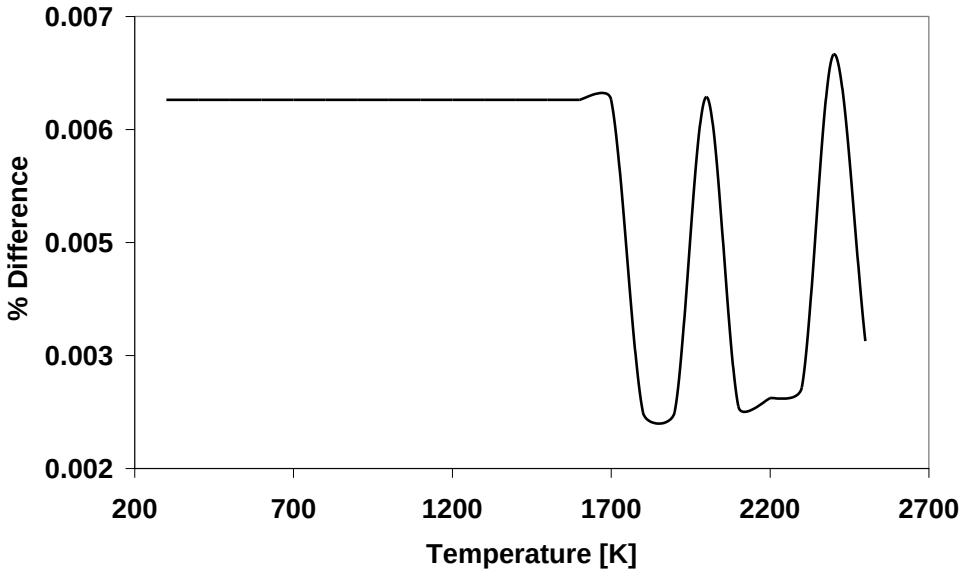

Figure 6.5: Comparison of Gas Constant, R, dry air at 10 atmospheres

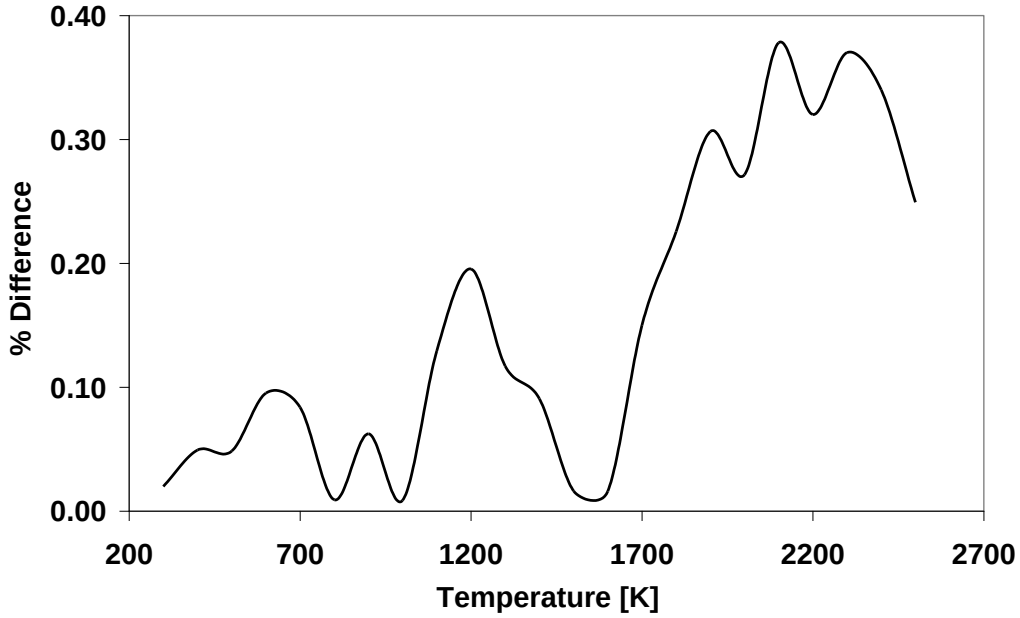

Figure 6.6: Comparison of isobaric heat capacity, dry air at 10 atmospheres

With reference to Figure 6.4, Figure 6.5 and Figure 6.6, it is observed that for isobaric heat capacity, the maximum error is 0.4 % whilst for Gamma, it is 0.1

%. Gas constant values agreed with greater accuracy as seen by the maximum error value slight above 0.006 %.

6.1.2 JetA Fuel

(Jones et al., 1984) presents the properties of combustion products of JetA fuel and dry air. The computations presented were performed using the NASA Lewis chemical equilibrium program documented in (Gordon, 1976). The molecular Hydrogen-Carbon ratio of JetA presented in (Jones et al., 1984) was 1.907 whilst that used for this work was 1.917.

Combustion properties were compared with tabulated JetA data for a FAR of 0.01, temperatures of 300[K], 1000[K], 2000[K], 2800[K], for 1 atmosphere and 50 atmospheres.

Figure 6.7, Figure 6.8 and Figure 6.9 are graphs of comparison of Gas constant, R, Isobaric heat capacity, C_p and ratio of heat capacities, γ for both 1 atmosphere and 50 atmospheres.

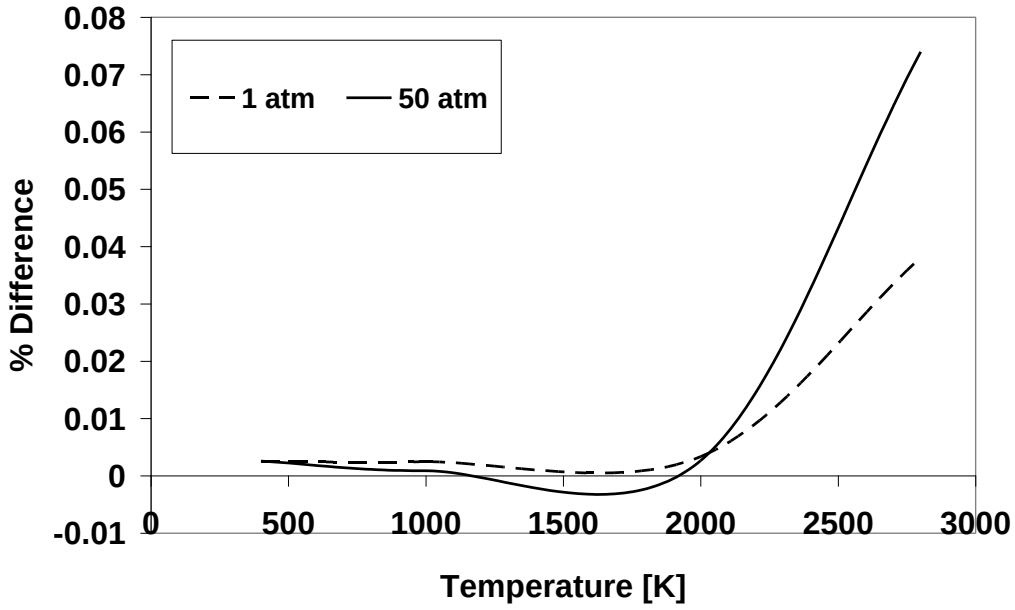

Figure 6.7: Comparison of Gas constant R, JetA fuel, FAR 0.01

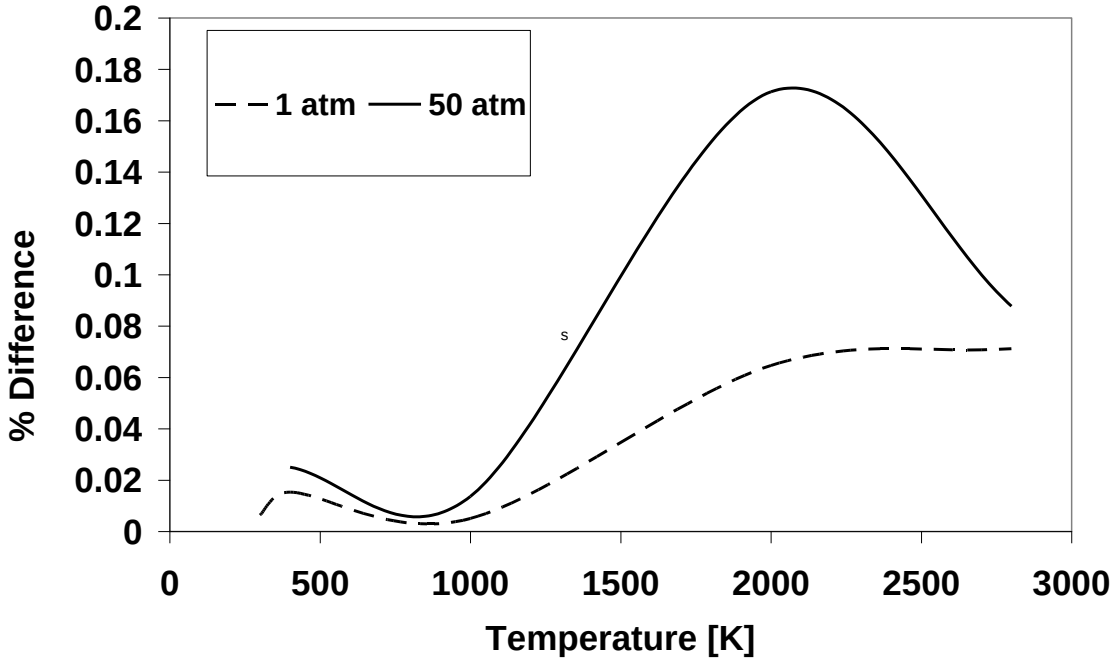

Figure 6.8: Comparison of Isobaric heat capacity, JetA Fuel, FAR 0.01

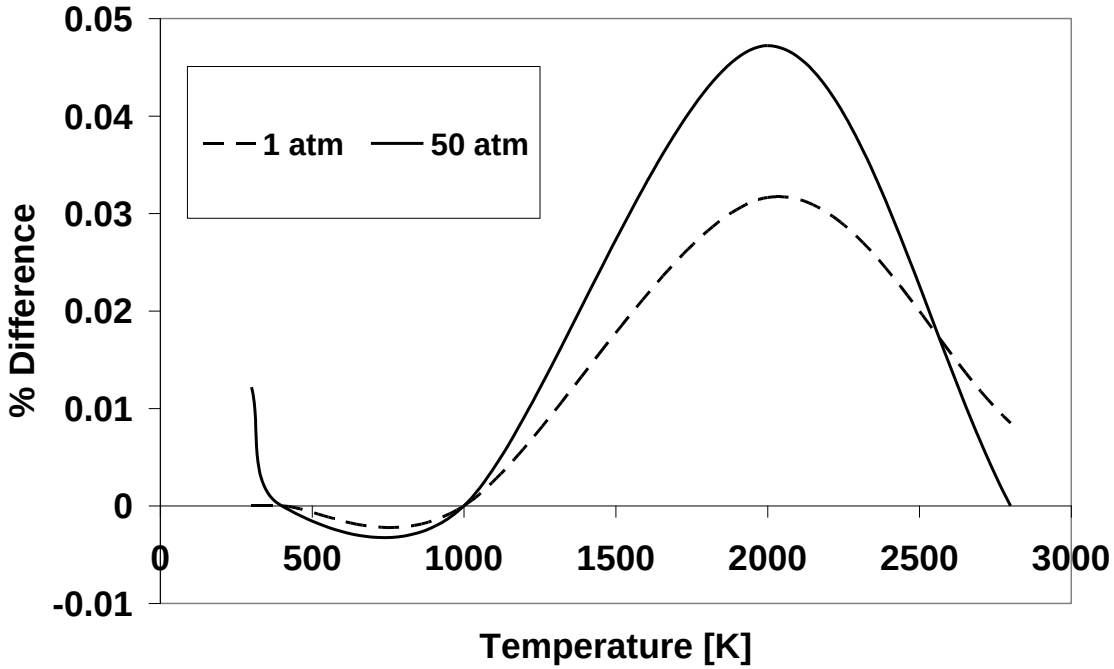

Figure 6.9: Comparison of ratio of heat capacities, JetA Fuel, FAR 0.01

From Figure 6.7, Figure 6.8 and Figure 6.9 it is observed that the maximum errors are 0.07%, 0.18% and 0.05% for Gas constant R, isobaric heat capacity C_p and ratio of heat capacities γ respectively. Such small values of maximum error indicate close agreement between values in literature and tabulated data.

6.1.3 Hydrogen Fuel

(Wear, 1985) presents properties of combustion of Hydrogen fuel and dry air. The computations were performed using the NASA Chemical equilibrium program documented in (Gordon, 1976).

Combustion properties were compared with tabulated Hydrogen fuel data for a FAR of 0.01, temperatures of 400[K], 1000[K], 2000[K], 2800[K], for 1 atmosphere and 50 atmospheres.

Figure 6.10, Figure 6.11 and Figure 6.12 are graphs of comparison of Gas constant, R, Isobaric heat capacity, C_p and ratio of heat capacities, γ for both 1 atmosphere and 50 atmospheres.

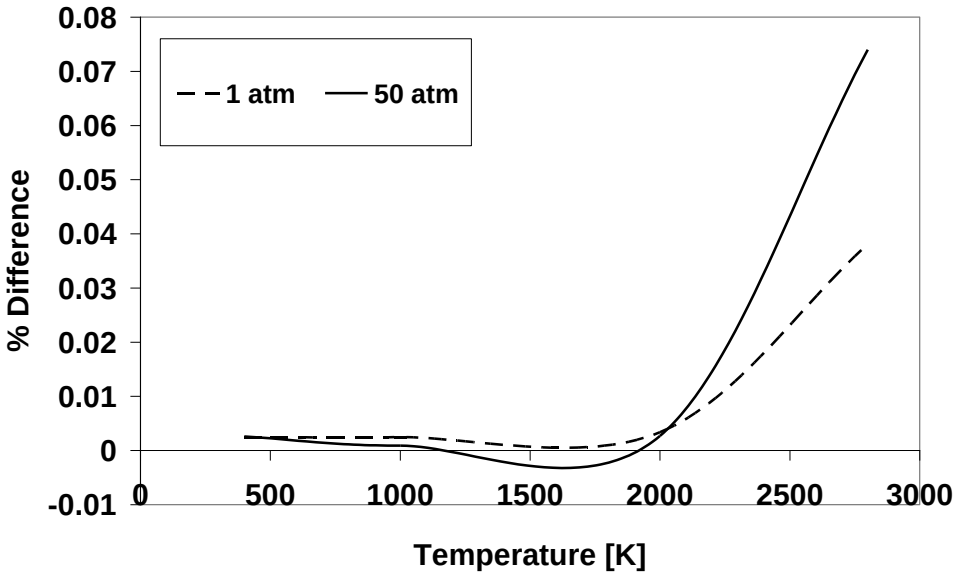

Figure 6.10: Comparison of Gas constant R, H_2 fuel, FAR 0.01

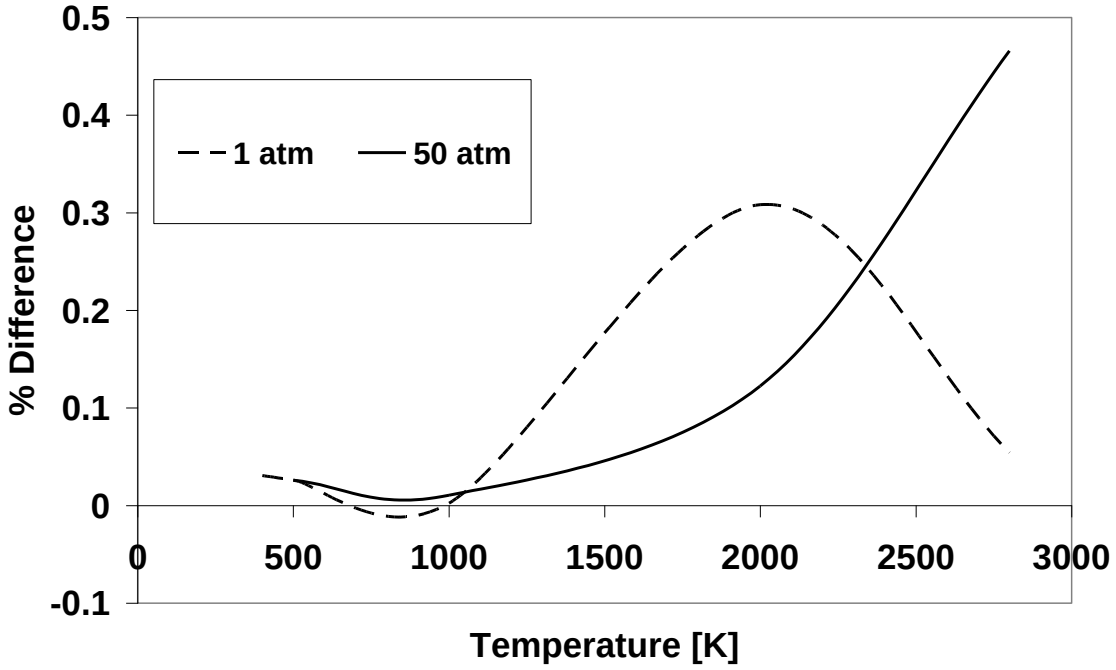

Figure 6.11: Comparison of Isobaric heat capacity, H_2 Fuel, FAR 0.01

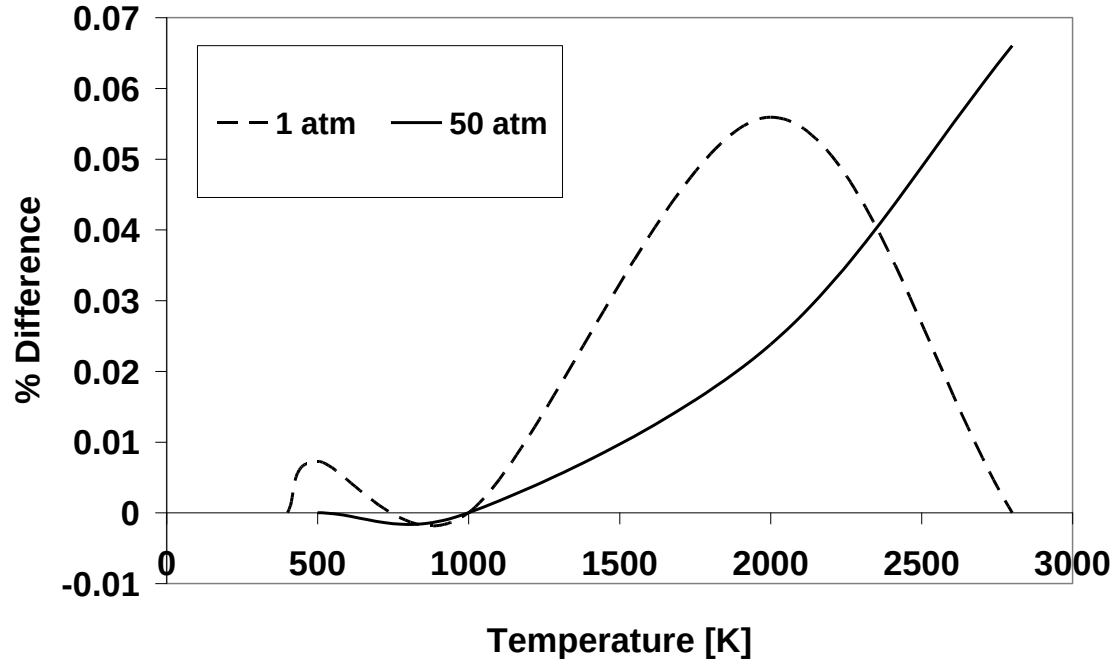

Figure 6.12: Comparison of ratio of heat capacities, H_2 Fuel, FAR 0.01

From Figure 6.10, Figure 6.11 and Figure 6.12, it is observed that the maximum errors are 0.07%, 0.5% and 0.07% for Gas constant R, isobaric heat capacity C_p and ratio of heat capacities γ respectively. Such small values of maximum error indicate close agreement between values in literature and tabulated data.

6.1.4 UK Natural Gas Fuel

Obtaining combustion properties of a specific natural gas may be a daunting task. This is because natural gases from different sources (even from the same country) will in most cases not be identical in as far as composition is concerned. However, it is possible to obtain natural gases with fairly similar/comparable compositions. Therefore, to validate the tabulated values of UK natural gas, the same were compared with the combustion properties of a natural gas presented by (Poferl et al., 1973). The compositions of the two natural gases composition are presented in Table 6.1. It is observed that apart from Methane, Ethane and Carbon dioxide, the other components compare fairly well. It needs to be re-stated that the purpose is not to check how well values of one natural gas compare to another but rather, if the tabulated values of UK natural gas are reasonable (and therefore dependable), even when compared to a natural gas with similar composition.

	Mole Fractions	
Component	**(Poferl et al., 1973)**	**UK Natural Gas**
Methane	0.875	0.926
Ethane	0.063	0.036
Propane	0.016	0.009
Butane	0.006	0.004
Pentane	0.002	0.003
Nitrogen	0.026	0.022
Carbon dioxide	0.012	

Table 6.1: Mole fractions of Natural gases

Comparisons were performed at a FAR of 0.01, a pressure of 20 atmospheres and temperatures ranging from 300[K] to 2800[K] in steps of 100 [K]. Figure 6.13, Figure 6.14, Figure 6.15 and Figure 6.16 are comparisons of the ratio of heat capacities γ, Gas constant R, isobaric heat capacity C_p and change in enthalpy, Δh, made between tabulated UK natural gas values and those obtained from (Poferl et al., 1973).

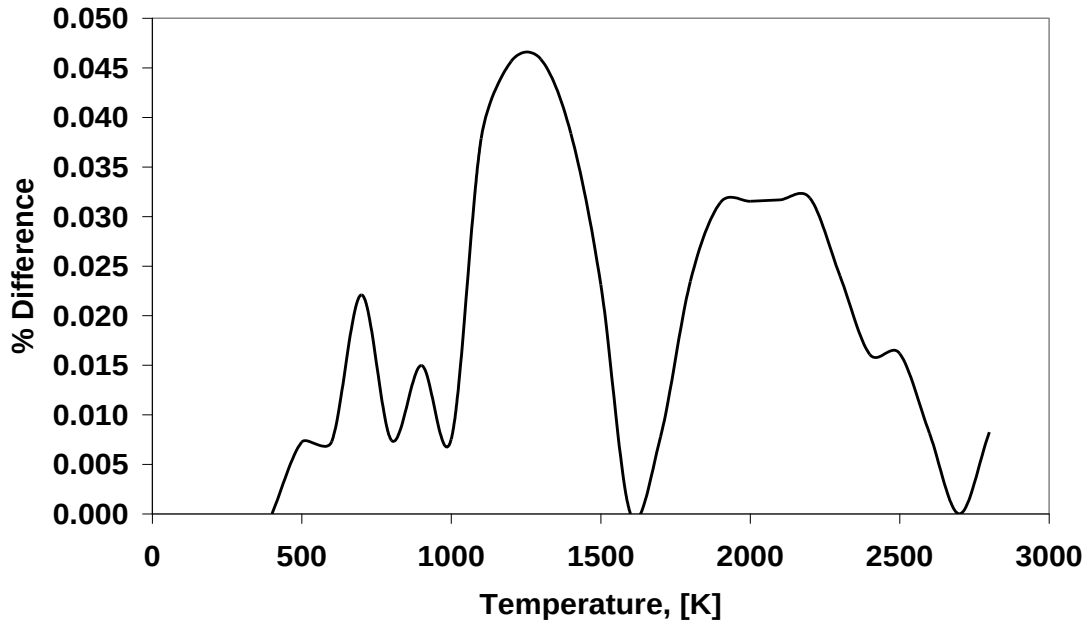

Figure 6.13: Comparison of ratio of heat capacities, UK Natural Gas Fuel, FAR 0.01, Pressure 20 Atm

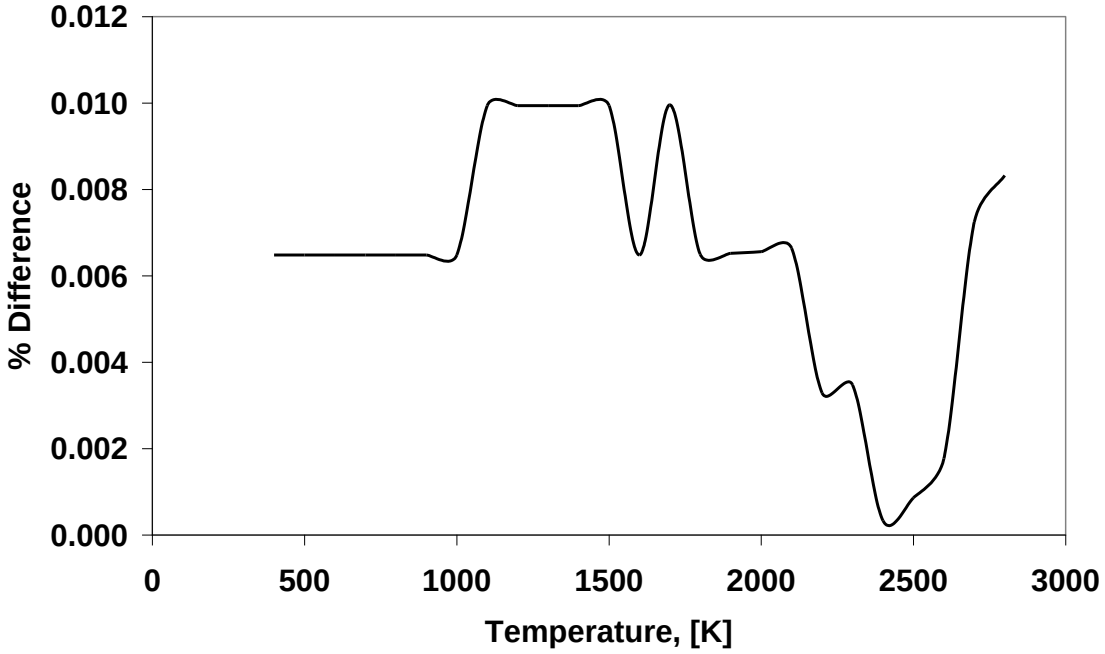

Figure 6.14: Comparison of Gas constant R, UK Natural Gas Fuel, FAR 0.01, Pressure 20 Atm

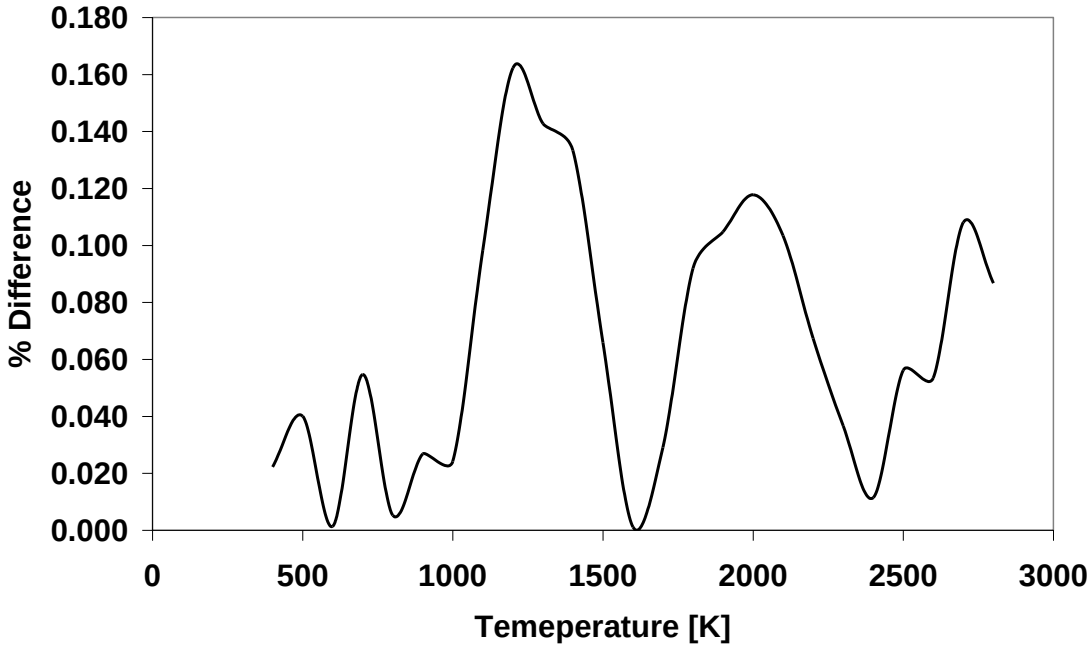

Figure 6.15: Comparison of isobaric heat capacity C_p, UK Natural Gas Fuel, FAR 0.01, Pressure 20 Atm

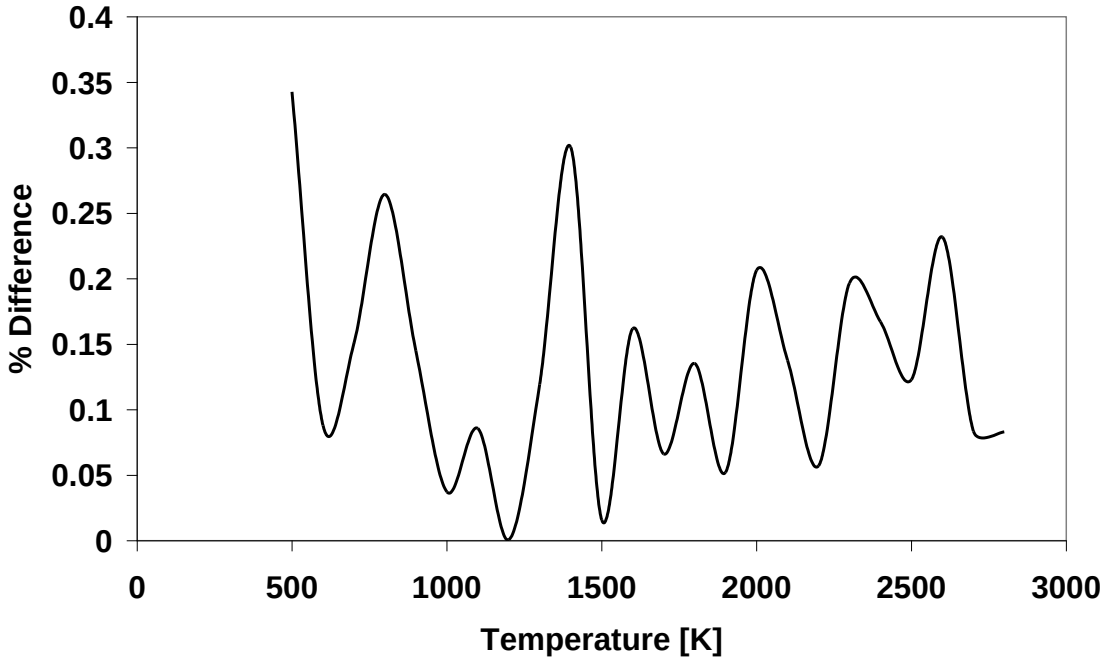

Figure 6.16: Comparison of ΔH, UK Natural Gas Fuel, FAR 0.01, Pressure 20 Atm

From Figure 6.13, Figure 6.14, Figure 6.15 and Figure 6.16, it is observed that the maximum percentage differences are 0.05 % for γ, 0.01 % for gas constant R, 0.16% for C_p and 0.35% for ΔH.

6.1.5 Diesel Fuel

(Gülder, 1988) presented empirical formulae by means of which the isobaric heat capacity, mean molecular weight and ratio of heat capacities of aviation fuel-air and diesel fuel-air systems can be calculated as functions of pressure, temperature, equivalence ratio and hydrogen-to-carbon atomic ratio of the fuel. The formulae were developed by fitting data from a detailed chemical equilibrium code to a functional expression. These formulae were used to obtain values of C_p, R and γ; subsequently, comparisons were made with

tabulated diesel-fuel data, for a FAR of 0.01 and pressure of 1 atmosphere and for temperature values of 500[K], 1000[K] and 1500[K].

Figure 6.17, Figure 6.18 and Figure 6.19 are the presentations of the percentage differences between tabulated diesel-fuel data and data obtained from (Gülder, 1988)

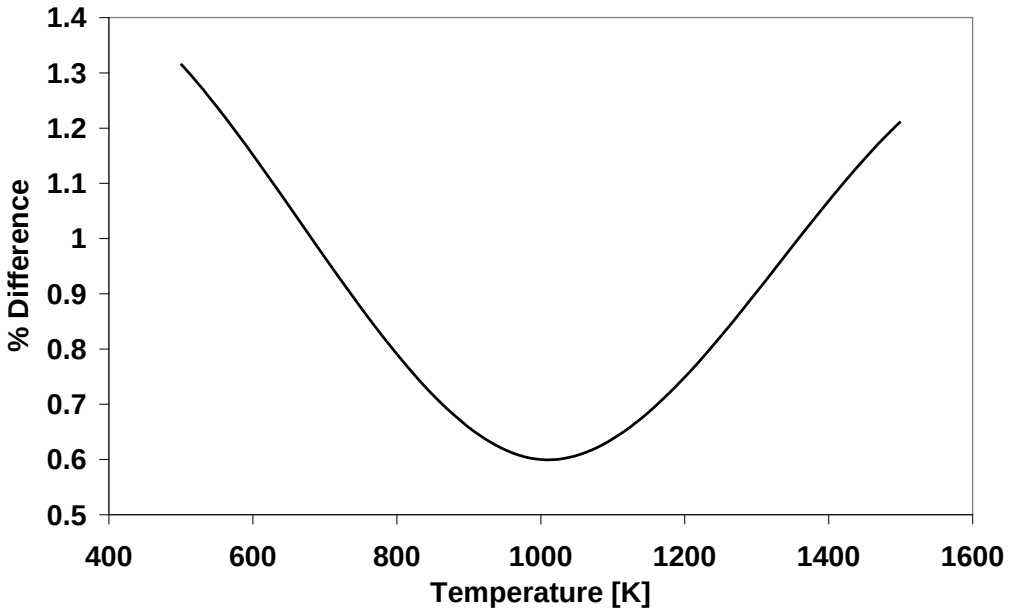

Figure 6.17: Comparison of Isobaric heat capacity C_p, diesel-fuel, FAR 0.01, Pressure 1 Atm

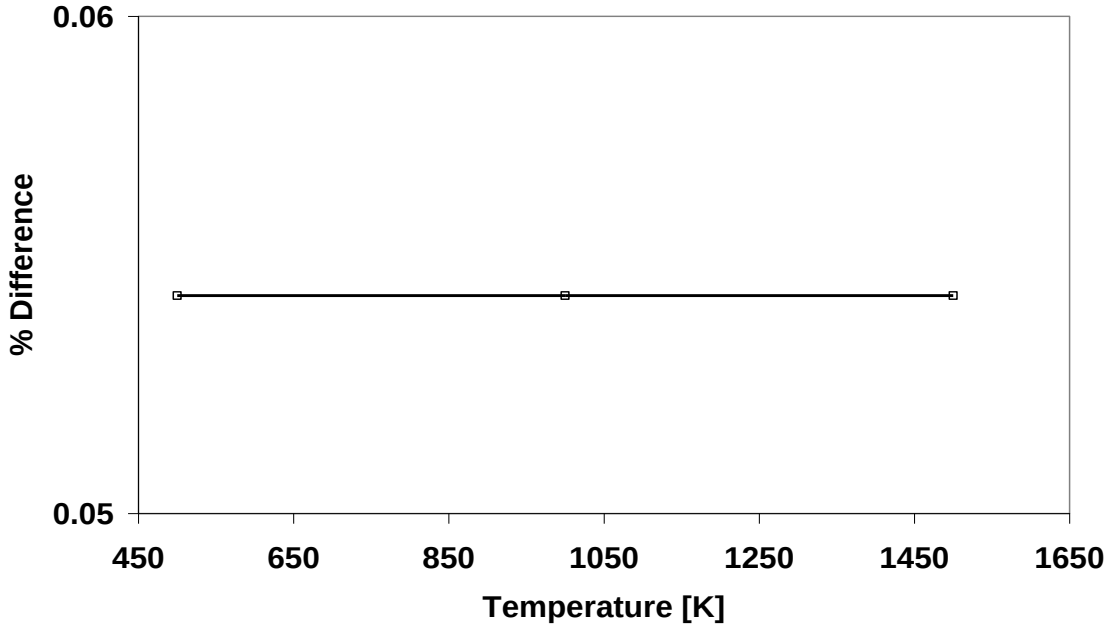

Figure 6.18: Comparison of Gas constant R, diesel-fuel, FAR 0.01, Pressure 1 Atm

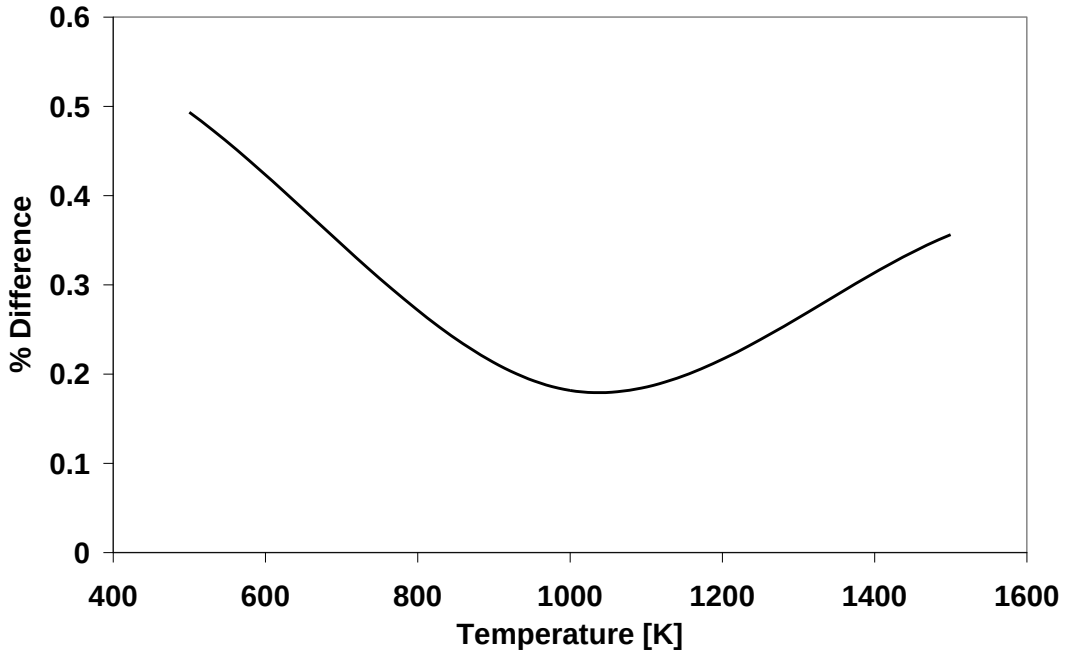

Figure 6.19: Comparison of ratio of heat capacities, diesel-fuel, FAR 0.01, Pressure 1 Atm

From Figure 6.17, Figure 6.18 and Figure 6.19, it is observed that maximum percentage differences are 1.3%, 0.05 % and 0.5 % for C_p, R and γ respectively.

6.1.6 Discussion of Fuel Data validation

It needs to be stated that the model used for this work will differ from the referenced models whose data was used for comparison; such differences will inevitably lead to percentage differences when combustion products are compared. One difference would be dissociation; if the referenced models did not consider dissociation (model used for this work considered dissociation), then the percentage differences between compared combustion properties will be large, for example, the dry air comparisons. Another difference would be the chemical composition of fuels considered; this would include Hydrogen-Carbon ratio of JetA and Diesel fuels and chemical composition and molar values of components of UK natural gas. Values used for JetA and Diesel in literature may not be identical to those used in this work, though any differences will be slight except in the case of UK natural gas.

Based on all the comparisons made in the previous section and considering all possible sources of percentage difference that have been mentioned, it can be concluded at this juncture that all the data presented in the fuel tables is dependable. Percentage differences between the same and values obtained from literature indicate that tabulated values are reasonable, that is, do not deviate significantly from data obtained from published sources. Therefore, the data can be used with confidence for further work. The selection of data points to be used with the interpolation routine now follows.

6.2 Data points selection criteria

Optimal data point selection was performed with the aim of optimising file-size and interpolation accuracy without compromising either one. File-size was an important consideration since large file sizes compromise computational speed. From experience, file sizes less than 30MB are not computationally burdensome; therefore, the aim was to keep file sizes below 30MB. To achieve this, optimal point selection was performed for each caloric property. The advantage of this method is that each caloric property will have just the right number of FARs, WARs, pressures and temperatures required to keep interpolation errors within 0.03 %.

The selection of points was done a dimension at a time, beginning with the temperature dimension (the four dimensions being Temperature, pressure, WAR and FAR).

6.2.1 Temperature

The initial temperature distribution was based on work by (Sethi V., 2008) who developed gas property tables using NASAs' Chemical equilibrium program (Gordon, 1994). This model employed linear interpolation between values for FAR, WAR, temperature and a fixed pressure of 50 bars. In this model, the temperature distribution was 200 [K] to 3000 [K] in steps of 50 [K]. This temperature distribution was deemed by (Sethi V., 2008) to be sufficient since only one pressure was considered; that is, dissociation at low pressures was not an issue. However, in light of dissociation at high temperatures and low pressures and subsequent interpolation accuracy, the temperature distribution was reviewed.

Figure 6.20 is a graph of comparisons of the dissociation and no-dissociation models for the Enthalpy, h of dry air.

From Figure 6.20 it can be observed that:

1. In the no-dissociation model, pressure makes no difference; the 1 Atm and 0.1 Atm lines are super-imposed upon each other;

2. Effects of dissociation are pronounced at high temperatures and low pressures; this is observed in the non-linearity of the 0.1 Atm pressure line. The reasons for this were discussed in an earlier chapter. It would be expected that at even lower pressures such as steam turbine exit pressures of 0.04 Atm, the effects of dissociation would be even more pronounced.

Therefore, in the interest of interpolation accuracy at high temperatures and low pressures, the temperature distribution above was reviewed; at temperatures above 2000 [K] the intervals were reduced to 25 [K]. This was sufficient to address non-linearity due to dissociation.

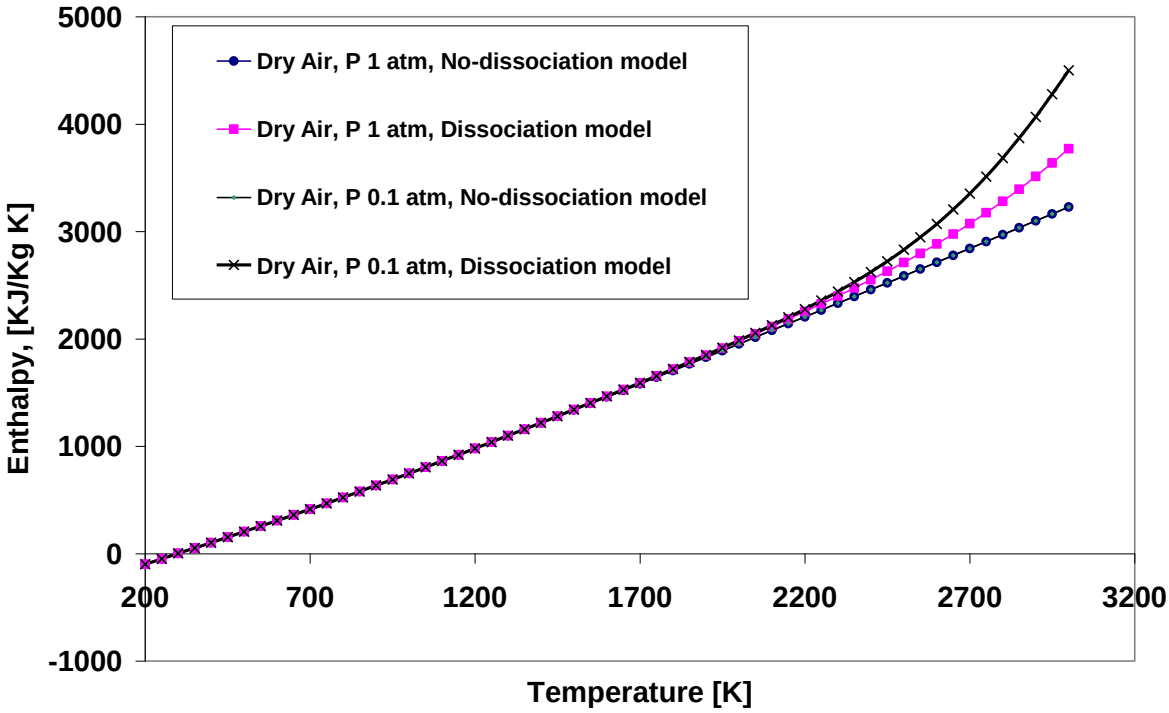

Figure 6.20: Comparing dissociation and no-dissociation models, Enthalpy of dry air

Figure 6.21 and Figure 6.22 are graphs of density and entropy of dry air, respectively, and at pressures of 1, 5 and 50 atmospheres. It is observed that for both properties, there exists a non-linearity at the initial temperature points, which then progresses into linearity. For density, this non-linearity becomes pronounced with increasing pressure. Therefore, to account for this non-linearity, the temperature distribution between 200 [K] and 400[K] was reviewed; the intervals between this temperatures were reduced to 25 [K], to account for the non-linearity of density and entropy properties.

To further improve interpolation accuracy, the interpolation algorithm utilised the Logarithm [base 10] of temperature as opposed to the actual value of temperature. Figure 6.23 and Figure 6.24 are plots of density and entropy respectively, for dry air, plotted against the logarithm of temperature as opposed to the actual temperature values. Compared to the plots of the actual values of temperature, (Figure 6.21 and Figure 6.22) it is observed that using the logarithm of temperature decreases non-linearity. This significantly improves interpolation accuracy.

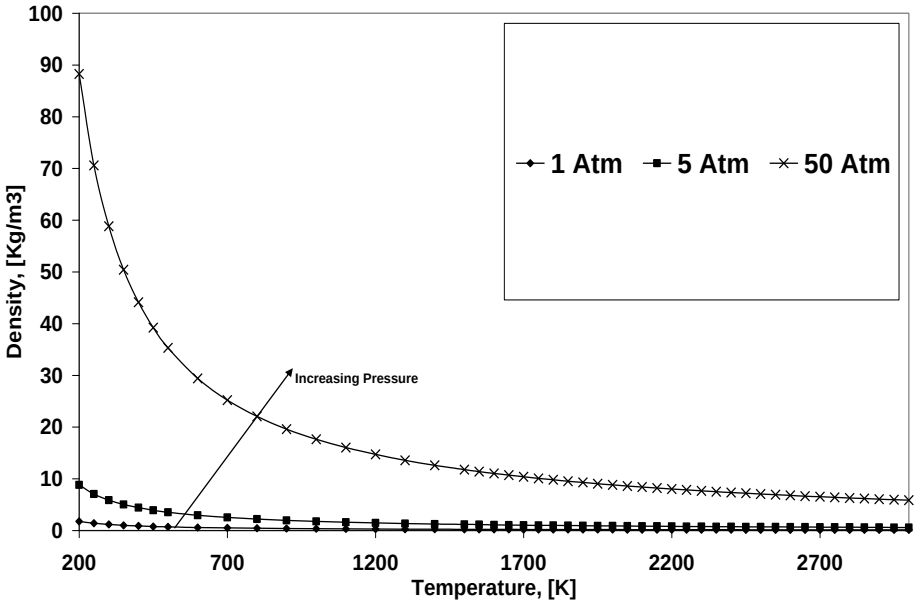

Figure 6.21: Density of dry air at various pressures

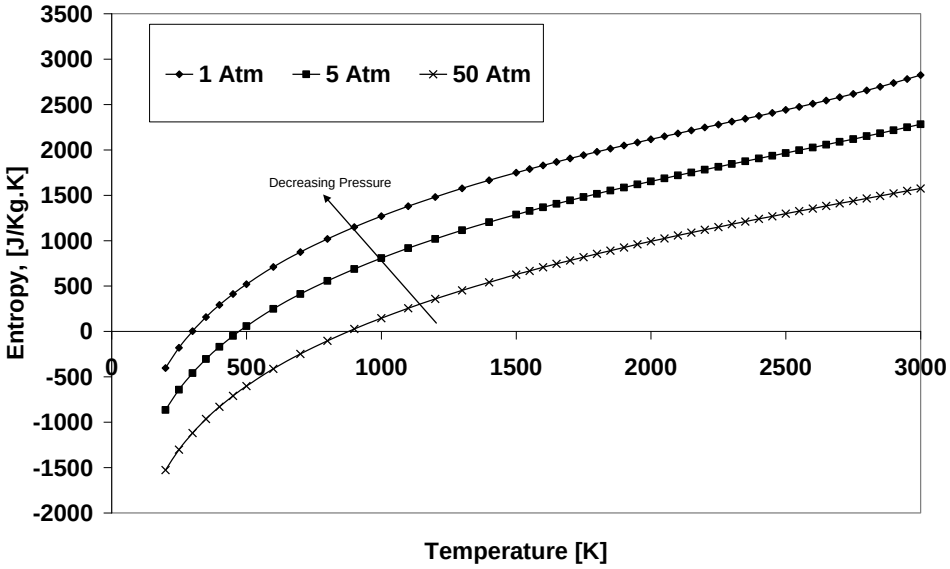

Figure 6.22: Entropy of dry air at various pressures

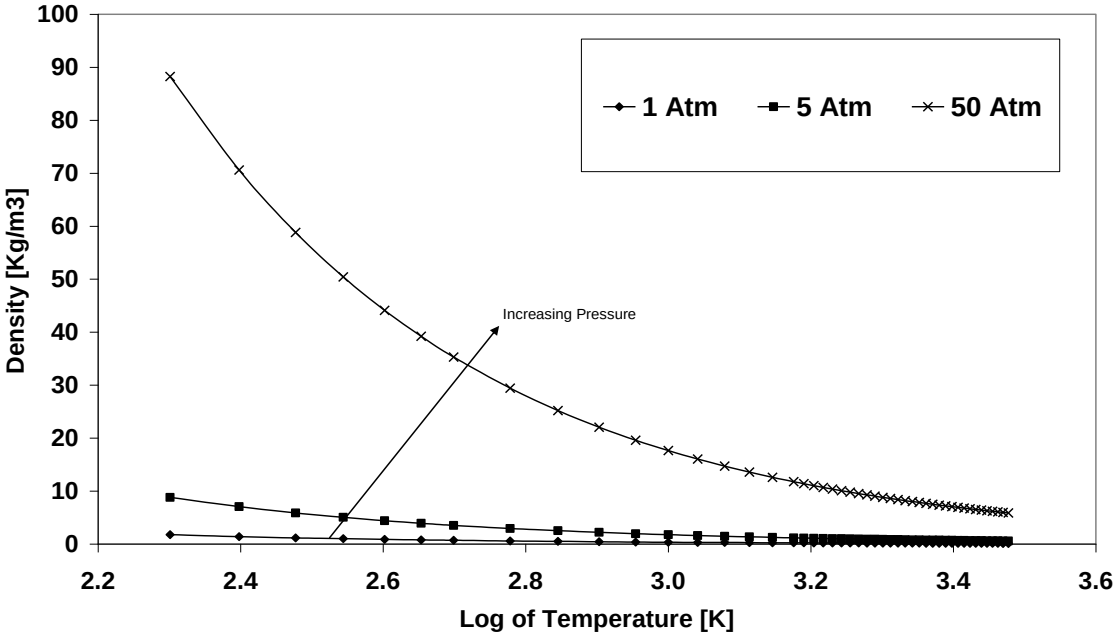

Figure 6.23: Plot of density against Logarithm of temperature, dry air

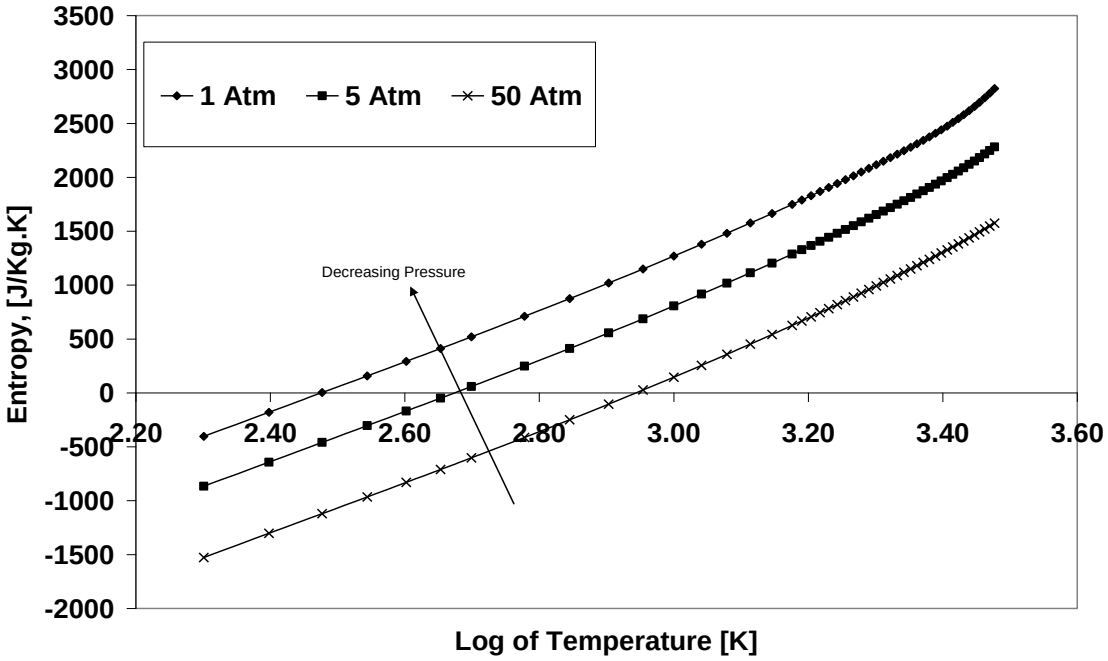

Figure 6.24: Plot of Entropy against logarithm of temperature, dry air

It needs to be stated that adding this extra temperatures did not reduce computational speed. With reference to Table 6.2, it can be observed that adding FARs is computationally expensive, since this implies adding all the WARs, Pressures and temperatures that form that particular FAR. Adding WARs is also computationally expensive as this implies adding all temperatures and pressures that form that WAR. Adding pressures is affordable depending on the number of pressures being added since this implies adding tables of temperatures (such as that presented in Appendix 1). Finally, adding temperatures implies adding lines to each individual pressure table; from experience, this does not add much to overall file-size. Therefore, well spaced temperatures can serve to eliminate the need to add pressure lines to improve interpolation accuracy.

Temperatures	Pressures	WARs	FARs
w number of temperatures form 1 pressure	*x* number of pressures form 1 WAR	*y* number of WARS form 1 FAR	All FARS combined form 1 Fuel-table

Increasing file-size ⟶

Table 6.2: Structure of fuel tables

Where,

- w, x, y and z are integers

The total number of temperatures (per table) was 75. Table 6.3 presents the summary of temperature distribution points.

Temperature Range, [K]	Explanation
198 – 199	Boundary points for the interpolation of temperatures $\leq$ 225 [K]
200 – 400, in steps of 25K	Takes care of the non-linearity of Density and Entropy caloric properties
400-1500 in steps of 100 K	Most properties exhibit linear properties at this range, hence, no need for concentrated temperature points.
1500-2000 in steps of 50K	Effects of dissociation begin to become pronounced, hence a reduction in temperature intervals to account for this.
2000-3000 in steps of 25 K	Takes care of pronounced effects of dissociation, that is, non-linearity.
3025-3050	Boundary points for the interpolation of temperatures $\geq$ 2975 K

Table 6.3: Distribution of temperature points for fuel tables

6.2.2 Pressure

As discussed in earlier sections, pressure plays a role in dissociation. Lower pressures favour dissociation than higher pressures. This can be observed in Figure 6.25 which is a plot of enthalpy of dry air at various pressures. The 50 atmosphere pressure line is close to the 200 atmosphere pressure line; both lines maintain some degree of linearity throughout the 200[K] to 3000 [K]

temperature range. Below 1 atmosphere, non-linearity that is caused by dissociation becomes pronounced.

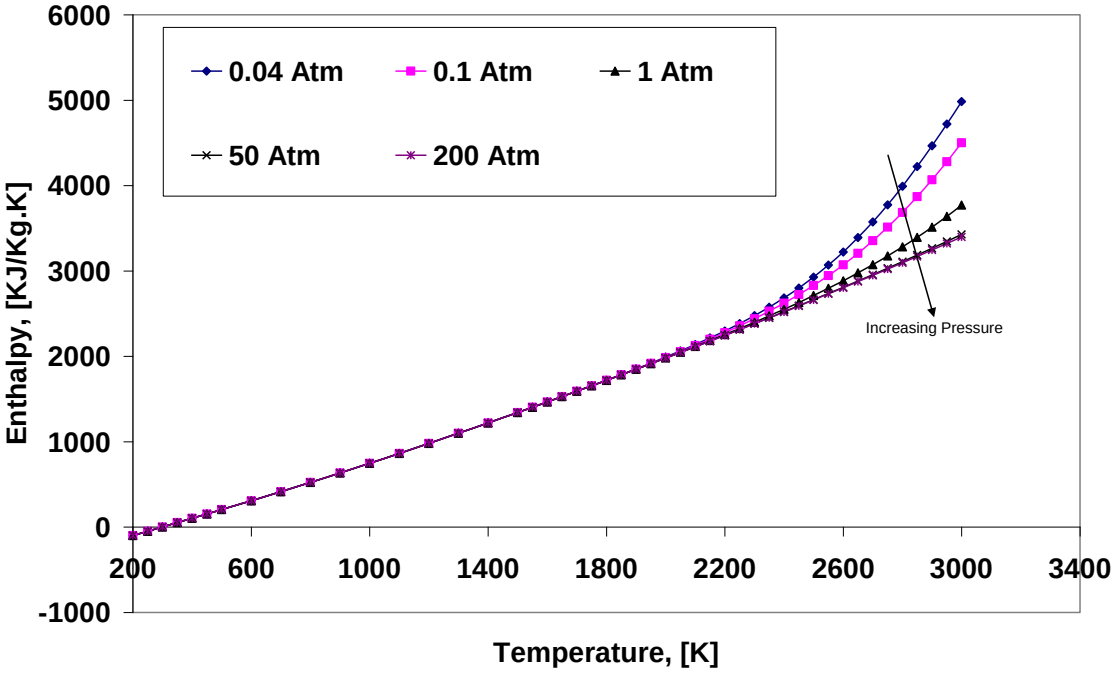

Figure 6.25: Influence of pressure on Enthalpy of dry air

Therefore when assigning pressure values, attention was given to the lower pressure values (pressures below 1 atmosphere).

The methodology used was thus:

1. Starting with 5 pressure values (in atmospheres) of 0.02, 0.2, 2, 20 and 200.
2. Since maximum interpolation error is in the middle of two points, then interpolation of respective caloric properties was carried out in between all pressure and temperature points and interpolation errors noted.
3. An interpolation error threshold was set as 0.03%; that is, the maximum allowable interpolation error. For all caloric properties except enthalpy, *h*

and entropy, *s*, the % error value was defined as relative error, presented in Equation 6.2

$$\%\, error = \left| \frac{GP_{\text{interpolated}} - GP_{\text{actual}}}{GP_{\text{actual}}} \right| \times 100 \qquad \textbf{(6.2)}$$

For entropy *s,* and enthalpy *h:* with reference to Figure 6.22 and Figure 6.25, it is observed that the pressure lines at some point cross the x axis. At this point on the x axis, the corresponding value on the y axis (enthalpy or entropy) would be zero (or a very small value). In such a situation, Equation 6.2 would fail since it would be a case of division by zero. In addition, if the value of GP_{actual} is significantly small, then the % error defined in Equation 6.2 will be large and in most cases greater than 0.03%. This is notwithstanding the fact that the absolute error, ($GP_{interpolated}$ - $Gp_{actual)}$ may be reasonably small Consider the case in Table 6.4 where the entropy of dry air was interpolated for the given temperatures and a pressure of 0.35 atmospheres.

It is observed that for 212.5 [K], even though the absolute error is slightly less than that of the value at 2512.5 [K], the relative error is however much larger and even unacceptable.

	T, 212.5 [K]	T, 2512.5 [K]
Gp_{actual} [J/Kg.K]	41.98	2767.9
$GP_{interpolated}$ [J/Kg.K]	42.2	2767.65
Absolute error, %	0.213	0.25
Relative error, %	0.504	0.009

Table 6.4: Relative and absolute errors of dry air at 0.35 atmospheres

Therefore, for enthalpy and entropy, a different definition of relative error was used and is presented in Equation 6.3.

$$\%\ error = \left| \frac{GP_{\text{interpolat ed}} - GP_{\text{actual}}}{GP_{\max}} \right| \times 100 \qquad \textbf{(6.3)}$$

Where,

- GP_{max} is the maximum value of enthalpy or entropy, that is, the value of enthalpy (or entropy) at the highest temperature, for a particular FAR, WAR and pressure.

4. If the interpolation error was found to be larger than 0.03%, then pressure values were added in between the two pressure points that demonstrated large interpolation errors. For example, between 2 and 20 atmospheres is 11 atmospheres. If interpolating for 11 atmospheres (and all in-between temperatures) produces interpolation errors greater than 0.03%, then a pressure of 11 atmospheres is added. The test then will be for pressures of 6.5 (between 2 and 11) and 15.5 (between 20 and 11) atmospheres. This was carried on until all caloric properties were within the 0.03 % interpolation error threshold.

The advantage of the aforementioned method is that each caloric property will have just the right number of pressures required for accurate interpolation, without redundancy. Any extra pressures may serve to reduce the interpolation error but at the cost of reduced computational speed. Therefore, the method presented produces computationally efficient file sizes.

Appendix 2 provides figures of interpolation errors of dry air for all caloric properties. From this plots, it is clear that interpolation error of mid-way temperature and pressure points are all below 0.03 %.

At this juncture, the specific pressures are not provided since it was anticipated that more may be added, to reduce interpolation errors during selection of WAR and FAR points. Therefore, all pressure points will be provided for each caloric

property after selection of WAR and FAR points has been presented (along with FAR and WAR points). The following section provides the selection criteria of WAR and FAR points.

6.2.3 FAR and WAR

WAR points were added onto the dry air points to produce moist air files. The method used was as follows:

1. Starting with five points, 0, 0.001, 0.025, 0.05, 0.075, 1, where the points 0, 0.001 and 1 are boundary points and 0.025, 0.05 and 0.075 are points at 25%, 50 % and 75%, respectively.

2. Interpolation was then performed in between each WAR, pressure and temperature for respective caloric properties and interpolation errors noted. If the interpolation error was greater than 0.03 %, then either a WAR or pressure was added, depending on which was more computationally efficient. That is,

$$P_{total,p} = nWAR \times P_{added} \quad \textbf{(6.4)}$$

And,

$$P_{total,war} = nWAR_{added} \times P \quad \textbf{(6.5)}$$

Where,

- $P_{total,p}$ is the total number of pressures after adding pressures to improve interpolation accuracy (as opposed to adding water-to-air ratios).
- nWAR are the number of Water to air ratios.
- P_{added} is the number of pressures that would need to be added to improve interpolation accuracy.

- $P_{total,war}$ is the total number of pressures after adding water-to-air ratios to improve interpolation accuracy (as opposed to adding pressures).

- $nWAR_{added}$ is the number of water-to-air ratios that would need to be added to improve interpolation accuracy.

- P is the number of pressures per water-to-air ratio.

Then, if $P_{total,p} < P_{total,war}$ then adding pressures is preferable to adding water--to-air Ratios. Else, adding water-to-air ratios would be preferable (file size being the issue of interest) to adding pressures.

This methodology was adopted for all caloric properties. In the case where pressures were added to reduce interpolation error (as opposed to adding a WAR), then that would lead to reduced interpolation errors of dry air (since there are now more pressures available than previously).

WAR, values were considered up to 0.95 with an additional value of 0.1 for interpolation. Any interpolation performed for values between 0.95 and 0.1 would have errors greater than 0.03% since the interpolation routine would be using 3 points prior to the interpolant and 1 point after the interpolant, as opposed to the method used to define the method, that is, two points before and two points after the interpolant. The assumption was made that for gas turbine calculations, most WAR values would be less than 0.95. In addition, a lack of a WAR point beyond 0.1 served to keep file sizes small.

The same methodology of selection of WAR points was adopted for selection of FAR points. That is, starting with 5 FAR points, 0, 0.001, 0.025, 0.05 and Stoichiometric; in-between values were then added where interpolation errors were greater than 0.03%. (Interpolation being performed midway between FAR, WAR, pressure and temperature points). These points were added onto the now selected temperature, pressure and WAR points

In addition, for FAR, only values up to stoichiometric were considered, with an additional FAR point of [1.8 $\times$ Stoichiometric], for *rich-burn, quick-mix, lean-burn* combustors (Tacina, 1990). Therefore, any interpolation performed for values between stoichiometric values and [1.8 $\times$ Stoichiometric], may have errors greater than 0.03%. The assumption that was made was that for gas turbine calculations, there will be no need to interpolate within this region, that is, between stoichiometric and [1.8 $\times$ Stoichiometric] since most applications will be either lean-burn (below stoichiometric), stoichiometric or at [1.8 $\times$ Stoichiometric]. The exclusion of values in this region served to keep file sizes minimal and thus computationally efficient.

As a reminder, the values of stoichiometric and [1.8 $\times$ Stoichiometric] for respective FARs are presented in Table 6.5. The 'Max FAR' values are the same as [1.8 $\times$ Stoichiometric].

	UK Natural Gas	Jet-A	Hydrogen	Diesel
$FAR_{stoichiometric}$	0.063	0.068	0.029	0.069
Max FAR	0.113	0.123	0.052	0.124

Table 6.5: Stoichiometric and maximum FARs for the 4 considered fuels

Appendices 3, 4, 5 and 6 are the plots of interpolation error for moist and fuelled air for mid-points of FAR, WAR, Pressure and temperature; from this plots, it is clear that all errors are within 0.03 %. Due to space limitations, only selected graphs (of interpolation error) are presented.

Having completed selection of all temperature, pressure, WAR and FAR points, they may now be presented. The temperature points are the same for all caloric properties and for all fuels and are already presented in Table 6.3. Table 6.6 to Table 6.12 present the FARs, WARs and Pressure points for each caloric property. These were the final points used to build respective fuel tables for

interpolation. From these tables, the advantages of optimal point selection are oberved.

1. For instance, density requires only 5 WARs as opposed to C_p which requires 15, for interpolation accuracy $\leq$ 0.03%. This is because density is not as sensitive to moisture as isobaric heat capacity, C_p. Therefore, using the same number of WARs for both properties would have served to reduce the accuracy of C_p and in addition, would have provided redundant points for density. This redundancy is what contributes to large file sizes which are computationally burdensome.

2. Gas-constant, R and Viscosity μ require less pressure points than all other caloric properties. Therefore, using the same number of pressure points for all properties would have served to place redundant points for R and μ; this would have served to further improve interpolation accuracy for R and μ but at the expense of computational efficiency (larger file sizes than necessary).

FAR				WAR	Pressure, Atm
Jet-A 12 points	UK Natural Gas 12 points	Hydrogen Fuel 8 points	Diesel 14 points	5 points	30 points
0	0	0	0	0	0.021
0.001	0.001	0.001	0.001	0.001	0.022 0.036
0.013	0.007	0.007	0.007	0.05	0.05 0.1
0.025	0.013	0.005	0.013	0.095	0.2 0.5
0.0375	0.025	0.013	0.025	0.1	0.625 1
0.05	0.0375	0.025	0.0375		1.5 2
0.06	0.05	0.029	0.05		2.75 3.5
0.062	0.06	0.052	0.055		5 6.25
0.064	0.061		0.06		7.5 10
0.066	0.062		0.062		12.5 15
0.068	0.063		0.064		17.5 30
0.123	0.113		0.066		50 80
			0.069		112.5 137.5
			0.124		167.5 187.5
					200 201
					202

Table 6.6: FAR, WAR and Pressure points for interpolation, density

FAR				WAR	Pressure, Atm
Jet-A 12 points	UK Natural Gas 11 points	Hydrogen Fuel 7 points	Diesel 12 points	11 points	31 points
0	0	0	0	0	0.021
0.001	0.001	0.001	0.001	0.001	0.022 0.036
0.013	0.013	0.005	0.013	0.00325	0.05 0.0635
0.025	0.025	0.013	0.025	0.0055	0.075 0.0875
0.0375	0.0375	0.025	0.05	0.01	0.1 0.125
0.05	0.05	0.029	0.055	0.025	0.15 0.175
0.06	0.06	0.052	0.06	0.05	0.2 0.275
0.062	0.061		0.062	0.075	0.35 0.425
0.064	0.062		0.064	0.0875	0.5 0.625
0.066	0.063		0.066	0.095	0.75 1
0.068	0.113		0.069	0.1	1.5 2
0.123			0.124		3.5 5
					7.5 10
					20 100
					150 200
					201 202

Table 6.7: FAR, WAR and Pressure points for interpolation, Enthalpy

FAR				WAR	Pressure, Atm
Jet-A 12 points	UK Natural Gas 11 points	Hydrogen Fuel 7 points	Diesel 13 points	11 points	40 points
0	0	0	0	0.0	0.021
0.001	0.001	0.001	0.001	0.001	0.022 0.026
0.013	0.013	0.005	0.013	0.002125	0.03 0.0325
0.025	0.025	0.013	0.025	0.0055	0.035 0.04
0.0375	0.0375	0.025	0.0375	0.01	0.045 0.05
0.05	0.05	0.029	0.05	0.025	0.0625 0.075 0.1
0.06	0.06	0.052	0.055	0.05	0.125 0.15
0.062	0.061		0.06	0.075	0.2 0.275
0.064	0.062		0.062	0.0875	0.35 0.425
0.066	0.063		0.064	0.095	0.5 0.625 0.75
0.068	0.113		0.066	0.1	1 1.25
0.123			0.069		1.5 2
			0.124		2.75 3.5
					5 7.5
					10 15
					20 40
					60 100
					150 175
					200 201
					202

Table 6.8: FAR, WAR and Pressure points for interpolation, Entropy

FAR				WAR	Pressure, Atm
Jet-A 12 points	UK Natural Gas 13 points	Hydrogen Fuel 10 points	Diesel 14 points	15 points	40 points
0	0	0	0	0.0	0.021
0.001	0.001	0.001	0.001	0.001	0.022 0.026
0.013	0.007	0.0025	0.013	0.0015	0.03 0.0325
0.025	0.013	0.004	0.025	0.002	0.035 0.04
0.0375	0.025	0.0055	0.0375	0.003	0.045 0.05
0.05	0.0375	0.007	0.05	0.005	0.0625 0.075
0.06	0.05	0.013	0.055	0.01	0.1 0.125
0.062	0.055	0.025	0.06	0.025	0.15 0.2
0.064	0.06	0.029	0.062	0.0375	0.275 0.35
0.066	0.061	0.052	0.064	0.05	0.425 0.5
0.068	0.062		0.066	0.0625	0.625 0.75
0.123	0.063		0.069	0.075	1 1.25
	0.113		0.124	0.0875	1.5 2
				0.095	2.75 3.5
				0.1	5 7.5
					10 15
					20 40
					60 100
					150 175
					200 201
					202

Table 6.9: FAR, WAR and Pressure points for interpolation, C_p

FAR				WAR	Pressure, Atm
Jet-A 9 points	UK Natural Gas 9 points	Hydrogen Fuel 7 points	Diesel 11 points	11 points	19 points
0	0	0	0	0.0	0.021
0.001	0.001	0.001	0.001	0.001	0.022 0.0415
0.025	0.025	0.005	0.013	0.00325	0.061 0.0805
0.05	0.05	0.013	0.025	0.0055	0.1 0.2
0.06	0.06	0.025	0.055	0.01	0.5 1
0.062	0.061	0.029	0.06	0.025	2 10
0.064	0.062	0.052	0.062	0.05	20 100
0.068	0.063		0.064	0.075	150 175
0.123	0.113		0.066	0.0875	185 200
			0.069	0.095	201 202
			0.124	0.1	

Table 6.10: FAR, WAR and Pressure points for interpolation, ratio of heat capacities

FAR				WAR	Pressure, Atm
Jet-A 8 points	UK Natural Gas 9 points	Hydrogen Fuel 7 points	Diesel 9 points	8 points	15 points
0	0	0	0	0.0	0.021
0.001	0.001	0.001	0.001	0.001	0.022 0.05
0.013	0.013	0.005	0.013	0.01	0.1 0.2
0.025	0.025	0.013	0.025	0.025	0.6 1
0.05	0.05	0.025	0.05	0.05	2 10
0.06	0.06	0.029	0.06	0.075	20 100
0.068	0.062	0.052	0.064	0.0875	150 200
0.123	0.063		0.069	0.1	201 202
	0.113		0.124		

Table 6.11: FAR, WAR and Pressure points for interpolation, Gas constant R

FAR				WAR	Pressure, Atm
Jet-A 8 points	UK Natural Gas 9 points	Hydrogen Fuel 7 points	Diesel 9 points	8 points	15 points
0	0	0	0	0.0	0.021
0.001	0.001	0.001	0.001	0.001	0.022 0.05
0.013	0.013	0.005	0.013	0.01	0.1 0.2
0.025	0.025	0.013	0.025	0.025	0.6 1
0.05	0.05	0.025	0.05	0.05	2 10
0.06	0.06	0.029	0.06	0.075	20 100
0.068	0.062	0.052	0.064	0.0875	150 200
0.123	0.063		0.069	0.1	201 202
	0.113		0.124		

Table 6.12: FAR, WAR and Pressure points for interpolation, Viscosity

Having validated the respective fuel data by comparing to published data and having chosen computationally efficient and accurate points for FAR, WAR, Pressure and temperature, the fuel tables could then be used together with the non-linear Spline interpolation algorithm, to run gas turbine simulation case studies. These are presented in the following section.

6.3 Case studies

In this section, the validated fuel data tables are used for case studies in an attempt to demonstrate their accuracy in gas turbine performance simulation. The non-linear interpolation routine in conjunction with the fuel data were used to run compression (dry and moist air) and expansion cases for three fuels, JET-A, Diesel and Hydrogen. The results obtained were compared with those obtained from a gas property model developed by (Mucino, 2007) based on polynomials developed by (Bücker, 2003). In addition, the non-linear interpolation results were compared to a model that employed a linear interpolation model, using the same fuel tables. NASAs' CEA software (Gordon and McBride, 1994) was used to calculate the baseline values, against which the performance calculations were compared. The performance parameters that were used for comparison are Compressor exit temperature and Compressor work for dry and moist air, Turbine exit temperature and Turbine work for Jet-A, Hydrogen and Diesel. The presentation of results now follows.

6.3.1 Case study 1: Compressor calculation, dry air

To demonstrate the effectiveness of the developed multi-fuel performance model, a compressor case was run for dry air. The compressor calculation is based on entropy change. The pressure rise is calculated as:

$$P_{out} = P_{in} \times PR \tag{6.6}$$

Where,

- P_{out} is the compressor exit pressure
- P_{in} is the compressor inlet pressure
- PR is the pressure ratio

Ideal conditions (ideal compressor exit temperature) were calculated from the entropy function, ϕ

$$\phi_{out,ideal} - \phi_{in} = R.\ln.PR \quad \textbf{(6.7)}$$

Where,

- R is the gas constant
- ϕ is the entropy function.

Based on the ideal conditions, ideal enthalpies were interpolated for from the fuel tables. Then based on the definition of isentropic efficiency presented in Equation 6.8, the temperature at compressor exit is calculated.

$$\eta_{is} = \frac{h_{exit,ideal} - h_{inlet}}{h_{exit} - h_{inlet}} = \frac{T_{exit,ideal} - T_{inlet}}{T_{exit} - T_{inlet}} \quad \textbf{(6.8)}$$

Where,

- T is the temperature
- h is the enthalpy

Therefore, compressor work, CW is given by,

$$CW = w\left(h_{exit} - h_{inlet}\right) \quad \textbf{(6.9)}$$

Where,

- w is the mass flow rate, Kg/s

Table 6.13 presents the parameters for the dry-air compressor calculation.

T_{inlet} [K]	288.15
P_{inlet} [Atm]	0.979
PR	10.459
FAR	0
WAR	0
$\eta_{compressor}$	0.78
W [Kg/s]	4.05

Table 6.13: Case parameters, compressor calculation, dry air

Table 6.14 and Figure 6.26 are the presentation of results for the dry air compressor calculation case. From these tables, it is observed that the non-linear interpolation method provides the best results for compressor exit temperature, T_2 and compressor work. The model by (Mucino, 2007) provides the least accurate results. The results provided by the linear interpolation method are close to those provided by the model by (Mucino, 2007) for both compressor exit temperature and compressor work.

	T_{exit} [K]	Compressor Work, [KW]
Actual Value	633.147	1415.4
Linear interpolation	638.9	1449.1
Non-linear interpolation	632.912	1415.259
(Mucino, 2007)	639.288	1450.083

Table 6.14: Comparison of Dry Air Compression simulation results

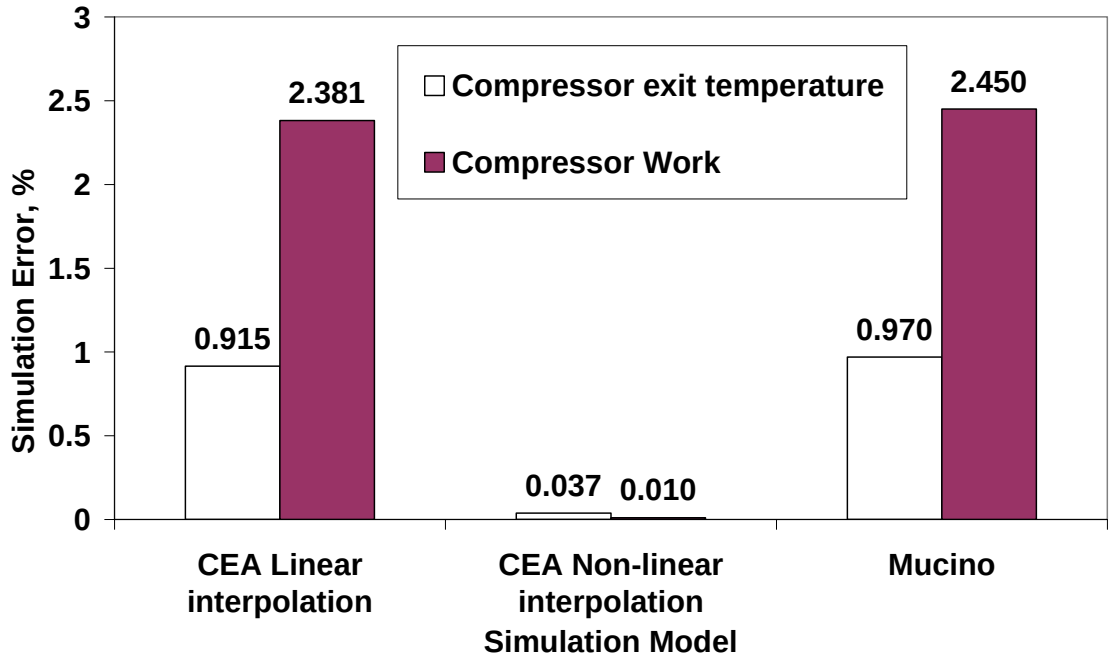

Figure 6.26: Comparison of simulation % errors for $T_{compressor\ exit}$ and Compressor work, dry air.

6.3.2 Case study 2: Compressor calculation, moist air

Case study 2 involves including moisture into the compression calculation. The case parameters are presented in Table 6.15.

T_{inlet} [K]	288.15
P_{inlet} [Atm]	0.979
PR	10.459
FAR	0
WAR	0.00618
$\eta_{compressor}$	0.78
W [Kg/s]	4.05

Table 6.15: Case parameters, compressor calculation, moist air

Table 6.16 and Figure 6.27 are the presentation of the moist air compressor calculations; from these, it is observed that the non-linear interpolation method gives the best results in terms of simulation error, when compared with linear interpolation and (Mucino, 2007) model. In addition, the errors provided by (Mucino, 2007) model have increased (when compared to dry air). However, the non-linear interpolation method remains consistent.

	$T_{exit,compressor}$ [K]	Compressor Work, [KW]
Actual Value	632.306	1419.53
Linear interpolation	629.594	1436.08
Non-linear interpolation	632.41	1419.67
(Mucino, 2007)	639.27	1457.98

Table 6.16: Comparison of moist air compression simulation results.

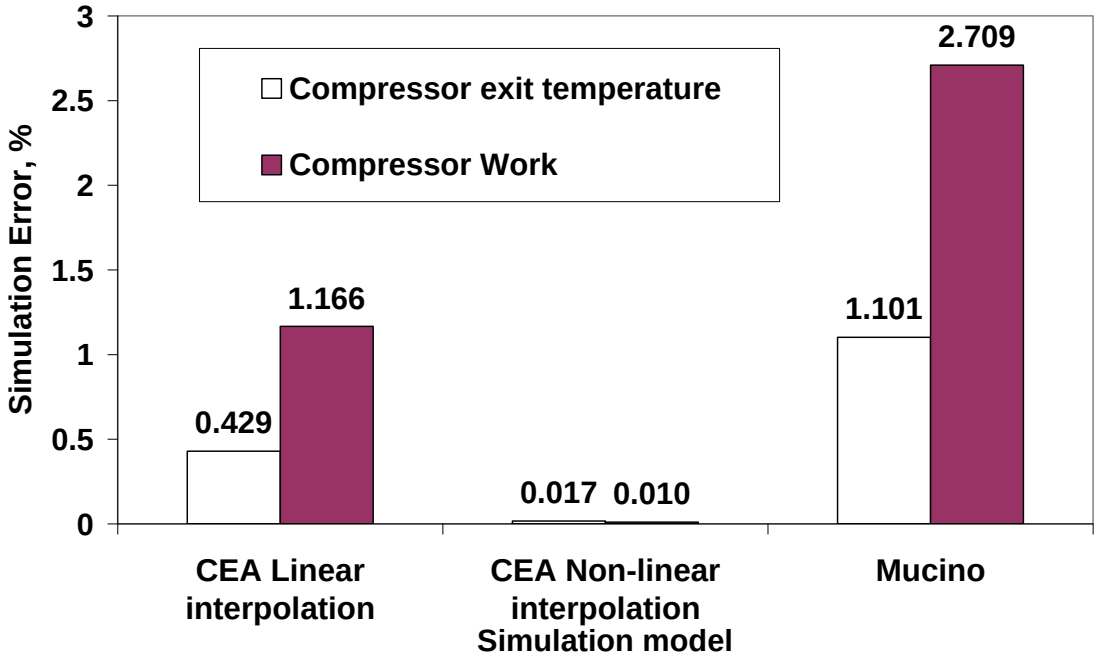

Figure 6.27: Comparison of simulation % errors for $T_{compressor\ exit}$ and Compressor work, moist air.

6.3.3 Case study 3: Compressor turbine calculation, Jet-A Fuel

The multi-fuel simulation method was also applied to compressor turbine calculation, using Jet-A as the fuel. Equation 6.8 can be modified for turbine calculation (expansion) as,

$$\eta_{is} = \frac{h_{inlet} - h_{outlet}}{h_{inlet} - h_{outlet,ideal}} = \frac{T_{inlet} - T_{exit}}{T_{inlet} - T_{ideal}} \quad \textbf{(6.10)}$$

The turbine TW, work can then be obtained as,

$$TW = w\left(h_{inlet} - h_{exit}\right) \quad \textbf{(6.11)}$$

Table 6.17 presents the parameters for the turbine calculation case with Jet-A as the fuel.

TET [K]	1397.02
P_{inlet} [Atm]	30.57
PR	0.261
FAR	0.0217
WAR	0.00618
$\eta_{turbine}$	0.865
W [Kg/s]	4.07

Table 6.17: Case parameters, compressor turbine calculation, Jet-A

The results obtained after running the turbine calculations are presented in Table 6.19 and Figure 6.28 for both turbine exit temperature and turbine work. It is observed that once again, the non-linear interpolation method gives the most accurate results. In addition, the results provided by the model by (Mucino, 2007) seem to be increasing in error, with increase in FAR (that is, the errors for Jet-A are greater than those of dry and moist air). This is further

confirmed by running another case for Jet–A fuel with parameters provided in Table 6.18, where FAR, WAR and TET have been increased to 0.0615, 0.053 and 1547.5 [K] respectively. The results of this are provided in Table 6.20 and Figure 6.29 where it is observed that results provided by the model by (Mucino, 2007) are unacceptably large. The author is of the inclination that at such high FAR and temperatures, dissociation could be playing a role in this large error; this model (Mucino, 2007) does not take dissociation into account. In addition, the linear results are also larger at higher FAR, WAR and temperature. The non-linear model however consistently provides accurate results.

TET [K]	1547.5
P_{inlet} [Atm]	30.57
PR	0.261
FAR	0.0615
WAR	0.053
$\eta_{turbine}$	0.865
W [Kg/s]	4.07

Table 6.18: Case parameters, compressor turbine calculation, Jet-A

	$T_{exit,turbine}$ [K]	Turbine Work, [KW]
Actual Value	1072.483	1605.128
Linear interpolation	1071.57	1604.7
Non-linear interpolation	1072.49	1605.035
(Mucino, 2007)	1013.93	1868.5

Table 6.19: Comparison of turbine simulation results, Jet-A fuel

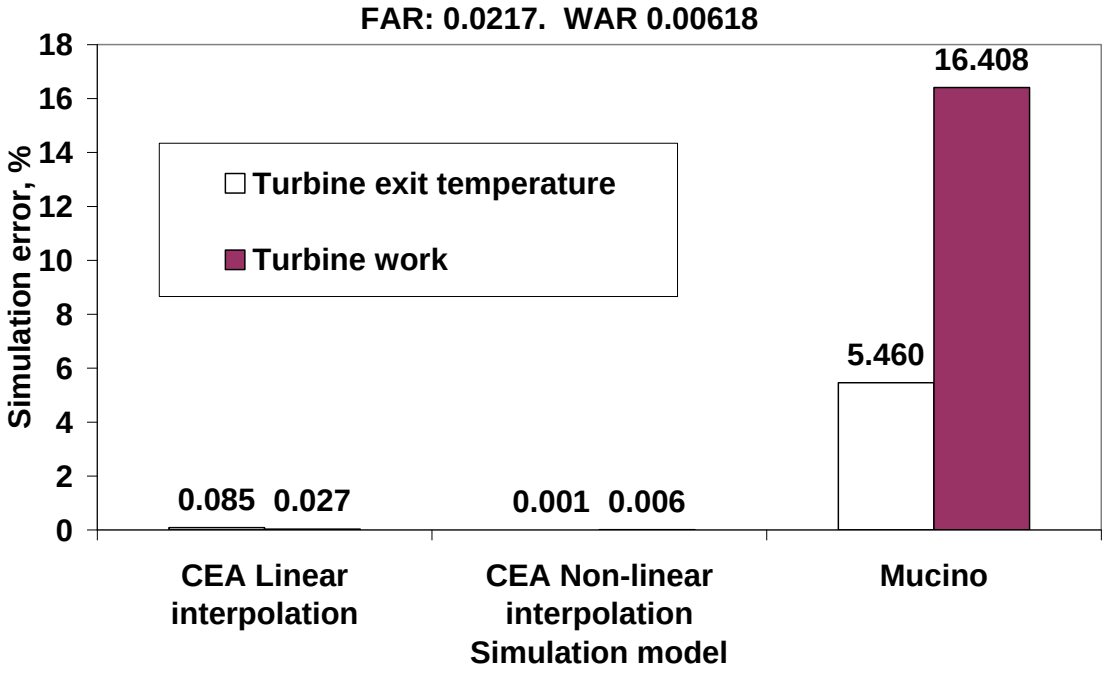

Figure 6.28: Comparison of simulation % errors, Jet-A

	$T_{exit,turbine}$ [K]	Turbine Work, [KW]
Actual Value	1209.452	1866.323
Linear interpolation	1215.032	1845.954
Non-linear interpolation	1209.04	1866.215
(Mucino, 2007)	1123.42	2315.79

Table 6.20: Comparison of turbine simulation results, FAR 0.0615 and WAR 0.053, Jet-A fuel

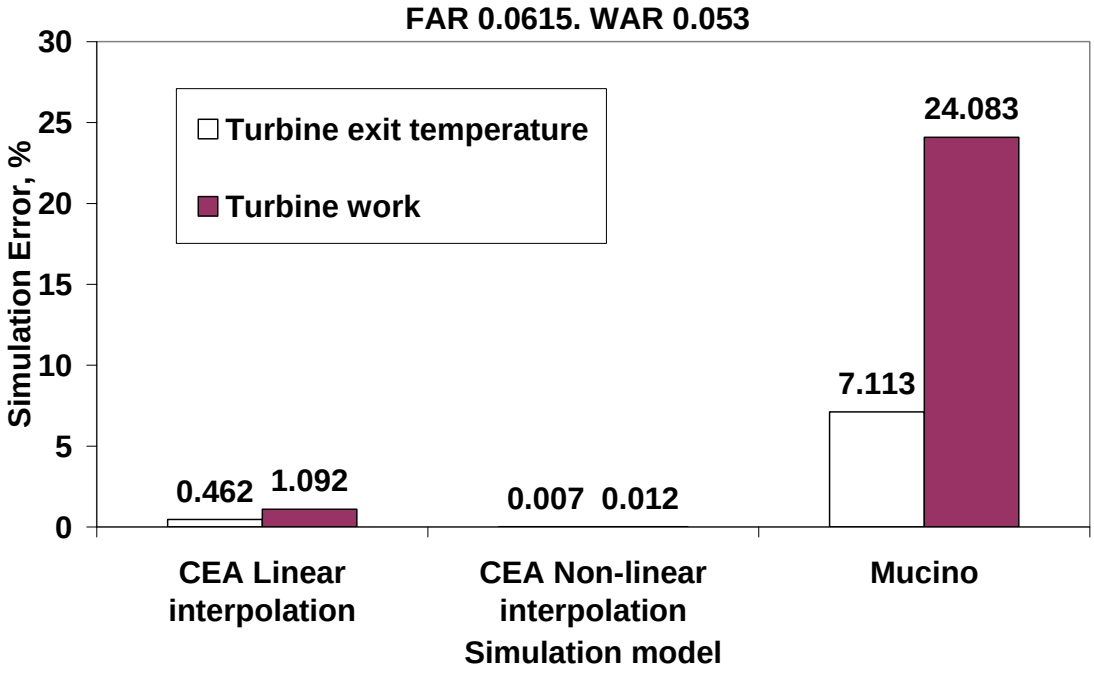

Figure 6.29: Comparison of simulation % errors, Jet-A, FAR 0.0615, WAR 0.053

6.3.4 Case study 4: Compressor turbine calculation, Hydrogen fuel

The multi-fuel simulation method was also applied to compressor turbine calculation, using Hydrogen as a fuel. The case parameters for this are presented in Table 6.21

TET [K]	1397.02
P_{inlet} [Atm]	30.57
PR	0.261
FAR	0.0217
WAR	0.00618
$\eta_{turbine}$	0.865
W [Kg/s]	4.07

Table 6.21: Case parameters, compressor turbine calculation, Hydrogen fuel

The results for this Hydrogen fuel simulation are presented in Table 6.22 and Figure 6.30. Once again, the non-linear interpolation method gives the most accurate results of the three methods.

	$T_{exit,turbine}$ [K]	Turbine Work, [KW]
Actual Value	1011.88	2159.99
Linear interpolation	1013.068	2153.3
Non-linear interpolation	1011.95	2159.6
(Mucino, 2007)	1013.993	2327.79

Table 6.22: Comparison of turbine simulation results, Hydrogen fuel

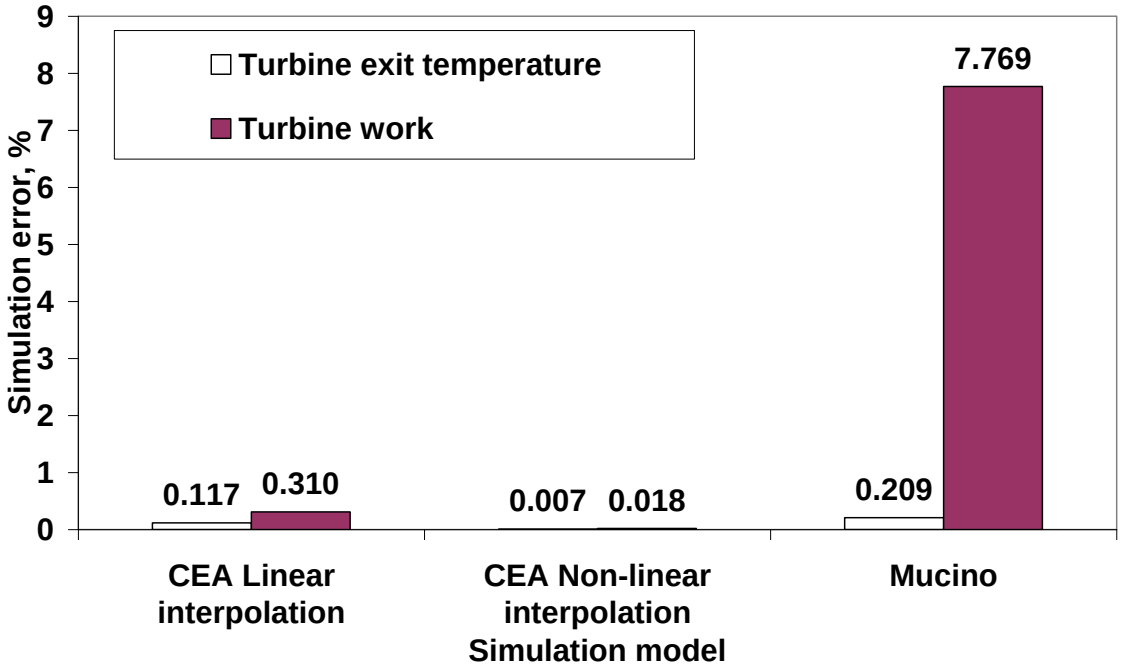

Figure 6.30: Comparison of simulation % errors, Hydrogen fuel

6.3.5 Case study 5: Compressor turbine calculation, Diesel fuel

The multi-fuel simulation method was also applied to compressor turbine calculation, using Diesel as a fuel. The case parameters for this are presented in Table 6.23

TET [K]	1397.02
P_{inlet} [Atm]	30.57
PR	0.261
FAR	0.0217
WAR	0.00618
$\eta_{turbine}$	0.865
W [Kg/s]	4.07

Table 6.23: Case parameters, compressor turbine calculation, Diesel fuel

The results for this Diesel fuel simulation are presented in Table 6.24 and Figure 6.31. Once again, the non-linear interpolation method gives the most accurate results of the three methods. The errors of the linear interpolation method have increased, compared to Jet-A and Hydrogen fuel. The same case applies to (Mucino, 2007) model

	$T_{exit,turbine}$ [K]	Turbine Work, [KW]
Actual Value	1166.46	1390.59
Linear interpolation	1071.609	1862.3
Non-linear interpolation	1166.98	1387.912
(Mucino, 2007)	1013.923	2149.216

Table 6.24: Comparison of turbine simulation results, Diesel fuel

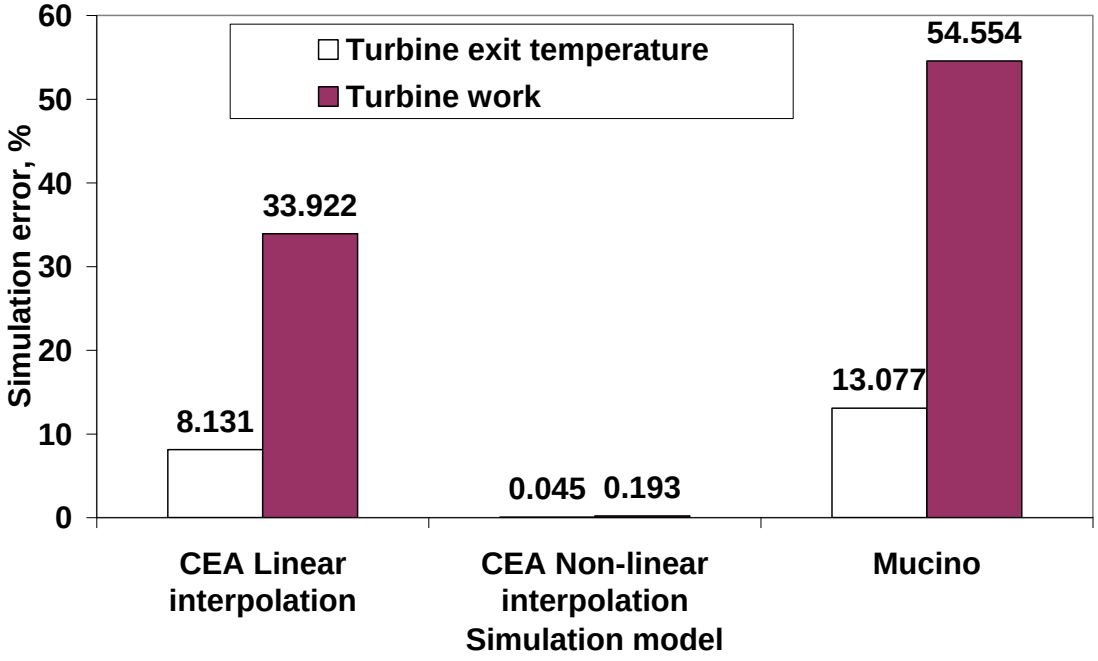

Figure 6.31: Comparison of simulation errors, Diesel fuel

6.4 Multi-fuel performance simulation discussion of results

This section aims to discuss the findings of the non-linear multi-fuel interpolation method and further reconcile them with the insights gained from the literature review.

From the literature review, the issues of real-gas effects (dissociation) and fuel chemistry were highlighted and it was concluded that they both need to be taken into account fully, if errors due to them are to be reduced. The Bücker polynomials (Bücker, 2003) polynomials are of order 10 and can be utilised to calculate enthalpy, h, entropy, s and isobaric heat capacity, C_p as a function of temperature for eight molecular gases: Nitrogen, Oxygen, Neon, Argon, Carbon monoxide, Water, Carbon dioxide and Sulphur dioxide. The gas properties for dry air are gained by adding the results according to their molar fractions and masses specified for air. Fuel-to-air ratio, FAR and Water-to-air ratio WAR are introduced by adapting molar fractions and masses accordingly. Other gas

properties like the ratio of heat capacities γ, gas constant R, can be calculated from the available molar fractions, mass fractions and gas properties. This method is relatively easy to implement and is not computationally expensive. However, its accuracy is restricted to very ideal cases in which the gas under consideration consists only of the eight gases mentioned. This has been demonstrated in the combustion case studies where, the errors obtained increase with addition of FAR. Real gas effects (specifically, dissociation) will rise considerably for moist air and combustion gases due to the presence of water and/or carbon dioxide, depending on the concentration of either (or both). For instance, for dry air (case study 1), the error in predicting compressor exit temperature was 0.97% and for moist air (case study 2), the error increased to 1.1%. The same was observed when FAR was increase from 0.02172 to 0.0615 and WAR from 0.00618 to WAR 0.053 (case study 3); the errors increase with increase in FAR.

In light of advancements in gas turbine technology that require temperatures above 2000 [K], or, conceptual design work for future technologies that require gas turbine temperatures above 2000 [K] and keeping the aforementioned issue of dissociation at high temperatures in mind, then an improved approach has been desirable.

Linear interpolation depends on approximating a function between two points. The accuracy of this method depends on the distance between these two points; if the points are sufficiently close, then the accuracy will be reasonably good. However, having sufficiently close points (of FAR, WAR, Pressure and temperature) comes with the penalty of large file sizes (in the case of fuel-tables method) and is thus computationally expensive. Non-linear interpolation (for this work, cubic-spline interpolation) acts as a solution to this problem since non-linear interpolation can better approximate any function, given four points. The improved accuracy of non-linear interpolation has been clearly demonstrated in all the case studies. In case study 5, the errors of the linear method increase significantly from other cases; this can be attributed to the

increased non-linearity of diesel caloric properties. However, the non-linear interpolation method produced errors below 0.2% (Case study 5). The non-linear interpolation method has also been demonstrated to consistently provide improved accuracy results in all cases.

The provided fuel tables have been produced using NASA's CEA program (Gordon and McBride, 1994) which is accepted as an industry standard. Therefore, the fuel tables in conjunction with the non-linear interpolation algorithm can be used as a tool that can provide mutual acceptance of results across engineering teams. The caloric properties provided in the fuel tables for FAR, WAR, Pressure and temperature exceed the typical values for gas turbine calculations; as such, the method can be used for conceptual work that covers parameters outside the typical ranges of current gas turbine calculations. These caloric properties were calculated with dissociation in mind; therefore any errors due to the same would be eliminated (as opposed to assuming no-dissociation).

Finally, the provided caloric properties are unique to each fuel; therefore, any errors due to assuming similar fuel chemistry across two different fuels would be eliminated.

7 CONCLUSIONS AND FURTHER WORK

At the onset of this project, two aims were clearly stated. This section aims to make conclusions based on these aims and further highlight any limitations that may require further work to be carried out in the future.

7.1 Non-linear WLS conclusions and further work

For the non-linear WLS part of the project, the aim was stated thus:

- **To investigate the fidelity of a non-linear weighted least squares diagnostics algorithm for fault quantification of gas path components.**

To fulfil this aim, a number of objectives were set out which included the review of diagnostic methods developed in the past with the aim of identifying key requirements for an advanced diagnostic method. Key requirements for an advanced diagnostic scheme were identified and which served as the frame-work for the development of the non-linear WLS algorithm. These included amongst others, based on non-linearity, ability to address measurement noise, based on a mathematical model and easily satisfied computational requirements. To work in conjunction with the non-linear WLS algorithm, two new weighting schemes were developed, WS1 and WS2. The non-linear WLS algorithm in conjunction with these two weighting methods was tested with application to four case studies, which involved the diagnostics of various gas path components using noisy simulated data. Three of the four studies involved the use of multiple measurement samples and one case study involved the use of a single measurement sample. The weighting methods were compared with the traditional weighting method of the reciprocal of variance and the non-linear WLS was compared to non-linear GPA. From the work that has been carried out, the following can therefore be concluded:

1. WS1 and WS2 produce reasonably small weights; this in turn reduces the probability of degradation of the influence co-efficient matrix

(measured by high matrix condition numbers) and will thus produce useful diagnostic results at all times. In comparison, the traditional method of using the reciprocal of variance is not stable in the sense that, it may or may not degrade the influence co-efficient matrix. In the case where it does, any produced diagnostic results will not be useful.

2. The non-linear weighted least squares method provides improved results over its linear counterpart and is therefore recommended over its linear counterpart. In addition, the method provides results that are improved in precision and accuracy over methods that do not account for measurement noise.

3. The non-linear WLS method in conjunction with WS1 and WS2 weighting methods can therefore be applied to the diagnostics of various gas path components, using noisy measurements and the results produced would be useful even for decision making in the context of engine maintainance schedules.

From this part of the project, two contributions to knowledge have been made:

1. The first is in the form of two new weighting methods WS1 and WS2 that have demonstrated improvements over the existing reciprocal-of-variance method. Both weighting methods produce weights that do not degrade influence co-efficient matrices and can thus be deemed stable. WS1 is further useful in weighting measurements in the absence of a sample of data. This stability is of real value to gas turbine users since it guarantees diagnostic results at all times. Such diagnostic results can then be used to make informed decisions. The ability (of WS1) to weight measurements using a single sample is of real value as well, since it means that in the absence of samples of data, one can still perform diagnostics and thereafter make informed decisions.

2. The second contribution is in the form of the non-linear WLS algorithm which works in conjunction with WS1 and WS2 weighting methods and

has been demonstrated to be a significant improvement over its linear counterpart. This diagnostic method would be of value to any gas turbine diagnostics department, in quantifying gas turbine component degradations even in the presence of measurement noise.

However, the method has its limitations which need to be addressed as further work.

- The developed method did not include a covariance matrix to address measurement errors. Therefore, any detected fault will be attributed to component deterioration even if the fault may actually be a measurement fault. Therefore, the current method can be improved to cover measurement faults by including a measurement error covariance matrix, in addition to the matrix of influence co-efficients.

- The developed method quantifies gas turbine faults but does not possess any fault isolation capability. That is, the method does not provide any means of predicting and/or isolating the degraded component. Work needs to be done in developing such a capability so that the method will be a fault isolation and quantification method.

- Other areas that desire some attention would include all other requirements for an advanced diagnostic scheme that were highlighted as findings from the literature review. For instance, the method could be used as part of a hybrid method with any other diagnostic scheme, where each component of the hybrid system benefits from mutual interaction. In addition, any weaknesses from any component would be complemented by the strengths of the other. Another example would be the inclusion of a component which allows the inclusion of past maintainance histories and records (e.g., Bayesian belief network or an expert system); such information would be used to further improve diagnostic results. This sort of hybrid method deserves some investigation with the aim of improving the non-linear WLS algorithm.

7.2 Multi-fuel performance simulation conclusion and further work

For the multi-fuel performance simulation part of the project, the following aim was stated:

- **To develop a multi-fuel and multi-caloric property to improve the potential of gas turbine performance simulation accuracy.**

To fulfil this aim, a number of objectives were laid out which began with a review of literature of simulation methods developed in the past. The ideal gas assumption was reviewed and it was concluded that apart from class-room instruction, the method is not accurate enough for gas turbine simulation. Dissociation as a phenomenon was reviewed and any errors due to the same were highlighted and discussed. It was concluded that dissociation should not be ignored and where possible, its effect should be modelled, for improved simulation accuracy and more so at high temperatures and low pressures. Models that fail to take fuel chemistry into account were also reviewed and it was concluded that, unless two different fuels are not significantly dissimilar in terms of their chemical composition, then for improved accuracy, they would need to be modelled separately. This conclusion applies more so to natural gases whose chemical compositions will vary based on their countries of origin.
A suitable technical model was identified as NASAs' CEA software based on the fact that it was the only one (compared to most models used in industry as acceptable standards today) that described the caloric properties of combustion gases with satisfactory accuracy over the temperature range of 200[K] to 3000[K]. This software was then used to produce fuel tables for four fuels, Jet-A, Diesel, Hydrogen and Natural gas from the United Kingdom. The fuel tables consisted of caloric properties density, enthalpy, entropy, isobaric heat capacity, ratio of heat capacities, the gas constant and viscosity. For each of these caloric properties, data points were selected for Fuel-to-air ratio, Water-to-air ratio, pressure and temperature with the aim of optimising file sizes. A non-

linear cubic-spline interpolation method was developed to work in conjunction with these fuel files.

Case studies for compressor and turbine simulation were carried out and from this work, the following conclusions can be made.

1. The cubic spline non-linear method provides improved accuracy as compared to the linear interpolation method. This is especially significant for caloric properties that exhibit significant non-linearity, e.g. density. This is also significant at high FARs and WARs. As such, the non-linear method is recommended over the linear interpolation method.
2. Polynomial based methods may be reasonably accurate for dry and moist air; however, when considering Fuel-to-air ratios, this accuracy reduces and more so at high Fuel-to-air ratios, high temperatures, where dissociation effects may be prevalent. The developed fuel tables unique to each fuel eliminate any errors that are a result of assuming similar fuel chemistry across fuels.

From this part of the project, a contribution to knowledge has been made in the form of a comprehensive and improved-accuracy simulation tool that can be used for gas turbine simulation and for multiple fuels. This is of value especially when it is part of a simulation and diagnostic suite where accurate simulation data is required for accurate detection of component degradation. In addition, since the fuel tables cover parameters of FAR, WAR Pressure and temperature that are beyond current gas turbine limits, the tool can as well be used for conceptual design purposes of future gas turbine technologies. In addition, the method is a frame-work for further development of more fuel tables by other users. Such additional fuels will use the same cubic-spline interpolation routine and as such, there is no limitation to the number of fuels that can be added. The method can also be used for classroom instruction where accurate caloric properties for different fuels can easily be obtained by running the non-linear interpolation.

The method does however have limitations that need to be addressed as further work.

- An improved interpolation method needs to be explored with the aim of reducing interpolation points and hence improving computational efficiency. This would also afford users the chance to add FAR points between stoichiometric values and *rich burn quick quench* values without stiff computational penalties.

REFERENCES

Afgan, N., Carvalho, M., Pilavachi, P., Tourlidakis, A., Olkhonski, G. and Martins, N. (2006), "An expert system concept for diagnosis and monitoring of gas turbine combustion chambers", *Journal of Applied Thermal Engineering,* vol. 26, no. 7, pp. 766-771.

ANSI/ASME PTC 4.4-1981, "Gas Turbine Heat Recovery Steam Generators, Performance Test Codes", *ASME, New York*.

Applebaum, E. and Ha'Emek, M. (2001), "Fuzzy Classification for Fault Isolation in Gas Turbine Engines". *Joint 9th IFSA World Congress and 20th NAFIPS International Conference.* vol. 1, pp. 292-297.

Baehr, H. and Diederichsen, C. (1988), "Berechnungsgleichungen für Enthalpie und Entropie der Komponenten von Luft und Verbrennungsgasen", *Brennstoff-Wärme-Kraft,* vol. 40, no. 12, pp. 30-33.

Barwell, M. (1987), "Compass-ground based engine monitoring program for general application." *SAE Technical Paper Series 871734, Aerospace Technology Conference and Exposition*, Long Beach, California

Bettocchi, R., Pinelli, M., Spina, P. and Venturini, M. (July 2007), "Artificial Intelligence for the Diagnostics of Gas Turbines—Part II: Neuro-Fuzzy Approach", *Journal of Engineering for Gas Turbines and Power*, vol. 129, issue 3, pp. 720-730.

Bettocchi, R., Pinelli, M., Spina, P. R. and Venturini, M. (July 2007), "Artificial Intelligence for the Diagnostics of Gas Turbines---Part I: Neural Network Approach", *Journal of Engineering for Gas Turbines and Power*, vol. 129, no. 3, pp. 711-719.

Brandt, F. (1999), "Brennstoffe und verbrennungsrechnung", Second ed, Vulkan-Verlag GmbH.

Bücker, D., Span, R. and Wagner, W. (January 2003), "Thermodynamic property models for moist air and combustion gases", *ASME Journal of Engineering for Gas Turbines and Power*, vol. 125, number 1 pp. 374-384.

Chen, T. and Sun, J. G. (2005), "Rough Set and Neural Network Based Fault Diagnosis for Aeroengine Gas Path", *ASME Turbo Expo 2005: Power for Land, Sea, and Air (GT2005)*, June 6–9, 2005 , Reno, Nevada, USA .

Collinge, K. and Schoff, K. (1987), "TEXMAS-an expert system for gas turbine engine diagnosis and more", AEROTECH '87: *Society of Automotive Engineers conference and exposition*, Long Beach, California, USA.

Crane Company (1988). "*Flow of fluids through valves, fittings, and pipes*." Technical Paper No. 410 (TP 410)

De Boor, C. (2001), '*A practical guide to splines'*, Springer-Verlag Publishers.

Denney, G. (1965), "F16 jet engine trending and diagnostics with neural networks", Proceedings of SPIE -*The International Society for Optical Engineering*, Vol. 1965, pp 419-422.

DePold, H. R. and Gass, F. D. (1999), "The application of expert systems and neural networks to gas turbine prognostics and diagnostics", J*ournal of Engineering for Gas Turbines and Power,* vol. 121, no. 4, pp. 607–612.

Demirci, S., Hajiyev, C. and Schwenke, A. (2008), "Fuzzy logic-based automated engine health monitoring for commercial aircraft", *Aircraft Engineering and Aerospace Technology*, vol. 80, no. 5, pp. 516-525.

Doel, D. (2003), "Interpretation of weighted-least-squares gas path analysis results", *Journal of Engineering for Gas Turbines and Power*, vol. 125, issue 3, pp. 624-634.

Doel, D. (1994), "TEMPER—a gas-path analysis tool for commercial jet engines", *Journal of Engineering for Gas Turbines and Power*, vol. 116, issue 1, pp. 82-90.

Doel, D. and LaPierre, L. (1989), "Diagnostic expert systems for gas turbine engines-status and prospects. *AIAA, ASME, SAE, and ASEE, Joint Propulsion Conference,* 25th, Monterey, CA; UNITED STATES; 10-13 July 1989. pp. 1989.

Dyson R.J.E., Doel, D.L.(1987). “CF-80 Condition Monitoring – The Engine manufacturing’s involvement in Data Acquisition and Analysis,” *AIAA-84-1412*.

Escher, P. and Singh, R. (1995), "An Object-Oriented Diagnostics Computer Program Suitable for Industrial Gas Turbines", *United 21st International Congress of Combustion Engines (CIMAC)*, Interlaken, Switzerland. pp. 15-18.

Escher, P. C. (2002), "Gas turbine data validation using gas path analysis", *ASME Turbo Expo 2002*, Amsterdam, Netherlands. pp. 45-51

Eustace, R. (1993), "Neural network fault diagnosis of a turbofan engine", *ISABE- International Symposium on Air Breathing Engines*, 11th , Tokyo, Japan, pp. 937-946.

Fast, M., Assadi, M. and De, S. (2009), "Development and multi-utility of an ANN model for an industrial gas turbine", *Journal of Applied Energy,* vol. 86, no. 1, pp. 9-17.

Ganguli, R. (2003), "Application of fuzzy logic for fault isolation of jet engines", *Journal of Engineering for Gas Turbines and Power (Transactions of the ASME),* vol. 125, no. 3, pp. 617-623.

Gesser, H. D. (2001), "Applied chemistry: a textbook for engineers and technologists"*, Kluwer Academic/Plenum Publishers*

Gordon, S. and McBride, B. J. (1976), "Computer program for calculation of complex chemical equilibrium compositions, rocket performance, incident and reflected shocks, and Chapman-Jouguet detonations", *NASA SP-273*, NASA, Washington (1976)

Gordon, S. and McBride, B. J. (1994), "Computer program for calculation of complex chemical equilibrium compositions and applications", *NASA reference publication,* vol. 1311, Washington, DC.

Guha, A. (2001), "An efficient generic method for calculating the properties of combustion products", Proceedings of the Institution of Mechanical Engineers, Part A: *Journal of Power and Energy,* vol. 215, issue. 3, pp. 375-387.

Gulati, A., Zedda, M. and Singh, R. (2000), "Gas turbine engine and sensor multiple operating point analysis using optimization techniques", *AIAA/ASME/SAE/ASEE Joint Propulsion Conference and Exhibit*, 36th, Huntsville, AL, USA

Gülder, Ö. L (1988), "Combustion Gas Properties: Part III—Prediction of the Thermodynamic Properties of Combustion Gases of Aviation and Diesel Fuels", *Journal of Engineering for Gas Turbines and Power,* vol. 110, pp. 94.

Hamilton, T. P. (1988), "HELIX: a helicopter diagnostic system based on qualitative physics", *Artificial Intelligence in Engineering*, vol. 3, issue. 3, pp. 141-150.

Jacobsen, R., Clarke, W., Penoncello, S. and McCarty, R. (1990), "A thermodynamic property formulation for air. I. Single-phase equation of state from 60 to 873 K at pressures to 70 MPa", *International Journal of Thermophysics,* vol. 11, issue. 1, pp. 169-177.

Jones, R., Trout, A., Wear, J. and McBride, B. (1984), "Combustion gas properties I-ASTM Jet A fuel and dry air", *NASA Technical paper* 2359.

Kamboukos, P., STAMATIS, A., Mathioudakis, K. and Oikonomou, P. (2001), "Optimising diagnostic effectiveness of mixed turbofans by means of adaptive modelling and choice of appropriate monitoring parameters", *Ageing Mechanisms and Control; Monitoring and Management of Gas turbine fleets for extended life and reduced costs Symposium*, Machester, UK, October 2001.

Kamboukos, P. and Mathioudakis, K. (2005), "Comparison of Linear and Nonlinear Gas Turbine Performance Diagnostics", *Journal of Engineering for Gas Turbines and Power (Transactions of the ASME),* vol. 127, issue. 1, pp. 49-56.

Kanelopoulos, K., Stamatis, A. and Mathioudakis, K. (June, 1997), "Incorporating neural networks into gas turbine performance diagnostics". *The 1997 International Gas Turbine & Aero-engine Congress & Exposition*; Orlando, FL, USA; pp 8.

Keenan, J. H. and Kaye, J. (1980), Gas tables: "*Thermodynamic properties of air products of combustion and component gases, compressible flow functions, including those of Ascher H. Shapiro and Gilbert M. Edelman*," Second edition, Wiley.

Kobayashi, T. and Simon, D. L. (2003), "Application of a bank of Kalman filters for aircraft engine fault diagnostics." *ASME Turbo Expo 2003*, Atlanta Georgia, USA. Number GT2003-38550, pp 461-470.

Konstantinos Kyprianidis, Sethi Vishal, Riti Singh, Pilidis Pericles, Ogaji Stephen and Anestis l. Kalfas (2009), "Thermo-Fluid modelling for gas turbines-Part1: Theoretical foundation and uncertainty analysis", *Proceedings of ASME Turbo Expo 2009*, Orlando, Fl, USA.

Kopytov, E., Labendik, V. and Yunusov, S. (2010), "Expert Systems for evaluating the aircraft power plants' technical condition", *Journal of Transport and Communication*, vol. 11, no. 1, pp. 31-37.

Kurzke, J. (2007), "About Simplifications in Gas Turbine Performance Calculations", *ASME Turbo Expo 2007*, Montreal, Canada. Number GT2007-27620, pp 493-501

Kyriazis, A. and Mathioudakis, K. (2009), "Enhanced Fault Localization Using Probabilistic Fusion With Gas Path Analysis Algorithms", *Journal of Engineering for Gas Turbines and Power*, vol. 131..

Lazalier, G., JACOX, J. and REYNOLDS, E. (1978), "A gas path performance diagnostic system to reduce J 75-P-17 engine overhaul costs", ASME, Transactions, *Journal of Engineering for Power*, vol. 100, pp. 691-697.

Lee, Y. K., Mavris, D. N., Volovoi, V. V., Yuan, M. and Fisher, T. (2010), "A Fault Diagnosis Method for Industrial Gas Turbines Using Bayesian Data Analysis", J*ournal of Engineering for Gas Turbines and Power,* vol. 132.

Li, Y. G. (2003), "A gas turbine diagnostic approach with transient measurements", Proceedings of the Institution of Mechanical Engineers, Part A: *Journal of Power and Energy,* vol. 217, issue. 2, pp. 169-177.

Li, Y.G;, E. Lo Gatto., and P.Pilidis (2006), "Gas turbine off-design performance adaptation using a genetic algorithm", *ASME Turbo Expo 2006: Power for Land, Sea, and Air (GT2006)*, May 8–11, 2006 , Barcelona, Spain

Li, Y. and Singh, R. (2005) "An advanced gas turbine diagnostics system-PYTHIA", *ISABE-2005*-1284

Lu, P. J., Zhang, M. C., Hsu, T. C. and Zhang, J. (2001), "An evaluation of engine faults diagnostics using artificial neural networks", *Journal of Engineering for Gas Turbines and Power,* vol. 123, issue 2, pp. 340-346.

Lunderstaedt, R. A. and Junk, R. H. (1997), "Application of the gas-path-analysis(GPA) for the non-stationary operation of a jet engine", *ISABE-International Symposium on Air Breathing Engines*, 13th Chattanooga, TN,USA. pp. 430-437.

Luppold, R., Roman, J., Gallops, G. and Kerr, L. (1989), "Estimating in-flight engine performance variations using Kalman filter concepts", *AIAA, ASME, SAE, and ASEE, Joint Propulsion Conference*, 25th , Monterey, CA, USA.

Marinai, L., Probert, D. and Singh, R. (2004), "Prospects for aero gas-turbine diagnostics: a review", *Journal of Applied Energy*, vol. 79, issue. 1, pp. 109-126.

MacIsaac, B. (1992), "Engine Performance and Health Monitoring Models Using Steady State and Transient Prediction Methods". A*dvisory Group for Aerospace Research and Development*, AGARD-LS-183

MCBRIDE, B.J., Gordon, S., RENO, M.A., (1993) "Coefficients for calculating thermodynamic and transport properties of individual species", *National Aeronautics and Space Administration. Memorandum 4513, Lewis Research Centre, Cleveland, OH.*

Meher-Homji, C. B. and Bhargava, R. (1994), "Condition monitoring and diagnostic aspects of gas turbine transient response", *International Journal of Turbo and Jet-Engines*, vol. 11, issue 1, pp. 99-111.

Merrington, G. (1989), "Fault diagnosis of gas turbine engines from transient data", *Journal of Engineering for Gas Turbines and Power,* vol. 111, pp. 237-243.

Merrington, G. (1988), "Identification of dynamic characteristics for fault isolation purposes in a gas turbine using closed-loop measurements", *AGARD-CP-448, Engine Condition Monitoring-Technology and Experience.*

Mucino, M. (2007), *CCGT Performance Simulation and Diagnostics for Operations Optimisation and Risk Management*, PhD Thesis, Cranfield University, Bedfordshire, England.

Mucino, M. and Li, Y. (2005), "A diagnostic system for gas turbines using GPA-index", *COMADEM Conference-2005-C007*.

Ogaji, S. O. T. and Singh, R. (2003), "Advanced engine diagnostics using artificial neural networks", *Applied Soft Computing Journal*, vol. 3, issue. 3, pp. 259-271.

Ogaji S.O.T., Li Y.G., Sampath S. and Singh R., "Gas Path Fault Diagnosis of a Turbofan Engine from Transient Data Using Artificial Neural Networks", *ASME Paper GT2003-38423*, ASME TURBO EXPO 2003, Atlanta, Georgia, USA, June 16-19, 2003.

Palmer, C. A. (1998), "Combining Bayesian belief networks with gas path analysis for test cell diagnostics and overhaul", *ASME 98*-GT-168.

Pawlak, Z. (1984), "Rough classification", *International Journal of Man-Machine Studies*, vol. 20, issue. 5, pp. 469-483.

Peterson C.; Sowa W.; Samuelsen, G.S (2002), "Performance of a Model Rich-Burn, Quick-Mix, Lean-Burn Combustor at Elevated Temperature and Pressure", *NASA/CR*—2002-211992, pp. 9-16.

Poferl, D. J., Svehla, R. A. and Lewandowski, K. (1969), "*Thermodynamic and Transport Properties of Air and the Combustion Products of Natural Gas and of ASTM-A-1 Fuel with Air*", NASA TN D-5452

Poferl, D. J. and Svehla, R. A. (1973), "*Thermodynamic and transport properties of air and its products of combustion with ASTMA-A-1 fuel and natural gas at 20, 30, and 40 atmospheres*", NASA TN D-7488

Provost, M. J. (1994), "The use of optimal estimation techniques in the analysis of gas turbines", PhD thesis, Cranfield University, School of Engineering, Bedfordshire, UK.

Provost, M. (1988), "COMPASS: a generalized ground-based monitoring system", *AGARD-CP-449*, Engine Condition Monitoring Technology and Experience

Romessis, C. and Mathioudakis, K. (2006), "Bayesian Network Approach for Gas Path Fault Diagnosis", *Journal of Engineering for Gas Turbines and Power,* vol. 128, issue 1, pp. 64-72.

Romessis, C., Stamatis, A. and Mathioudakis, K. (2001), "Setting Up a Belief Network for Turbofan Diagnosis with the Aid of an Engine Performance Model", *International Symposium on Air Breathing Engines*, 15th, Bangalore, India.

Ross, T. J. (2004), "Fuzzy logic with engineering applications", John Wiley & Sons Inc.

Sampath S., Li Y.G., Ogaji S.O.T. and Singh R., "Fault Diagnosis of a Two Spool Turbo-Fan Engine Using Transient Data: A Genetic Algorithm Approach", *ASME Paper GT2003-38300,* ASME TURBO EXPO 2003, Atlanta, Georgia, USA, June 16-19, 2003.

Sethi V. (2008), "*Advanced Performance Simulation of Gas Turbine Components and Fluid Thermodynamic Properties*", PhD thesis, Cranfield University, Cranfield, Bedfordshire.

Sethi, V., Diara, F., Atabak, S., Jackson, A., Bala, A. and Pilidis, P. (2008), "Advanced Modeling of Fluid Thermodynamic Properties for Gas Turbine Performance Simulation", *ASME TURBO EXPO 2008,* GT2008-51126, Berlin, Germany.

Shah, R., LaPierre, L., Costen, P., Doel, D., Co, G. E. and Syracuse, N. (1988), "JET-X: jet engine troubleshooting expert system", *Proceedings of the International Workshop on Artificial Intelligence for Industrial Applications,* pp. 135-139.

Simani, S. (2005), "Identification and fault diagnosis of a simulated model of an industrial gas turbine", *IEEE Transactions on Industrial Informatics*, vol. 1, issue. 3, pp. 202-216.

Simona, D. and Simonb, D. L. (2009), "Constrained Kalman filtering via density function truncation for turbofan engine health estimation", *International Journal of Systems Science,* vol. 41, issue. 2, pp. 159-171.

Siu, C., Shen, Q., Milne, R. (1996), "Tmdoctor: a Fuzzy Rule-and Case-Based Expert System for Turbo-machinery Diagnosis." *Proceedings of IFAC Fault Detection, Supervision and Safety for Technical Processes,* Kingston Upon Hull, UK, Vol 2.

Society of Automotive Engineers (1999), "Gas Turbine Engine Steady-state and Transient Performance Presentation for Digital Computer Programs", *SAE AS681* Rev. H, Warrendale, PA

Stamatis, A., Mathioudakis, K., Papailiou, K. and Berios, G. (1991), "Jet engine fault detection with discrete operating points gas path analysis", *Journal of Propulsion and Power,* vol. 7, pp. 1043-1048.

Stamatis, A.,Mathioudakis, K., Papailiou, K. and Smith, M. (1990), "Gas turbine component fault identification by means of adaptive performance modelling", *ASME, International Gas Turbine and Aeroengine Congress and Exposition,* Brussels, Belgium.

Staples, L. and Saravanamuttoo, H. (1975), "An engine analyzer program for helicopter turbo-shaft power-plants", *NATO/AGARD Specialists Meeting in Diagnostics and Engine Condition Monitoring*, Liege, Belgium.

Stroud, K. A. and Booth, D. J. (2001), *Engineering mathematics,* Industrial Press Inc.

Svehla, Roger A. (1964); "*Thermodynamic and Transport Properties for the Hydrogen-Oxygen System*", NASA SP-3011.

TACINA, R. (1990), "Low NO (x) potential of gas turbine engines", *AIAA, Aerospace Sciences Meeting*, Reno, Nevada, USA, pp. 1990

Tang, G., Yates, C. L. and Chen, D. (1998), "Comparative study of two neural networks applied to jet engine fault diagnosis", *AIAA/ASME/SAE/ASEE Joint Propulsion Conference & Exhibit,* 34th Cleveland, OH.

Tang, G., Yates, C. L., Zhang, J. and Chen, D. (1999), "A practical intelligent system for condition monitoring and fault diagnosis of jet engines", *AIAA/ASME/SAE/ASEE Joint Propulsion Conference and Exhibit*, 35th, Los Angeles, CA.

Torella, G. and Torella, R. (1999), "Probabilistic expert systems for the diagnostics and trouble-shooting of gas turbine apparatuses", *AIAA/ASME/SAE/ASEE Joint Propulsion Conference and Exhibit*, 35th , Los Angeles, CA.

Trusler, J. (1991), *Physical acoustics and metrology of fluids*, Institute of Physics Publishing Inc.

Urban, L. A. and Volponi, A. J. (1992), "Mathematical methods of relative engine performance diagnostics", SAE Technical paper series,1992.

Urban, L. (1975), "Parameter Selection for Multiple Fault Diagnostics of Gas turbine Engines", J*ournal of Engineering for Power*, vol. 4, issue. 4, pp. 225-230.

Van Wylen, G. J., Sonntag, R. E. and Borgnakke, C. (1994), *Fundamentals of classical thermodynamics,* John Wiley & Sons.

Volponi, A. J., Brotherton, T., Luppold, R. and Simon, D. L. (2003), "Development of an information fusion system for engine diagnostics and health management", *AIAA 2004-6461, AIAA 1st Intelligent Systems Technical Conference,* Chicago, Illinois.

Volponi, A., DePold, H., Ganguli, R. and Daguang, C. (2003b), "The Use of Kalman Filter and Neural Network Methodologies in Gas Turbine Performance Diagnostics: A Comparative Study", J*ournal of Engineering for Gas Turbines and Power*, vol. 125, pp. 917.

Walsh, P. P., Fletcher, P. and InterScience, W. (1998), *Gas turbine performance,* Blackwell Science Oxford, Malden, MA.

Wear, J., Jones, R., MCbride, B. and Beyerle, R. (1985), "*Combustion gas properties. Part 3: Hydrogen gas fuel and dry air*", NASA Technical Paper 2477.

Wilcock, R., Young, J. and Horlock, J. (2002), "Gas properties as a limit to gas turbine performance", *ASME Turbo Expo*, Amsterdam, The Netherlands, 2002. pp 799-807

Yoon, J. E., Lee, J. J., Kim, T. S. and Sohn, J. L. (2008), "Analysis of performance deterioration of a micro gas turbine and the use of neural network for predicting deteriorated component characteristics", *Journal of mechanical science and technology,* vol. 22, no. 12, pp. 2516-2525.

Zedda, M. and Singh, R. (2002), "Gas turbine engine and sensor fault diagnosis using optimization techniques", *Journal of Propulsion and Power,* vol. 18, issue. 5, pp. 1019-1025.

APPENDIX 1: Typical Fuel data table

FAR 0.000 WAR 0.00000 P 0.020

# t	h_abs	s_abs	R_spec	cp	gam	vis
2.0000E+02	-9.8466E+04	7.1860E+02	2.8705E+02	1.0024E+03	1.4013E+00	1.3625E-05
2.5000E+02	-4.8333E+04	9.4240E+02	2.8705E+02	1.0031E+03	1.4009E+00	1.6302E-05
3.0000E+02	1.8588E+03	1.1254E+03	2.8705E+02	1.0048E+03	1.3999E+00	1.8746E-05
3.5000E+02	5.2176E+04	1.2805E+03	2.8705E+02	1.0082E+03	1.3981E+00	2.1020E-05
4.0000E+02	1.0271E+05	1.4155E+03	2.8705E+02	1.0135E+03	1.3952E+00	2.3163E-05
4.5000E+02	1.5355E+05	1.5352E+03	2.8705E+02	1.0206E+03	1.3913E+00	2.5199E-05
5.0000E+02	2.0480E+05	1.6432E+03	2.8705E+02	1.0295E+03	1.3866E+00	2.7148E-05
5.5000E+02	2.5653E+05	1.7418E+03	2.8705E+02	1.0398E+03	1.3814E+00	2.9023E-05
6.0000E+02	3.0879E+05	1.8328E+03	2.8705E+02	1.0510E+03	1.3757E+00	3.0832E-05
6.5000E+02	3.6164E+05	1.9173E+03	2.8705E+02	1.0628E+03	1.3700E+00	3.2585E-05
7.0000E+02	4.1508E+05	1.9965E+03	2.8705E+02	1.0749E+03	1.3643E+00	3.4288E-05
7.5000E+02	4.6913E+05	2.0711E+03	2.8705E+02	1.0870E+03	1.3588E+00	3.5946E-05
8.0000E+02	5.2378E+05	2.1417E+03	2.8705E+02	1.0988E+03	1.3536E+00	3.7563E-05
8.5000E+02	5.7901E+05	2.2086E+03	2.8705E+02	1.1103E+03	1.3487E+00	3.9142E-05
9.0000E+02	6.3480E+05	2.2724E+03	2.8705E+02	1.1213E+03	1.3441E+00	4.0688E-05
9.5000E+02	6.9113E+05	2.3333E+03	2.8705E+02	1.1319E+03	1.3398E+00	4.2202E-05
1.0000E+03	7.4798E+05	2.3916E+03	2.8705E+02	1.1421E+03	1.3357E+00	4.3688E-05
1.0500E+03	8.0533E+05	2.4476E+03	2.8705E+02	1.1520E+03	1.3319E+00	4.5144E-05
1.1000E+03	8.6317E+05	2.5014E+03	2.8705E+02	1.1614E+03	1.3283E+00	4.6572E-05
1.1500E+03	9.2147E+05	2.5532E+03	2.8705E+02	1.1705E+03	1.3249E+00	4.7975E-05
1.2000E+03	9.8022E+05	2.6032E+03	2.8705E+02	1.1793E+03	1.3217E+00	4.9355E-05
1.2500E+03	1.0394E+06	2.6515E+03	2.8705E+02	1.1879E+03	1.3186E+00	5.0716E-05
1.3000E+03	1.0990E+06	2.6983E+03	2.8705E+02	1.1965E+03	1.3157E+00	5.2059E-05
1.3500E+03	1.1590E+06	2.7436E+03	2.8705E+02	1.2049E+03	1.3127E+00	5.3385E-05
1.4000E+03	1.2195E+06	2.7876E+03	2.8705E+02	1.2135E+03	1.3099E+00	5.4697E-05
1.4500E+03	1.2804E+06	2.8303E+03	2.8705E+02	1.2222E+03	1.3070E+00	5.5994E-05
1.5000E+03	1.3417E+06	2.8719E+03	2.8705E+02	1.2313E+03	1.3041E+00	5.7279E-05
1.5500E+03	1.4035E+06	2.9124E+03	2.8705E+02	1.2409E+03	1.3011E+00	5.8553E-05
1.6000E+03	1.4658E+06	2.9520E+03	2.8706E+02	1.2514E+03	1.2980E+00	5.9815E-05
1.6500E+03	1.5287E+06	2.9907E+03	2.8706E+02	1.2632E+03	1.2946E+00	6.1066E-05
1.7000E+03	1.5922E+06	3.0286E+03	2.8707E+02	1.2768E+03	1.2910E+00	6.2309E-05
1.7500E+03	1.6564E+06	3.0658E+03	2.8708E+02	1.2931E+03	1.2868E+00	6.3542E-05
1.8000E+03	1.7215E+06	3.1025E+03	2.8711E+02	1.3130E+03	1.2821E+00	6.4767E-05
1.8500E+03	1.7878E+06	3.1388E+03	2.8714E+02	1.3377E+03	1.2766E+00	6.5985E-05
1.9000E+03	1.8554E+06	3.1748E+03	2.8719E+02	1.3688E+03	1.2703E+00	6.7196E-05
1.9500E+03	1.9248E+06	3.2108E+03	2.8726E+02	1.4082E+03	1.2630E+00	6.8401E-05
2.0000E+03	1.9964E+06	3.2468E+03	2.8736E+02	1.4580E+03	1.2547E+00	6.9602E-05
2.0500E+03	2.0708E+06	3.2838E+03	2.8750E+02	1.5208E+03	1.2454E+00	7.0800E-05
2.1000E+03	2.1487E+06	3.3218E+03	2.8769E+02	1.5994E+03	1.2352E+00	7.1997E-05
2.1500E+03	2.2311E+06	3.3598E+03	2.8794E+02	1.6969E+03	1.2244E+00	7.3195E-05
2.2000E+03	2.3188E+06	3.4008E+03	2.8828E+02	1.8167E+03	1.2131E+00	7.4395E-05
2.2500E+03	2.4132E+06	3.4428E+03	2.8871E+02	1.9619E+03	1.2018E+00	7.5601E-05
2.3000E+03	2.5155E+06	3.4878E+03	2.8927E+02	2.1358E+03	1.1908E+00	7.6816E-05
2.3500E+03	2.6273E+06	3.5358E+03	2.8999E+02	2.3410E+03	1.1804E+00	7.8044E-05
2.4000E+03	2.7501E+06	3.5878E+03	2.9087E+02	2.5796E+03	1.1709E+00	7.9288E-05
2.4500E+03	2.8858E+06	3.6438E+03	2.9196E+02	2.8521E+03	1.1625E+00	8.0552E-05
2.5000E+03	3.0359E+06	3.7048E+03	2.9329E+02	3.1575E+03	1.1552E+00	8.1841E-05
2.5500E+03	3.2020E+06	3.7698E+03	2.9487E+02	3.4922E+03	1.1491E+00	8.3158E-05
2.6000E+03	3.3855E+06	3.8418E+03	2.9673E+02	3.8493E+03	1.1441E+00	8.4508E-05
2.6500E+03	3.5872E+06	3.9178E+03	2.9890E+02	4.2183E+03	1.1403E+00	8.5891E-05
2.7000E+03	3.8073E+06	4.0008E+03	3.0136E+02	4.5842E+03	1.1376E+00	8.7310E-05
2.7500E+03	4.0452E+06	4.0878E+03	3.0412E+02	4.9276E+03	1.1360E+00	8.8763E-05
2.8000E+03	4.2993E+06	4.1798E+03	3.0715E+02	5.2256E+03	1.1353E+00	9.0248E-05
2.8500E+03	4.5666E+06	4.2738E+03	3.1040E+02	5.4534E+03	1.1356E+00	9.1759E-05
2.9000E+03	4.8431E+06	4.3698E+03	3.1382E+02	5.5879E+03	1.1368E+00	9.3288E-05
2.9500E+03	5.1235E+06	4.4658E+03	3.1731E+02	5.6112E+03	1.1391E+00	9.4825E-05
3.0000E+03	5.4022E+06	4.5598E+03	3.2077E+02	5.5158E+03	1.1423E+00	9.6362E-05
3.1500E+03	6.1724E+06	4.8108E+03	3.3019E+02	4.6336E+03	1.1593E+00	1.0087E-04
3.3000E+03	6.7773E+06	4.9978E+03	3.3695E+02	3.4477E+03	1.1874E+00	1.0511E-04

Figure A1.1: Typical fuel data table

APPENDIX 2: DRY AIR INTERPOLATION ERRORS

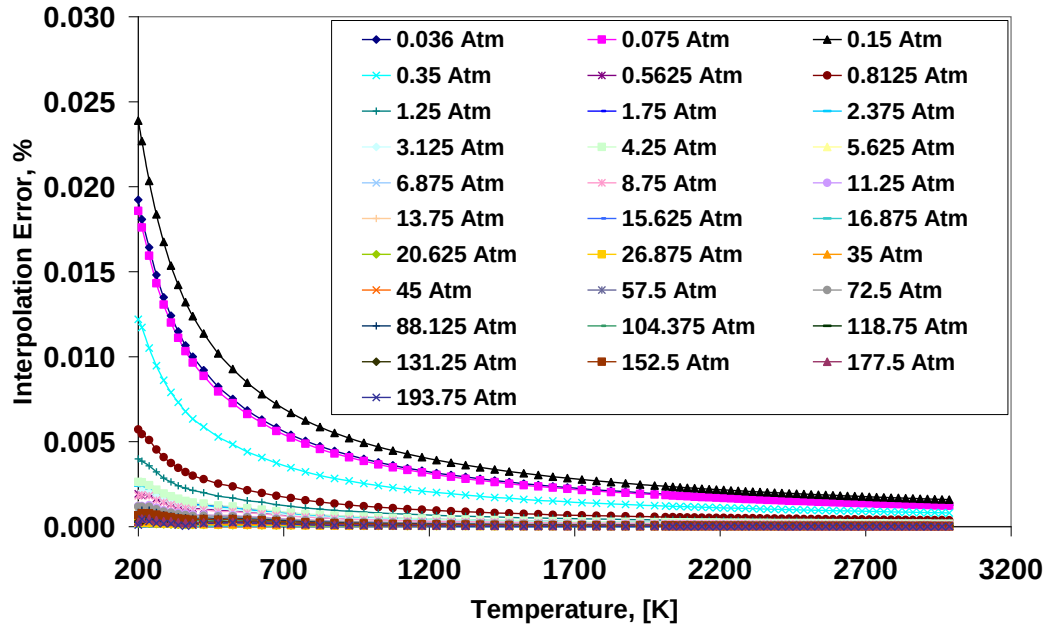

Figure A2.1: interpolation errors, dry air, density

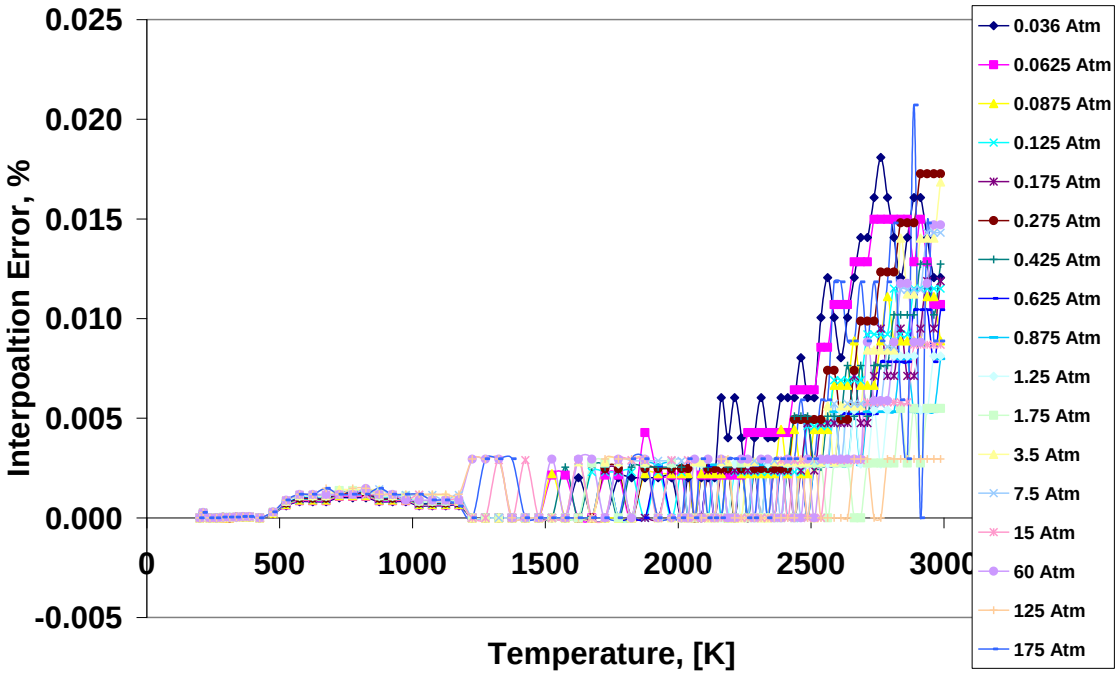

Figure A2.2: Interpolation errors, dry air, Enthalpy

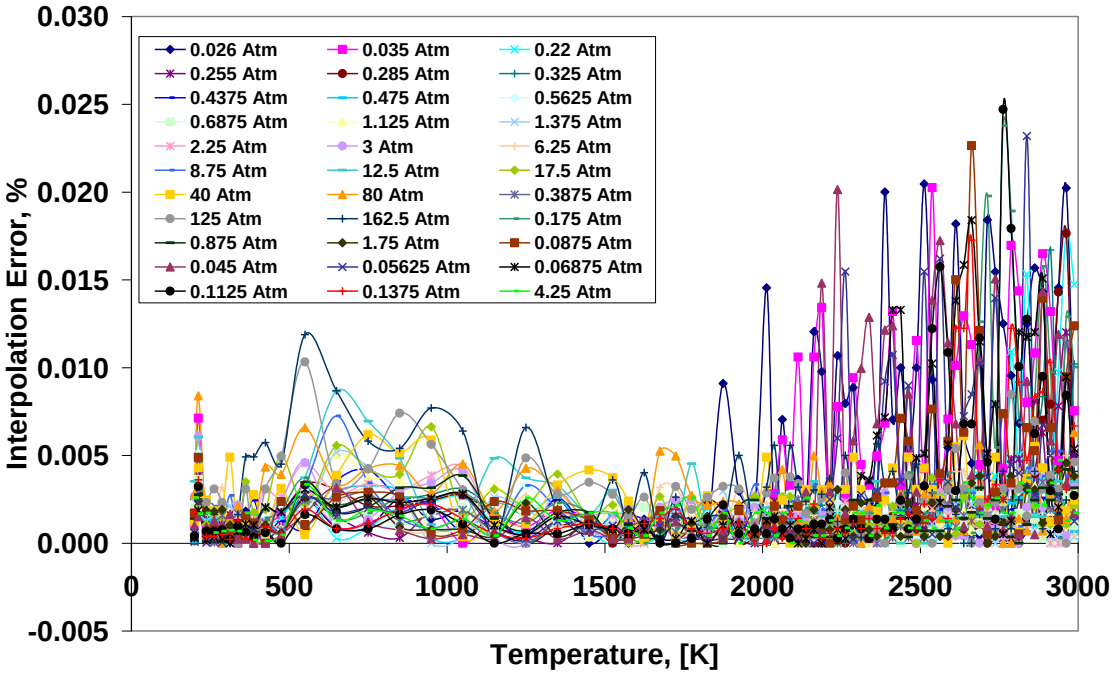

Figure A2.3: Interpolation error, dry air, entropy

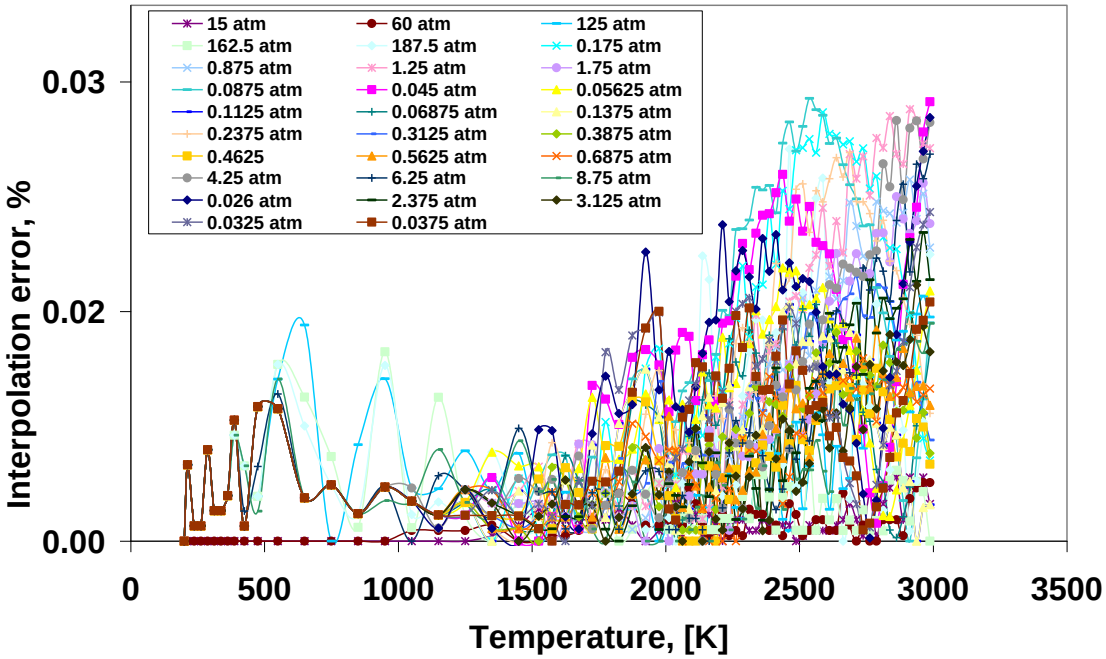

Figure A2. 4: Interpolation errors, dry air, Isobaric heat Capacity

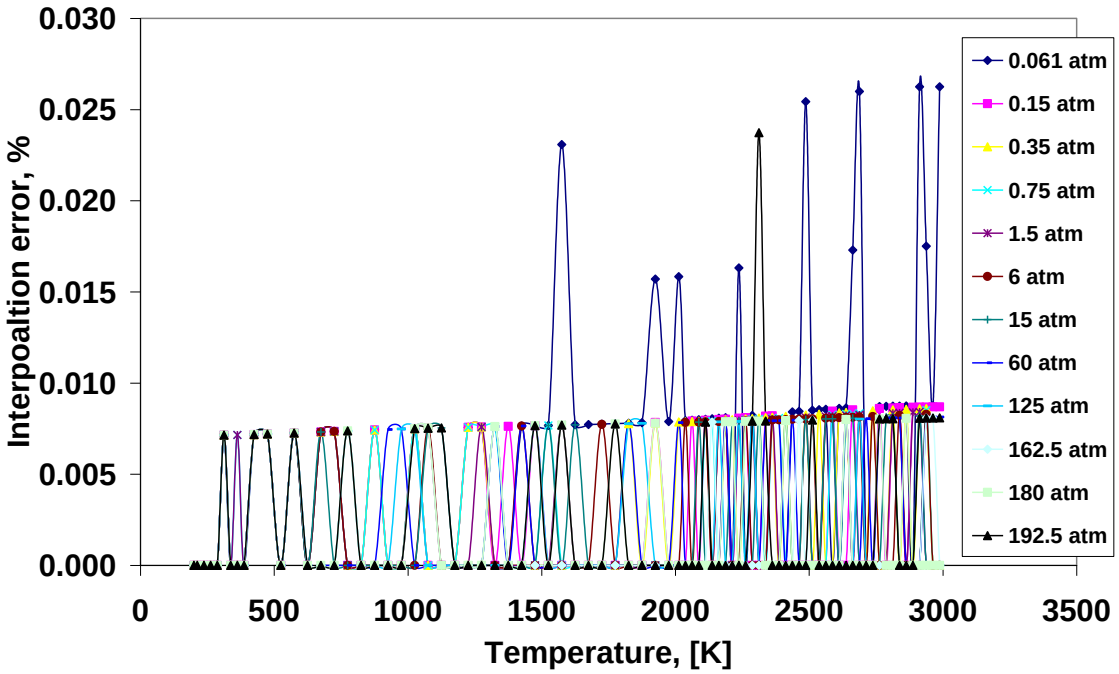

Figure A2. 5: Interpolation errors, dry air, ratio of heat capacities

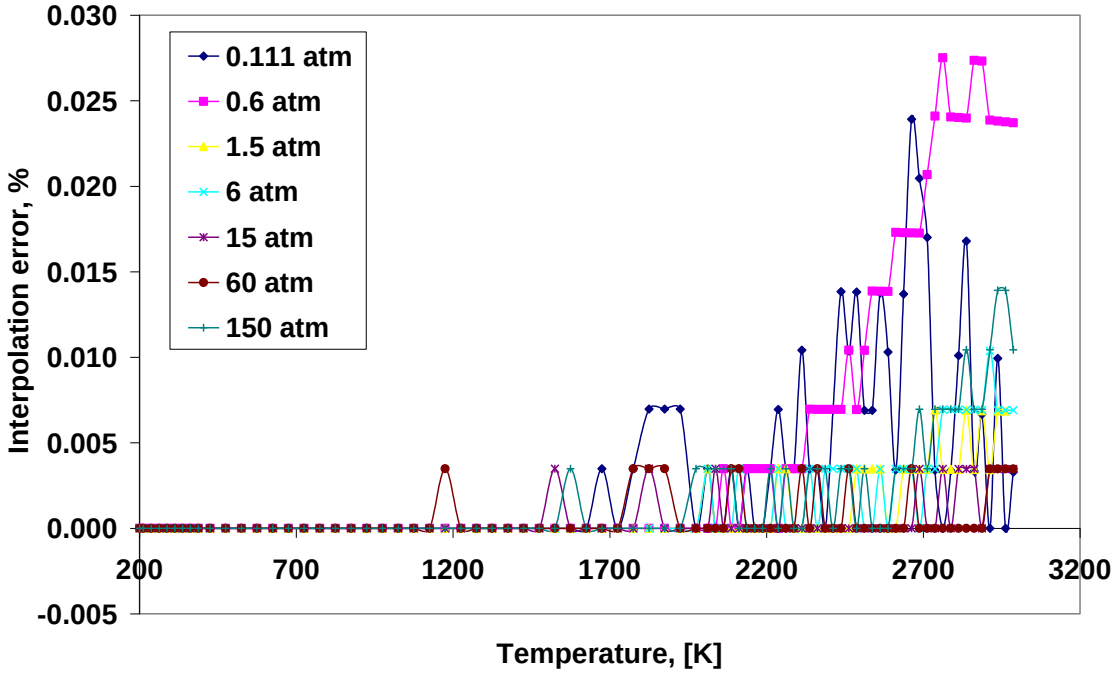

Figure A2.6: Interpolation errors, dry air, Gas constant, R

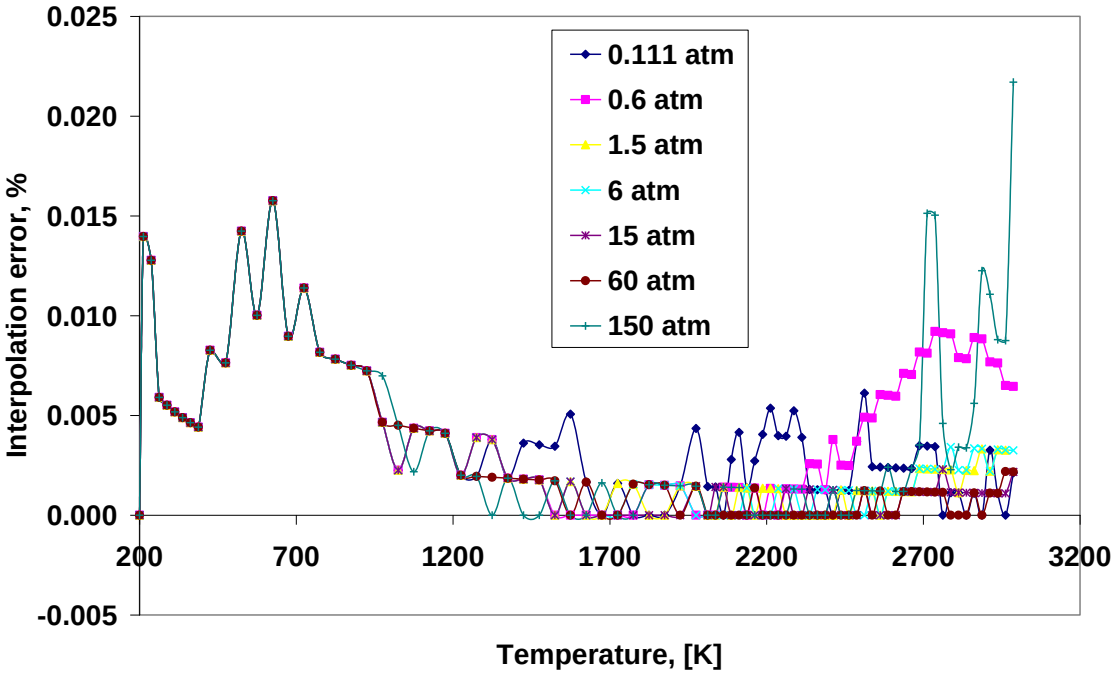

Figure A2. 7: Interpolation errors, dry air, Viscosity

APPENDIX 3: MOIST AIR INTERPOLATION ERRORS

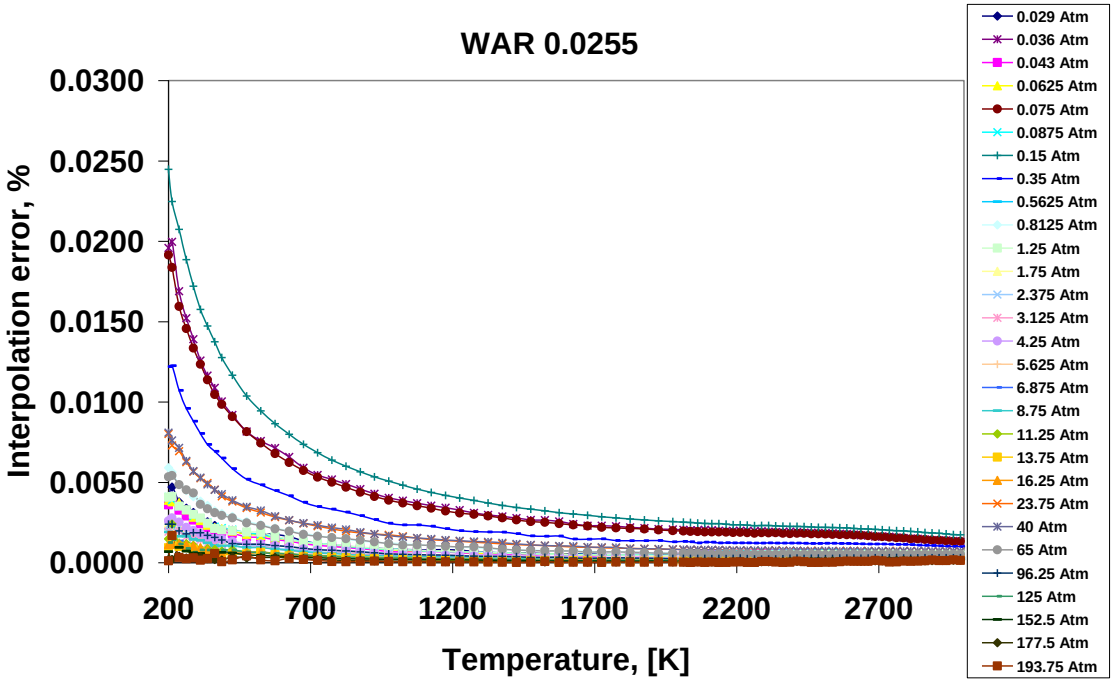

Figure A3.1: Interpolation errors, moist air, WAR 0.0255, density

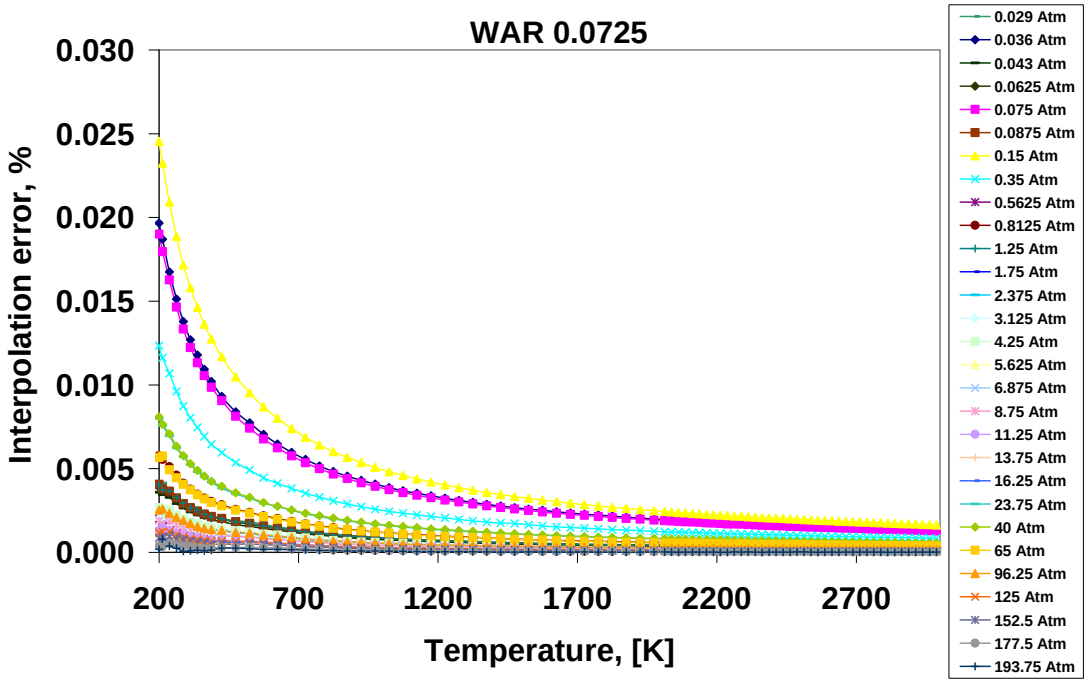

Figure A3.2: Interpolation errors, moist air, WAR 0.0725, density

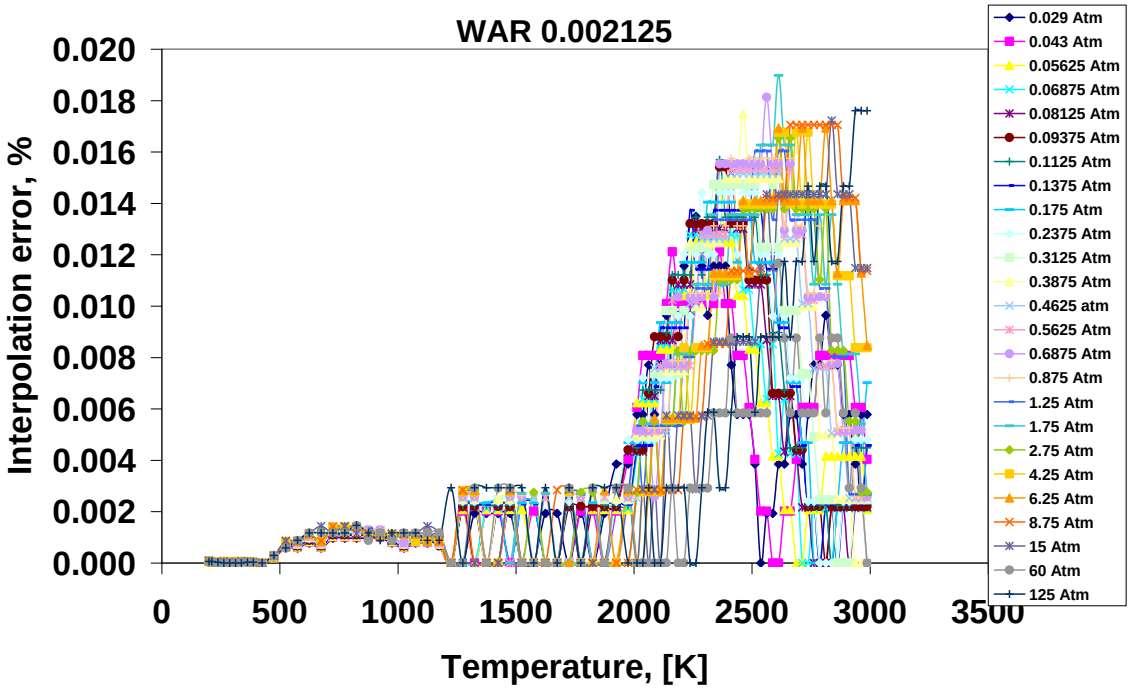

Figure A3.3: Interpolation error, moist air, WAR 0.002125, enthalpy

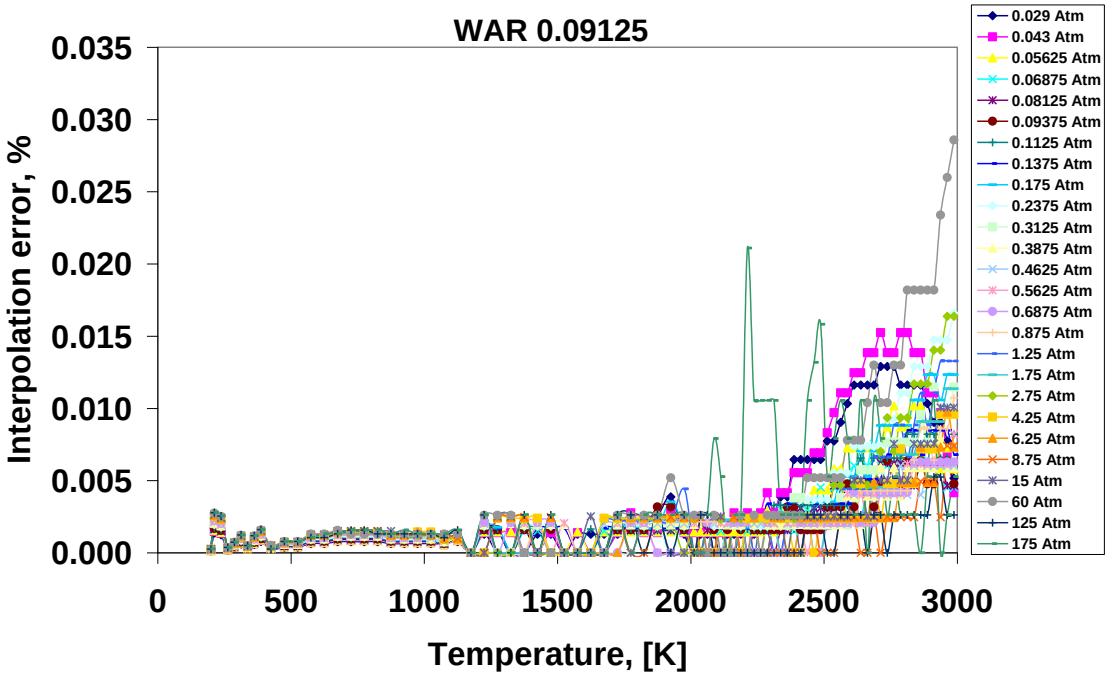

Figure A3.4: Interpolation error, moist air, WAR 0.09125, enthalpy

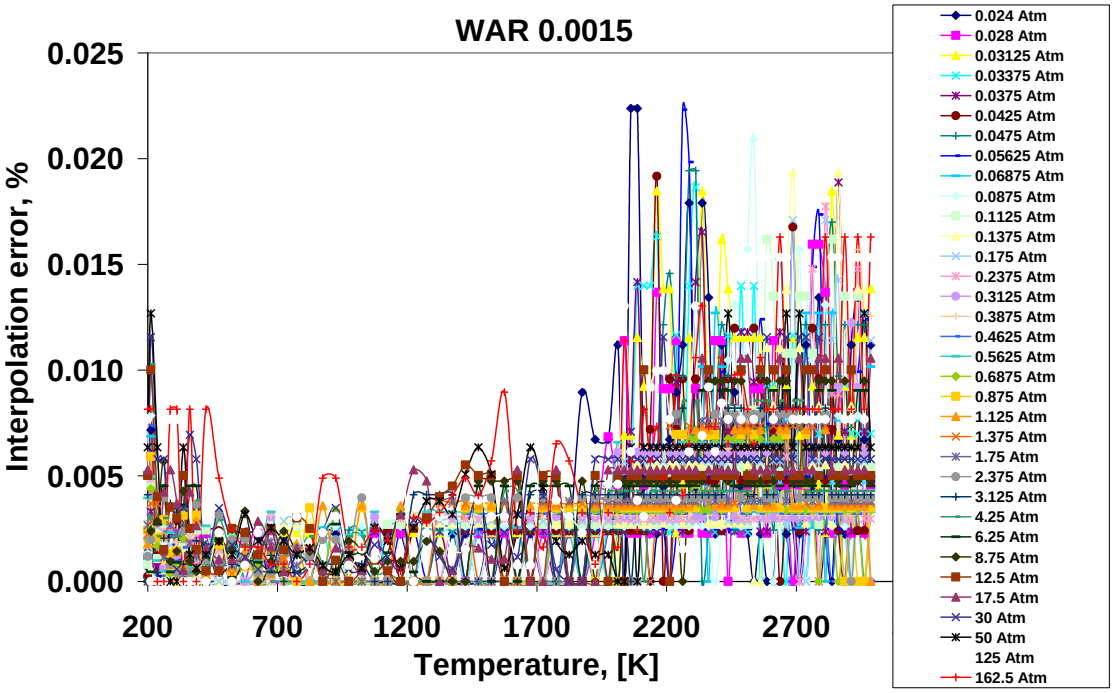

Figure A3.5: Interpolation error, moist air, WAR 0.015, Entropy

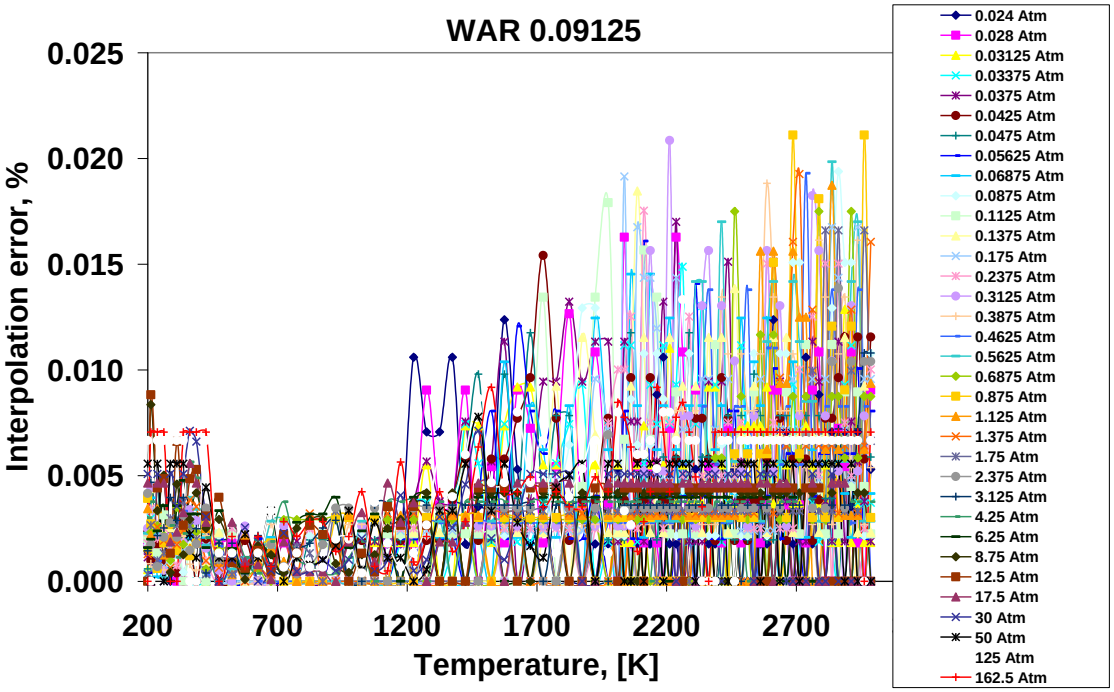

Figure A3. 6: Interpolation error, moist air, WAR 0.09125, Entropy

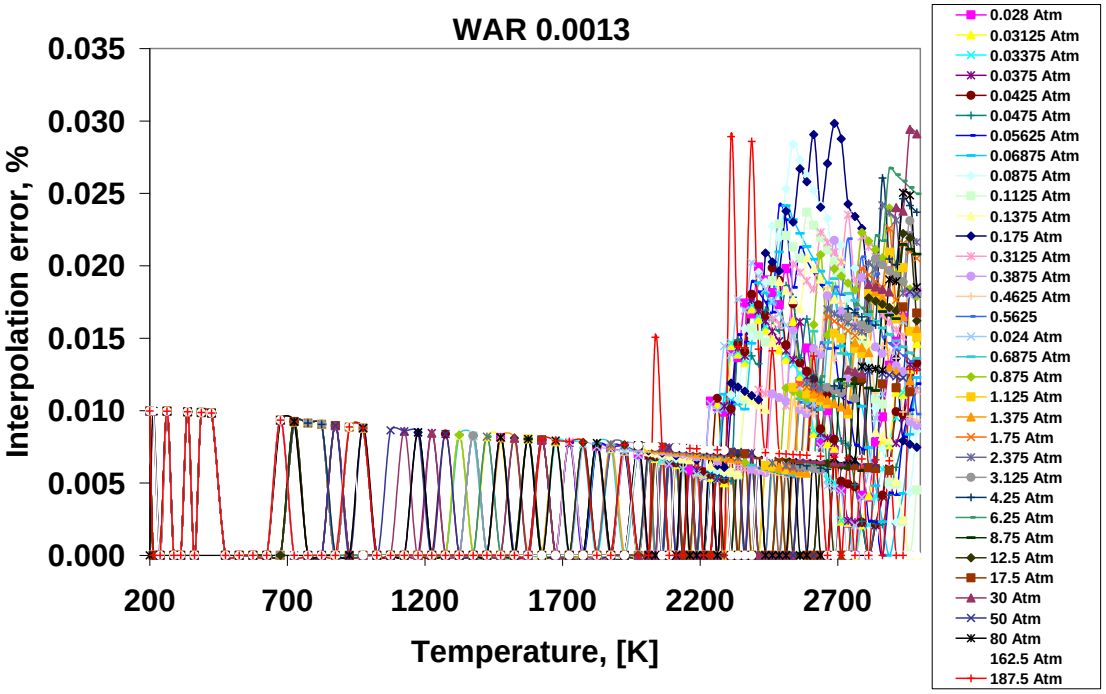

Figure A3.7: Interpolation error, moist air, WAR 0.0013, C_p

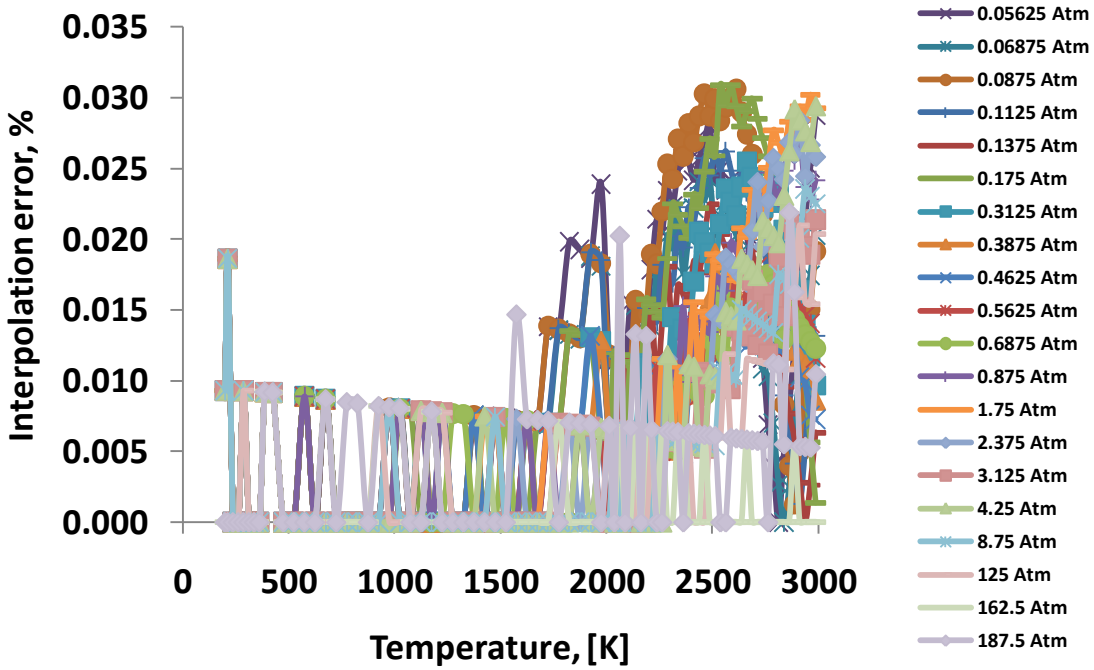

Figure A3.8: Interpolation error, moist air, WAR 0.09125, C_p

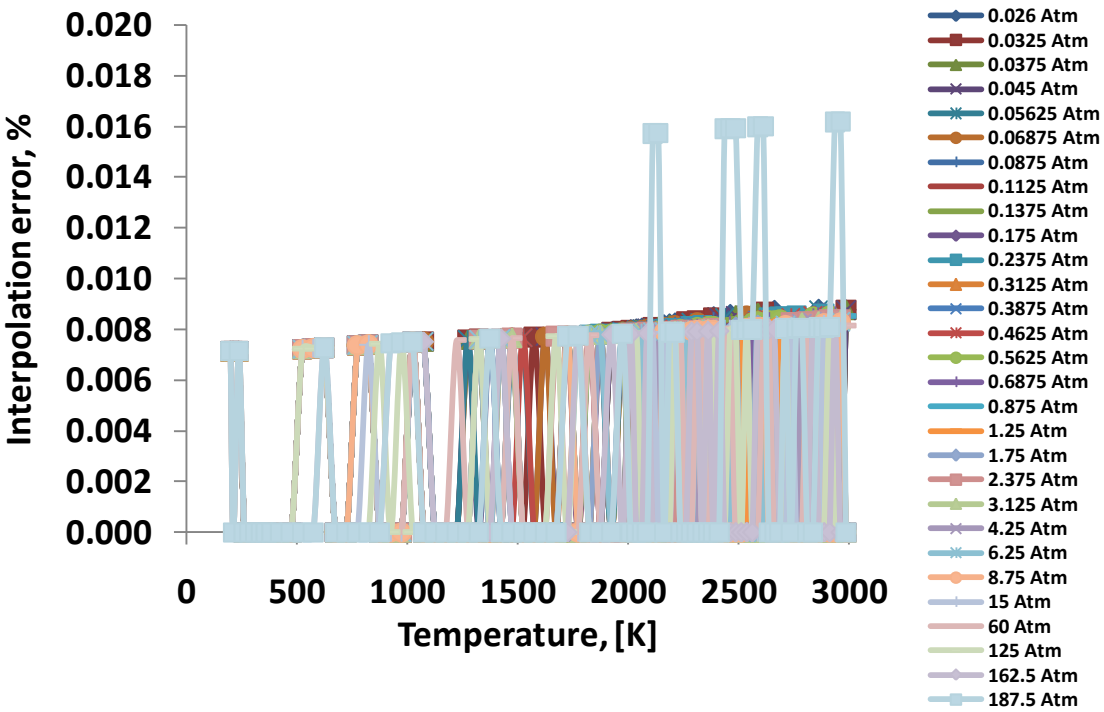

Figure A3.9: Interpolation error, moist air, WAR 0.0015625 ratio of heat capacities

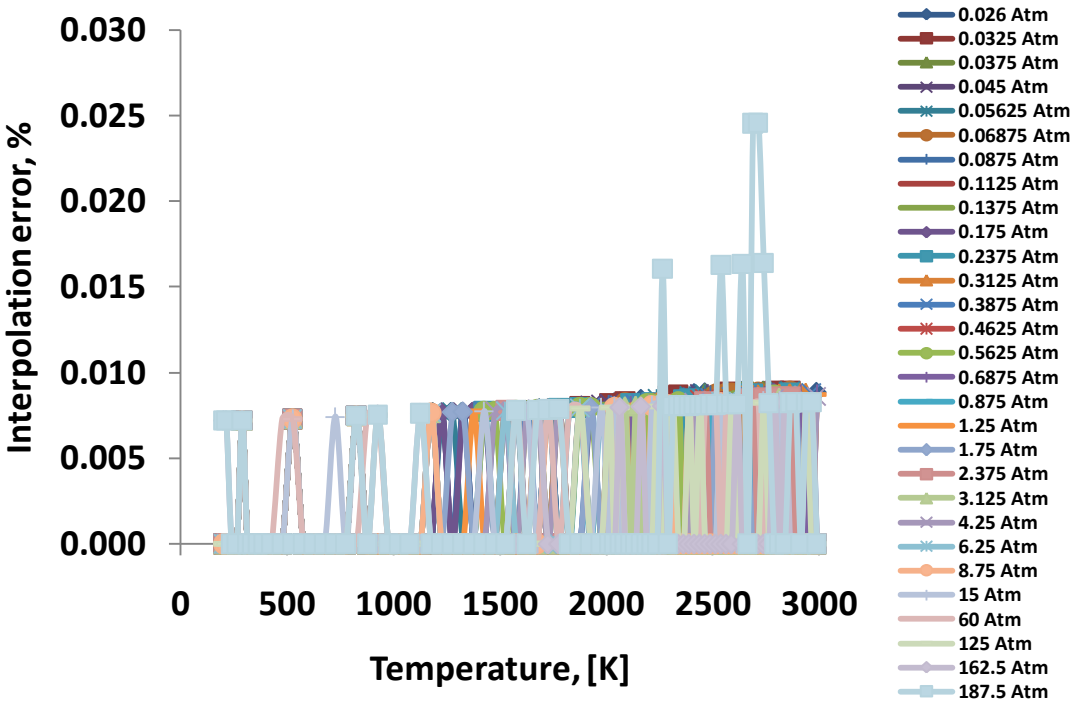

Figure A3.10: Interpolation error, moist air, WAR 0.09125, ratio of heat capacities

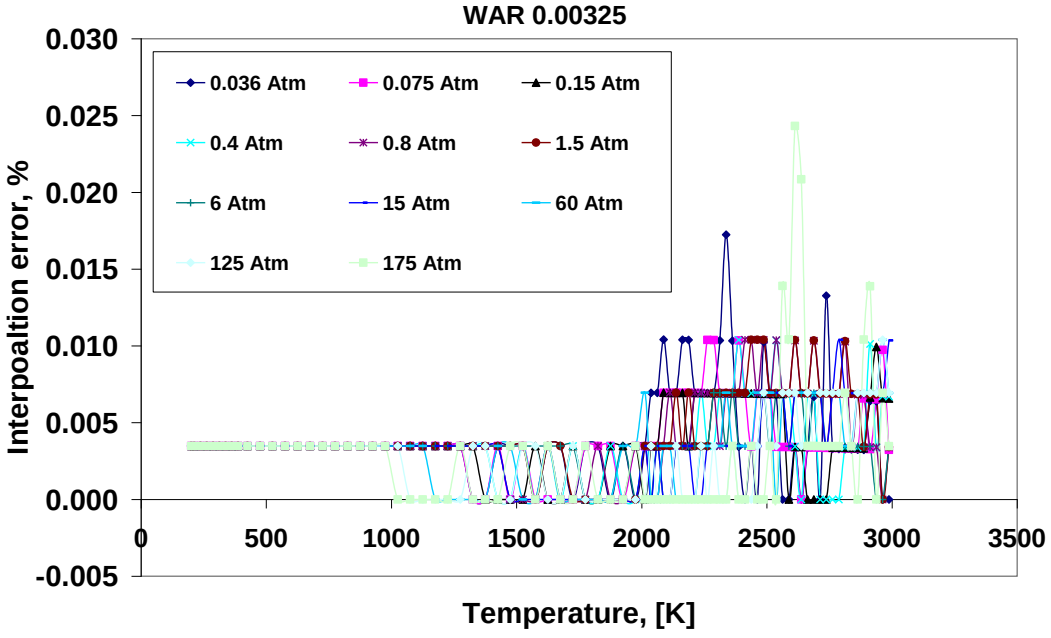

Figure A3.11: Interpolation error, moist air, WAR 0.00325, Gas constant, R

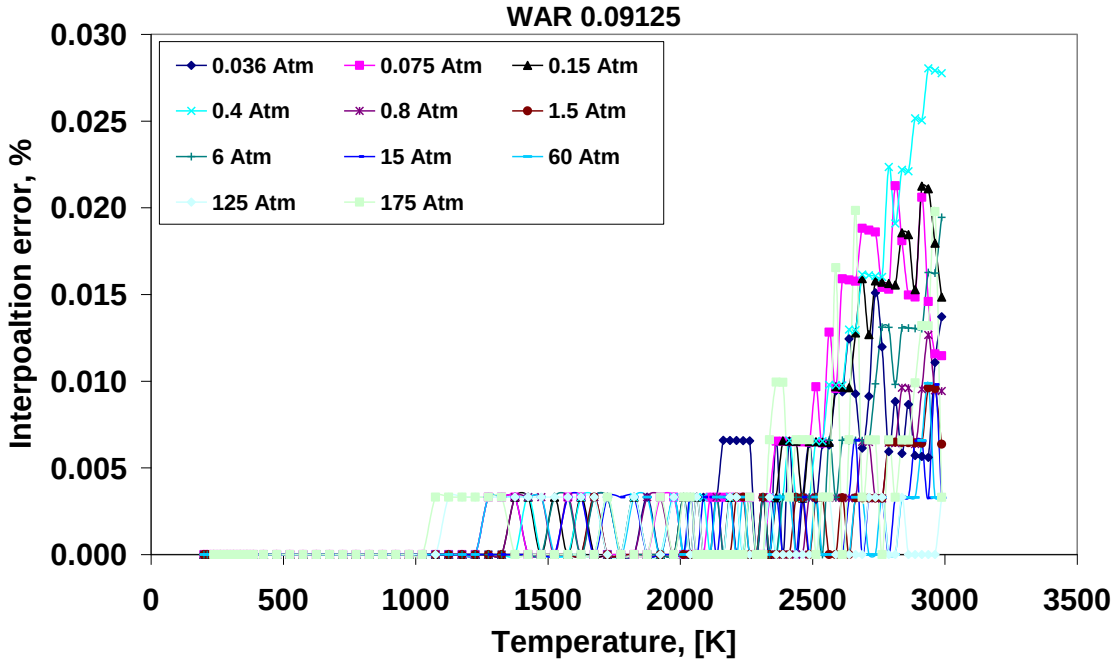

Figure A3.12: Interpolation error, moist air, WAR 0.09125, Gas constant, R

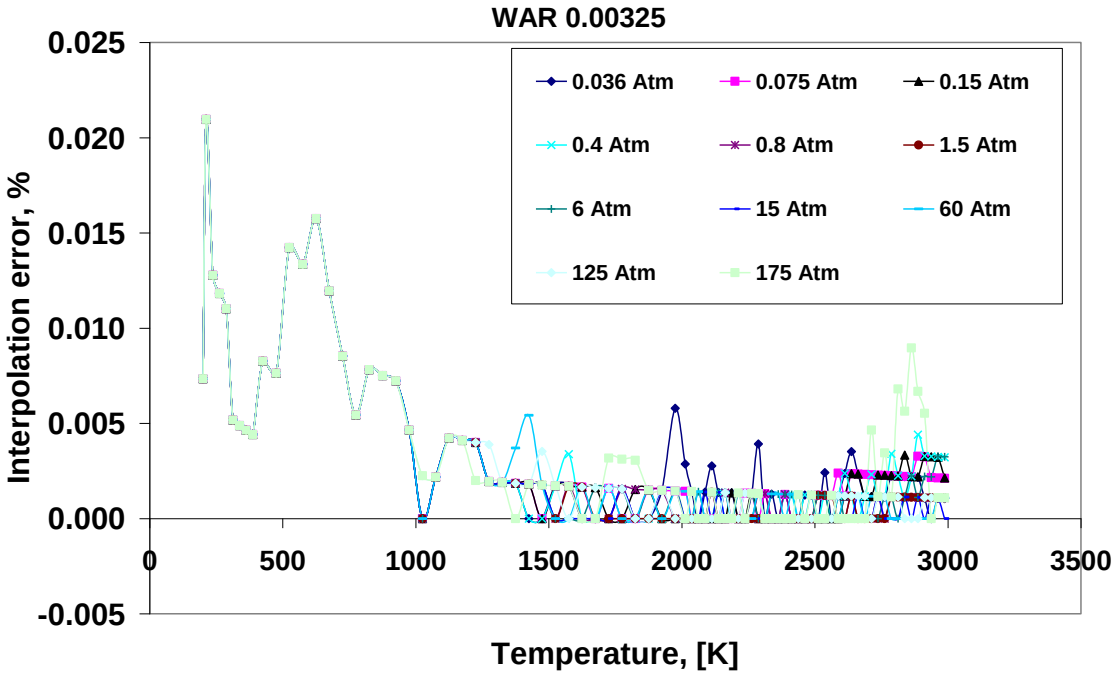

Figure A3.13: Interpolation error, moist air, WAR 0.00325, viscosity

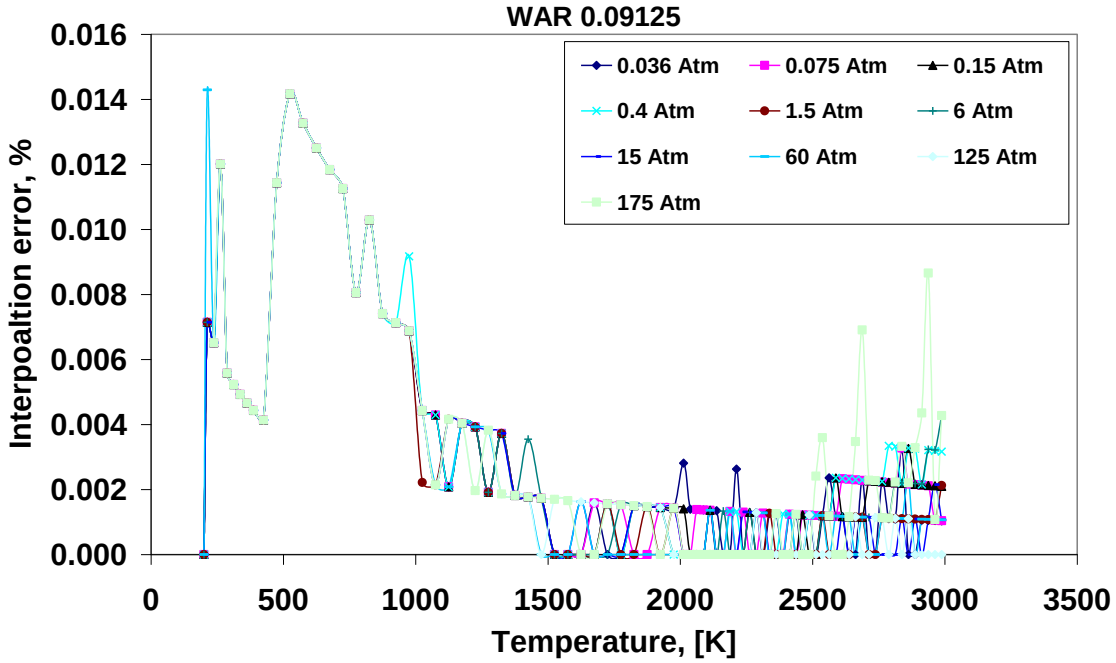

Figure A3.14: Interpolation error, moist air, WAR 0.09125, Viscosity

APPENDIX 4: JET A FUEL INTERPOLATION ERRORS

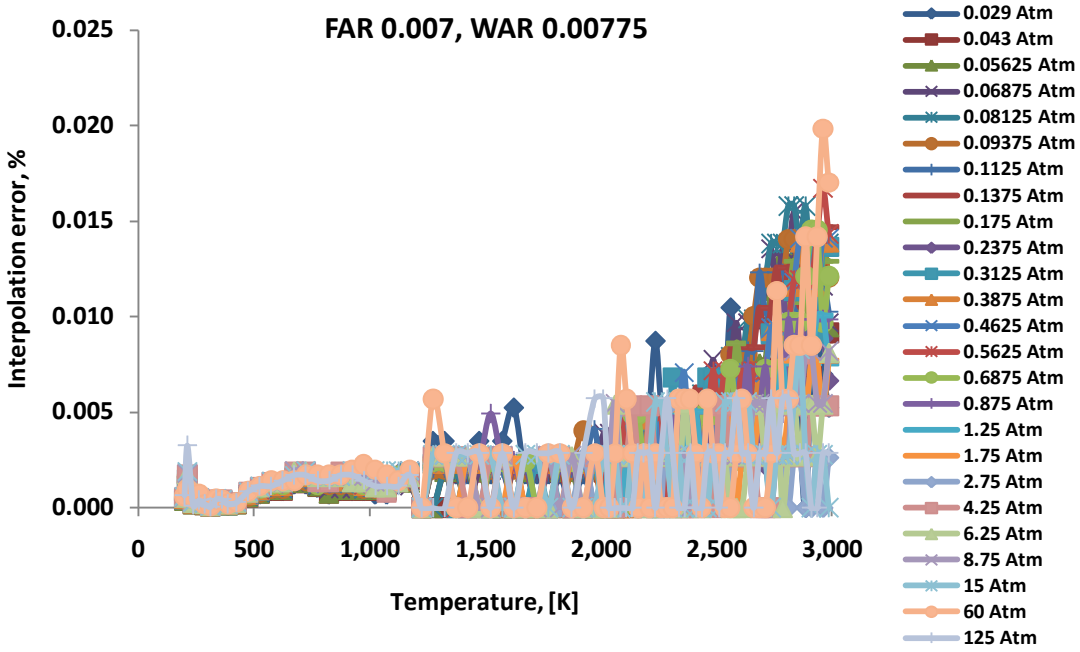

Figure A4.1: Interpolation errors, JetA FAR 0.007, WAR 0.00775, Enthalpy

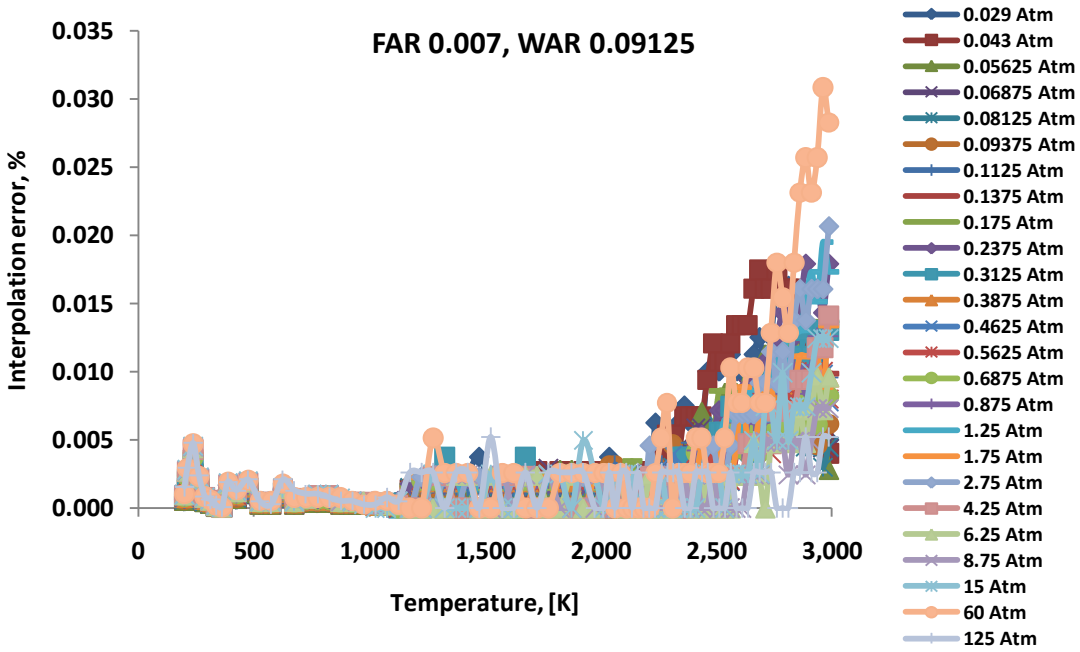

Figure A4.2: Interpolation errors, JetA FAR 0.007, WAR 0.09125, Enthalpy

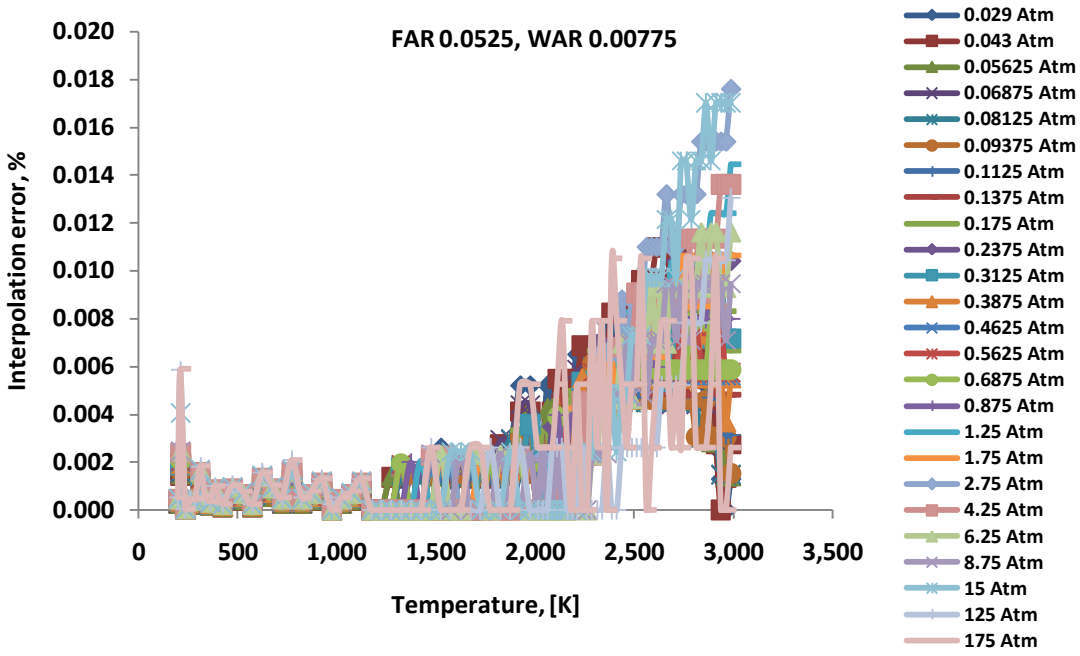

Figure A4.3: Interpolation errors, JetA FAR 0.0525, WAR 0.00775, Enthalpy

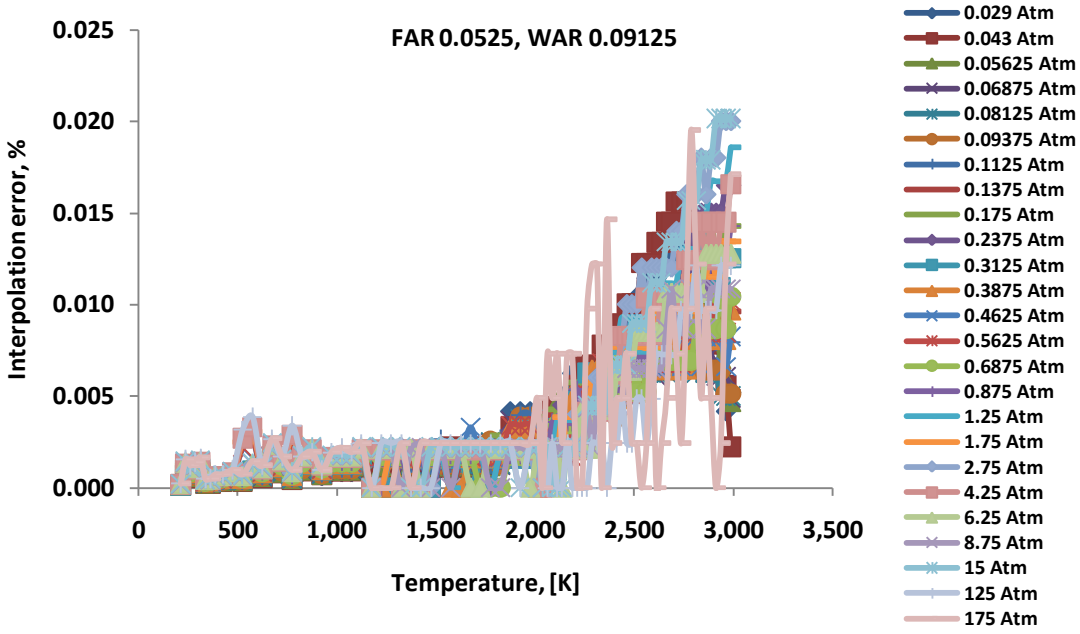

Figure A4.4: Interpolation errors, JetA FAR 0.0525, WAR 0.09125, Enthalpy

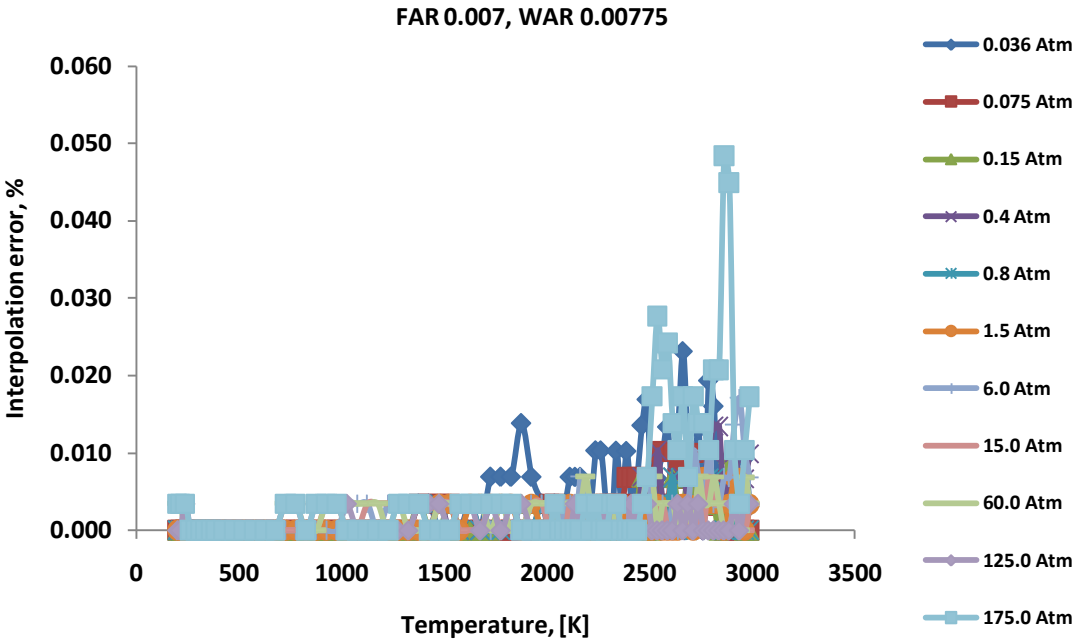

Figure A4.5: Interpolation errors, JetA FAR 0.007, WAR 0.00775, Gas constant, R

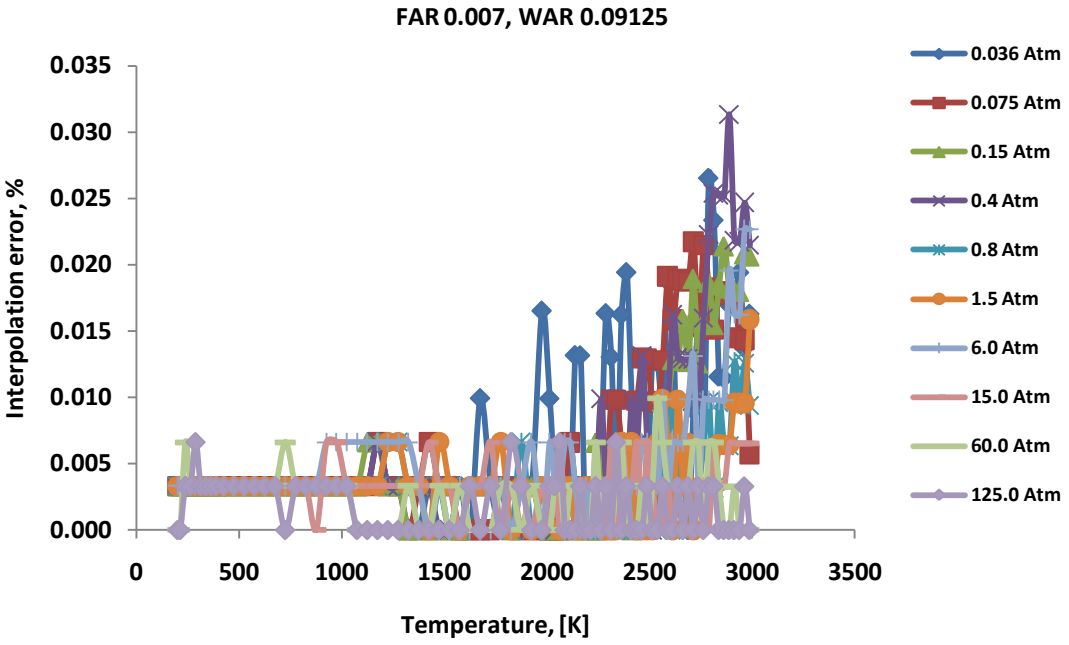

Figure A4.6: Interpolation errors, JetA FAR 0.007, WAR 0.09125, Gas constant, R

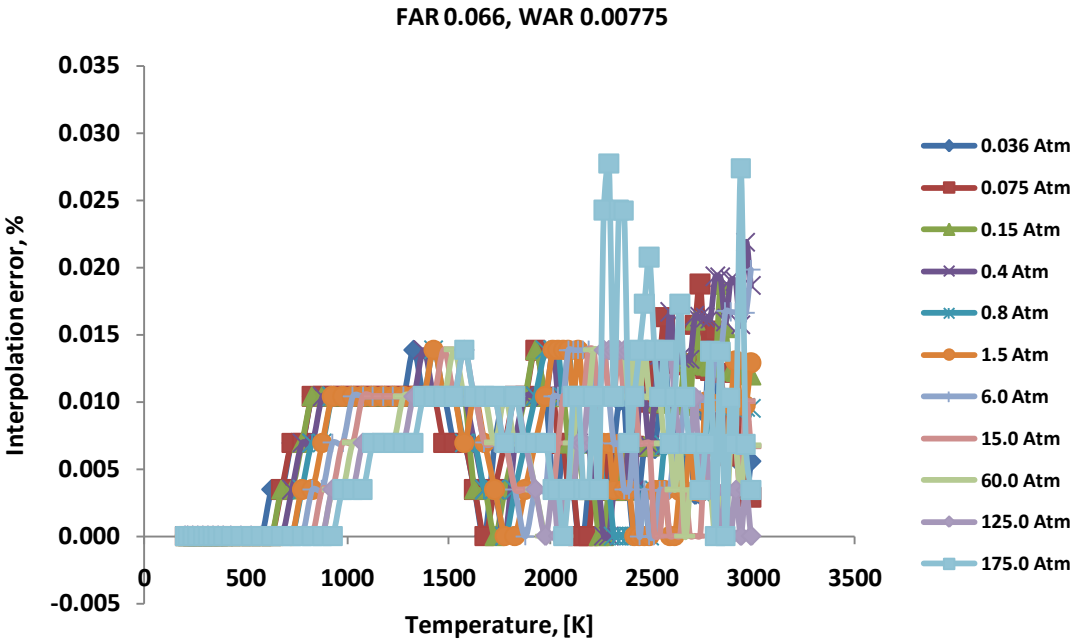

Figure A4.7: Interpolation errors, JetA FAR 0.066 WAR 0.00775, Gas constant, R

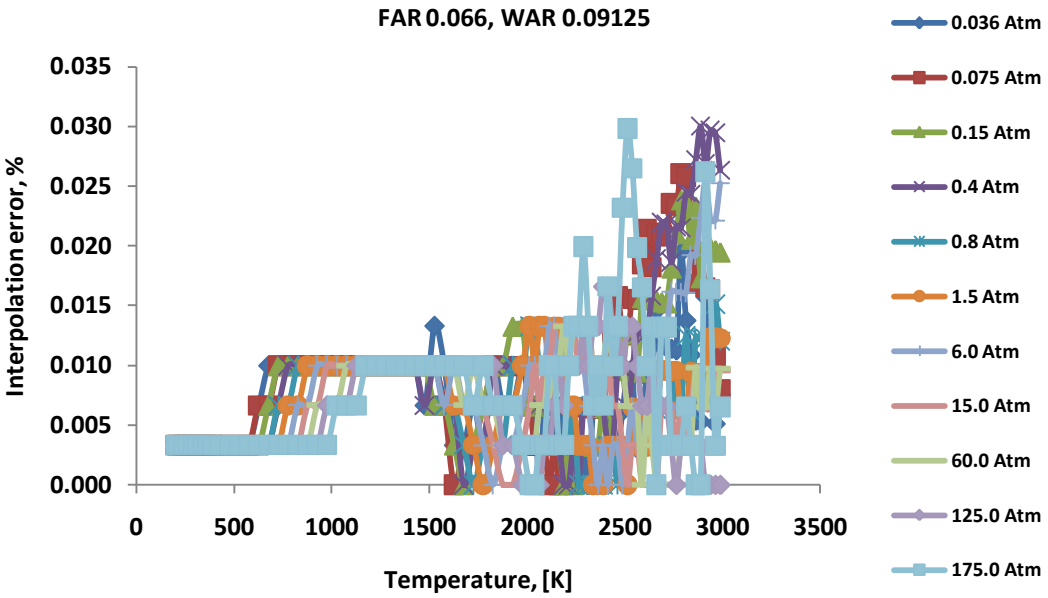

Figure A4.8: Interpolation errors, JetA FAR 0.066 WAR 0.09125, Gas constant, R

APPENDIX 5: DIESEL FUEL INTERPOLATION ERRORS

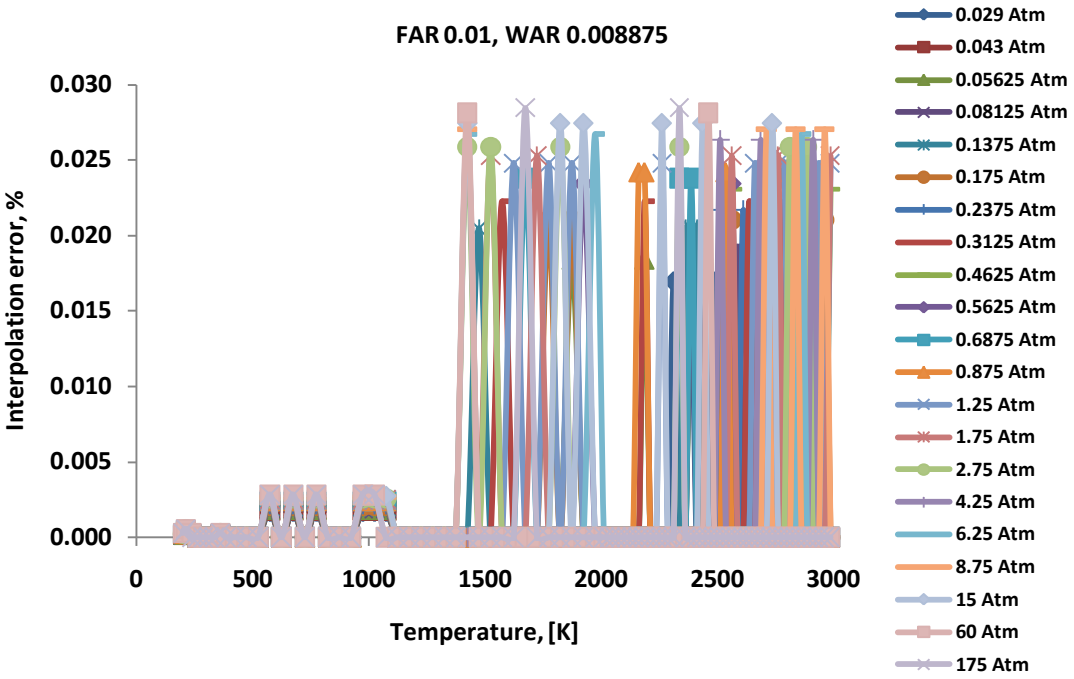

Figure A5.1: Interpolation errors, Diesel fuel FAR 0.01 WAR 0.008875, Enthalpy

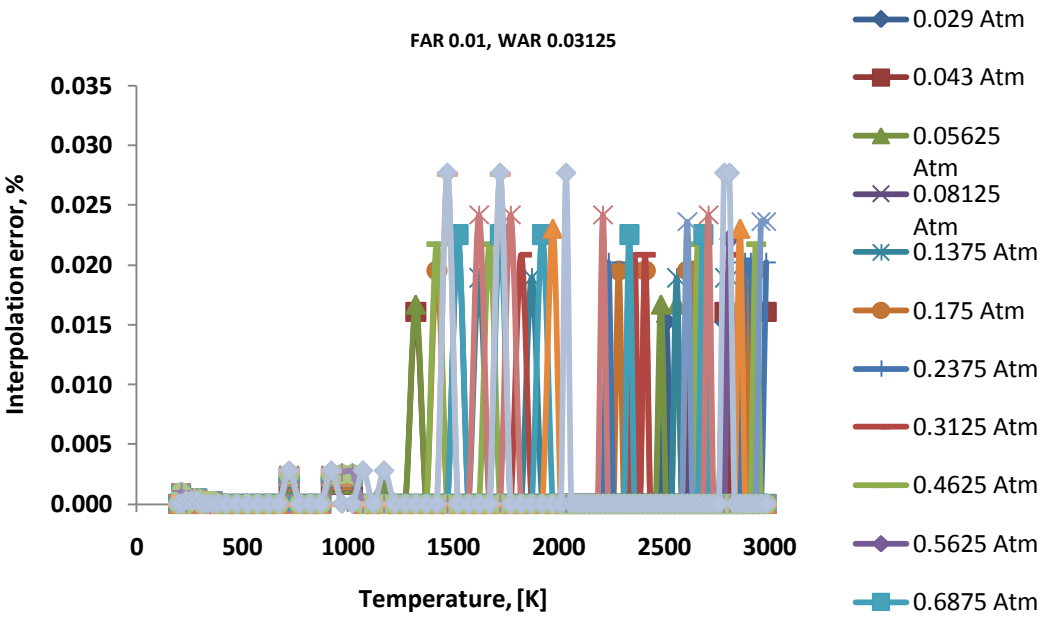

Figure A5.2: Interpolation errors, Diesel fuel FAR 0.01 WAR 0.03125, Enthalpy

APPENDIX 6: HYDROGEN FUEL INTERPOLATION ERRORS

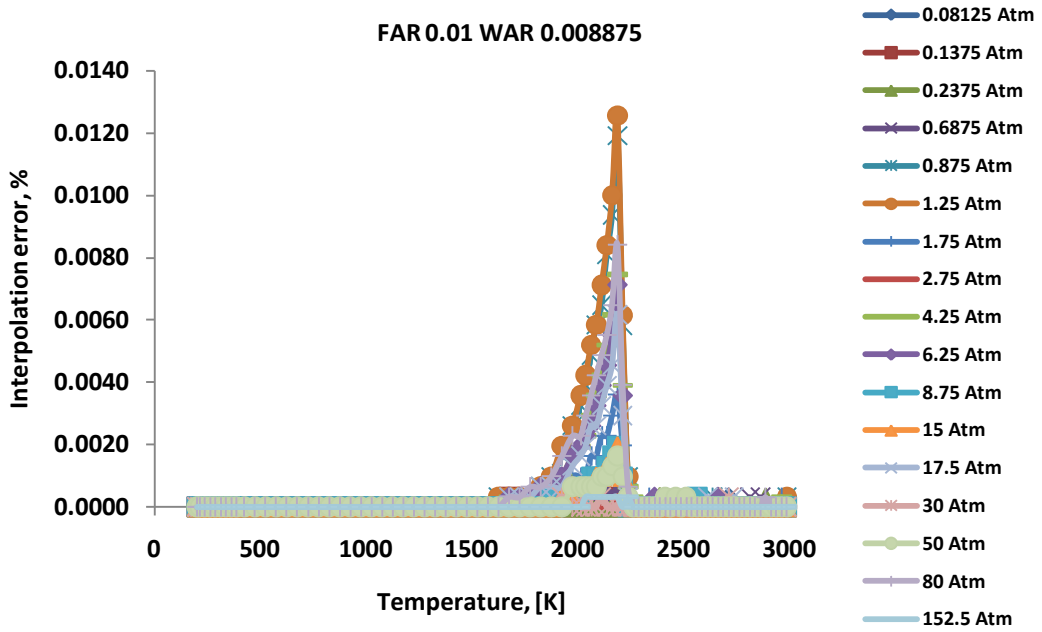

Figure A6.1: Interpolation errors, Hydrogen fuel FAR 0.01 WAR 0.008875, Gas constant, R

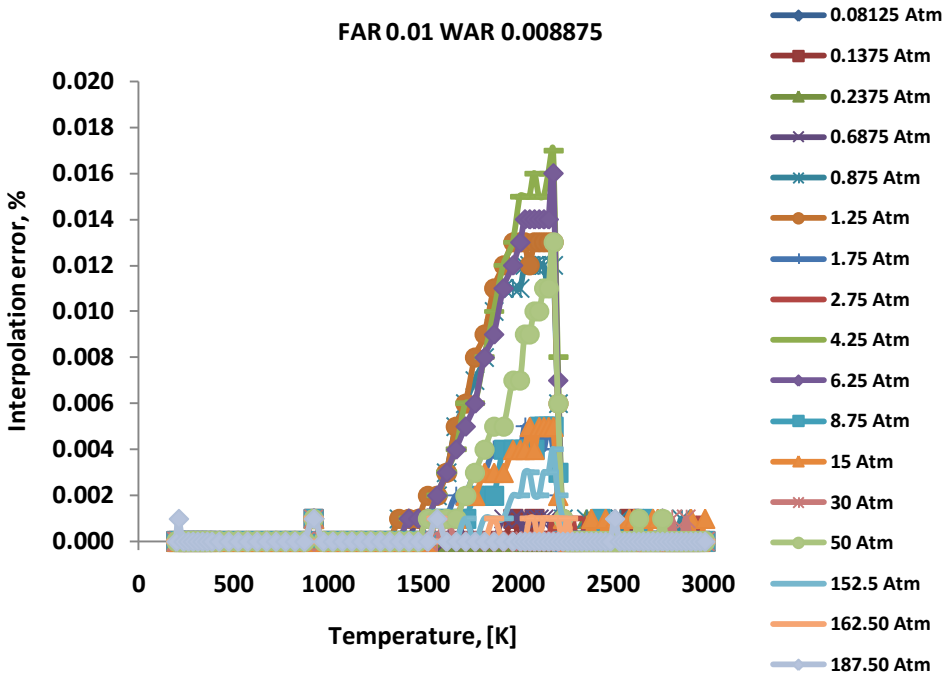

Figure A6.2: Interpolation errors, Hydrogen fuel FAR 0.01 WAR 0.008875, ratio of heat capacities